INVESTIGATING THE MOLECULAR MECHANISMS OF FRACTION SIZE SENSITIVITY IN IRRADIATED CELLS

DAVID MCBAY

Thesis submitted for the degree of Doctor of Philosophy

Supervisors

Professor Jessica Downs

Professor John Yarnold

Professor Penny Jeggo

Dr Navita Somaiah

Declaration

I hereby declare all the work presented in this thesis is my own unless where otherwise stated.

I hereby declare that this thesis has not been and will not be submitted in whole or in part to another University for the award of any other degree.

Signed:

Date:

Acknowledgements

At the start of my PhD I joined the Downs' laboratory as a collaborative student at the Genome Damage and Stability Centre (GDSC), University of Sussex. Reflecting back over the last four years, I could not have hoped to have joined a more supportive group. I want to take this opportunity to thank them first for their expertise, friendship and guidance. Despite having a relatively distinct project from the main focus of the group, there was never a lab meeting I hosted that left without a substantial amount of insight. More importantly, I've always felt part of a slightly crazy family who all look out for each other and make the day-to-day experience so much better for it. So a big thank you Suzi, Pete, Connie, Sarah, Federica, Karen, Susana, Alison, Geoffrey, Youwen, Noa and Pedro.

I want to also extend my thanks to the wider community at the ICR, especially to the technicians and service staff who have facilitated my research in a world-class environment. A particular thank you to James for introducing me to the complexities of sequencing analysis and programming and to Alice for her expertise and selfless work under tight deadlines; our collaboration was one of the most personally rewarding areas of my research. Finally, a thank you to my fellow PhD students: the best possible support network when experiments fail.

On a more personal note, I have to thank the group of people who allowed me to switch off and reset. As part of the University of London Canoe Polo Club I have made friends for life and countless memories that I will

cherish.

To my family, it is impossible to thank you for everything you have done for me; in particular, your support as I moved to London and encouragement to follow my interests. I may have not always articulated it, but your support was the bedrock to my studies.

To Eleanor, thank you for being with me through the thick and thin; the first year and a half of my PhD was particularly difficult. Words cannot express how much your belief, comfort, and encouragement meant to me.

Finally, to my four supervisors. Collaborations can be challenging, but your mentorship has developed me into a far better scientist and person than I was at the start of this journey. Navita, thank you for your expert insight and for reminding me of the clinical relevance of my research, which was a personal motivator. Penny, thank you for your teaching and critical thinking, both of which were inspirational to me. John, thank you for challenging me and for teaching me the value of precision. Jessica, thank you for taking me into your lab and for your door always being open as my first call for discussion and support. Many of my fellow students recoil in horror when they find out I have four supervisors, but I can honestly say I feel extremely lucky to have had not one but four fantastic supervisors. I hope this project has been as rewarding an experience for you as it was for me.

Abstract

Fractionated radiotherapy is used clinically when it spares healthy tissue relative to the cancer; the healthy tissue is described as more fraction size sensitive. However, a molecular understanding of the mechanisms that determine this sensitivity are limited. The recently demonstrated response of breast and prostate cancers to hypofractionation highlights the need understand the mechanisms of fraction size sensitivity in order to improve dose regimens. We must also develop biomarkers and drugs that leverage this sensitivity to individualise and improve radiotherapy outcomes. DNA double-strand breaks (DSB) are the most deleterious form of damage caused by irradiation due to their potential for misrepair. The cell cycle stage influences the availability of DSB repair pathways. There is a tight inverse association between fraction size sensitivity and proliferation rate. We hypothesise that the enhanced fidelity of Homologous Recombination (HR) repair in S/G_2 phase decreases fraction size sensitivity through a reduction of misrepair. Using a non-cancerous repair-proficient fibroblast model, we show that fraction size sensitivity is comparable across all cell cycle phases by clonogenic survival. Chromosome aberration analyses are consistent with survival and suggest that mis-repair events in G_1 and G_2 phase cells are spared by fractionation. We conclude that the availability of HR in G_2 does not impact fraction size sensitivity. Using γ-H2AX foci as a surrogate for DSBs we show that induction and kinetics of repair do not alter between fractions, however after complete repair persistent foci are shown to increase with dose and are spared with fractionation, suggesting a role for unrepaired DSBs. The chromatin

environment can impact repair pathway choice, we demonstrate through global changes to chromatin state with histone deacetylase inhibition (HDAC) and CRISPR-Cas9 guided BRG1 mutations that these changes do not impact fraction size sensitivity. Finally, a single cell sequencing approach begins to establish a mutational signature for irradiation.

Table of Contents

List of Figures

List of Abbreviations

53BP1	P53 binding protein 1
AR	Adaptive response
AT	Ataxia-telangiectasia
ATM	Ataxia telangiectasia mutated
ATR	ATM and Rad-3 related
BAM	Binary alignment map
BLM	BLM RecQ like helicase
BRCA1	BRCA1 DNA repair associated
BRG1	Nuclear protein BRG1
BSA	Bovine serum albumin
Cas9n	Cas9 Nickase
CDK9	Cyclin-dependent kinase 9
ChIP-seq	Chromatin immunoprecipitation-sequencing
Chk2	Checkpoint kinase 2
Chk2	Checkpoint kinase 1
CHO	Chinese hamster ovary
c-NHEJ	Canonical non-homologous end-joining
CRISPR	Clustered regularly interspaced short palindromic repeats
CtIP	CTBP-interacting protein
DDR	DNA damage response
DITR	Damage-induced transcriptional repression

DMEM	Dulbecco’s modified eagle medium
DNA	Deoxyribonucleic acid
DNA-PKcs	DNA-dependent protein kinase catalytic subunit
DNA-SCARS	DNA segments with chromatin alterations reinforcing senescence
DSB	Double-strand breaks
ECL	Enhanced chemiluminescence
EXD2	Exonuclease 3'-5' domain containing 2
EXO1	Exonuclease 1
FACS	Fluorescence-activated cell sorting
FBC	Fetal bovine serum
GDSC	Genome Damage and Stability Centre
Gy	Gray
H2AX	H2A histone family member X
H3K36me3	H3K36me3 histone
HAS	HiSeq Analysis Software v2.1
HAT	Histone acetyltransferase
HDAC	Histone deacetylases
HDR	High dose rate
HPC	High performance computing
HR	Homologous recombination
hTERT	Human telomerase reverse transcriptase
ICR	Institute of Cancer Research

IR	Ionising radiation
IRIF	Irradiation-induced foci
LDR	Low dose rate
LDS	Lithium dodecyl sulfate
LigIV	DNA Ligase IV
LPL	Lethal potentially lethal
LQ	Linear-quadratic
LQC	Linear-quadratic-cubic
MDC1	Mediator of DNA damage checkpoint protein 1
MMEJ	Micro-homology mediated end-Joining
MMSET	Nuclear receptor binding SET domain protein 2
MR Linac	Magnetic resonance linear accelerator
Mre11	MRE11 homolog, double strand break repair nuclease
MRI	Magnetic resonance imaging
MRN	Mre11/Rad50/Nbs1
Nbs1	Nijmegen breakage syndrome 1
NHEJ	Non-homologous end-joining
p53	Tumour protein p53
PALB2	Partner and localizer of BRCA2
PBAF	Polybromo-associated BRG1- or HBRM-associated factor complex
PBS	Phosphate-buffered saline
PCC	Premature chromatin condensation

PCR	Polymerase chain reaction
PFGE	Pulsed-field gel electrophoresis
PML	Promyelocytic leukaemia
PNKP	Polynucleotide kinase phosphatase
Pol μ	DNA polymerase μ
Pol λ	DNA polymerase λ
Rad50	RAD50 double strand break repair protein
Rad51	RAD51 recombinase
RAD51B	RAD51 paralog B
RAD51C	RAD51 paralog C
RAD51D	RAD51 paralog D
RBE	Relative biological effectiveness
RCF	Relative centrifugal force
RIF1	Replication timing regulatory factor 1
RNA	Ribonucleic acid
RNF168	Ring finger protein 168
RNF8	Ring finger protein 8
ROS	Reactive oxygen species
RPA	Replication protein A
SAHA	Suberanilohydroxamic acid
SEM	Standard error of the mean
SD	Standard deviation
sgRNA	Single guide ribonucleic acid

SMARCA4	SWI/SNF related, matrix associated, actin dependent regulator of chromatin, subfamily a, member 4
SNP	single-nucleotide polymorphism
SSB	Single-strand breaks
ssDNA	Single-stranded DNA
TBST	Tris-buffered saline
Tdt	Terminal deoxynucleotidyl transferase
TOPOIIIa	Type I topoisomerase
TRIP12	Thyroid hormone receptor interactor 12
UBR5	Ubiquitin protein ligase E3 component n-recognin 5
USA	United States of America
WGS	Whole genome sequencing
XLF	X-ray repair cross-complementing protein 1
XRCC2	X-ray repair cross-complementing protein 2
XRCC3	X-ray repair cross-complementing protein 3
XRCC4	X-ray repair cross-complementing protein 4
γH2AX	Gamma histone 2AX

1 Introduction

Dose fractionation schedules for curative radiotherapy have been derived from proven clinical practice. By splitting the overall dose into a series of fractions, we spare fraction size *sensitive* healthy tissue, relative to the fraction size *insensitive* cancer. Despite the advances made in the Deoxyribose Nucleic Acid (DNA) repair field, for instance how DNA damage is sensed, repair pathway choice is made and fulfilled, and checkpoint controls are implemented, this knowledge has not been robustly applied to elucidate a molecular understanding of fractionation sensitivity. We do not yet fully understand the molecular basis of the therapeutic method utilised in the treatment of 50% of cancer cases globally (Tobias 1996, Delaney et al. 2005). Determining this could aid biomarker discovery to personalise patient care and define drug targets that can ultimately improve radiotherapy outcomes. In order to question the intersection between evolved clinical practice and our molecular knowledge of DNA repair, we must first consider the relevant background knowledge of each.

1.1 Physical Nature of Ionizing Radiation

Radiation describes the transmission of energy as either electromagnetic waves or particles over any given distance. The electromagnetic spectrum encompasses all forms of radiation, from those with the lowest frequency and longest wavelength; radio waves, to the highest and shortest; Gamma rays (γ-rays). Radiation of sufficient energy (>10 electronvolts) is able to transfer energy to electrons within atoms it is travelling

through, exciting them to displacement. Electron loss creates an ionised molecule; this radiation is therefore characterized as Ionising Radiation (IR). Radiotherapy utilises this property to therapeutically target damage. The most prevalent forms of IR utilised are X-rays and γ-rays. The significant difference between X-rays and γ-rays is how they are produced; X-rays are produced by an electric device (extranuclear) whilst γ-rays are produced by decaying radioactive isotopes (intranuclear) (Hall and Giaccia 2012). They are broadly considered, with the same dose, to have the same relative biological effectiveness (RBE) although this is challenged in the literature between high and low X-ray dose rate delivery (Hill 2004). The dose rate determines the amount of time taken to deliver a unit of energy and contributes to RBE differences between IR modalities. High dose rate (HDR) delivers more energy at a time, low dose rate (LDR) less energy at a time. The dose-rate effect is particularly important for brachytherapy where an internal radiation source is used. The research work in this thesis was predominantly performed with X-ray radiation; γ-ray use will be clearly stated otherwise, the dose rate is given for both.

1.1.1 Chemical Damage to DNA from Irradiation

Cellular damage from radiation can occur through cytoplasmic interaction and via the signalling mediated bystander effect; however, the most deleterious damage befalls DNA (Desouky, Ding, and Zhou 2015, Zhou et al. 2009, Morgan 2003). DNA encodes the genetic information required for life through the sequence of four chemically distinct nucleosides attached to a sugar-phosphate backbone, each forming a nucleotide. The nucleotides of this

strand are bound by hydrogen bonds to complementary nucleotides of an antiparallel strand (cytosine to guanine and adenine to thymine) to form the renowned double helix structure. The chemical structure of DNA is susceptible to damage by ionisation, either directly or indirectly. Direct damage occurs when an excited electron interacts immediately with the DNA, whilst indirect damage occurs when an excited electron reacts with an independent molecule to generate a highly reactive free radical, which then interacts with DNA. For x-ray and γ-rays, the indirect effect is dominant and is mostly mediated through free radical production from water molecules (Hall and Giaccia 2012). A variety of DNA lesions can be caused by IR. These include base damage, sugar damage, DNA–DNA crosslinks, single-strand breaks (SSB) and double-strand breaks (DSB).

1.1.2 Double-Strand Breaks

Double-strand breaks are formed when both backbone strands are broken and these are considered the most deleterious form of damage from irradiation. An unrepaired DSB is a critical lesion; if left unrepaired, it will lead to the loss of a chromosome arm at next mitosis (Chapman, Taylor, and Boulton 2012). There is a direct association between the number of unrepaired DSBs and functional cell death in bacteriophage, bacteria and lower eukaryotes. Further, DSB repair-deficient mammalian cell mutants are more radiosensitive than wild-type counterparts (Iliakis 1991). To maintain genome stability, DSB repair pathways have evolved, the fidelity of which are crucial to evading cell death. Lower fidelity repair (misrepair) events range from small junctional deletions to larger deletions and rearrangements via interaction with

other DSBs. Rearrangements are significant aberrations, toxic if unbalanced; they can also lead to the development of additionally derived DSBs through problems encountered during cell cycle progression. These chromosome aberrations include dicentric chromosomes, complex chromatid exchanges, centric rings and acentric fragments. They result in instability of the genome and lead to functional cell death by either checkpoint mediated permanent cell cycle arrest, mitotic catastrophe or controlled apoptosis (Davis and Chen 2013). It is important to note that other forms of DNA damage, aside from DSBs, can also be relevant to cell survival. However, research is strongly weighted to considering the repair of DSBs due to the direct association between DSBs and survival without repair or with misrepair, drawn from the classical cytological observation of large scale aberrations (Cornforth and Bedford 1987, Bedford and Cornforth 1987).

1.2 Curative Radiotherapy

1.2.1 Principals and Clinical Use

Radiation biology is applied clinically to treat cancer through curative radiotherapy. External beam radiation therapy is the most common delivery method and is utilised to treat cancers of the head and neck, breast, cervix, prostate and eye. Fifty per cent of cancer treatment globally is estimated to include radiotherapy treatment (Delaney et al. 2005, Tobias 1996). In order for radiotherapy to be successful, tumour eradication or control must be achieved whilst limiting damage to the surrounding normal healthy tissue. This balance creates a narrow therapeutic window. A substantial focus of research has been

to improve the targeting of the tumour volume as precisely as possible to decrease normal tissue side effects and improve dose delivery to the cancer. The most recent advance is the use of an MRI (Magnetic Resonance Imaging) machine twinned with a radiotherapy machine, the Magnetic Resonance Linear Accelerator (MR Linac), to accurately map, target and deliver dose to the tumour volume in real-time (Lagendijk et al. 2008). However, even with the best targeting, radiation has to pass through surrounding tissue. The most important facet of radiotherapy is, therefore, the relationship between the absorbed dose of radiation and the resulting biological response for both the cancer and the healthy surrounding tissue.

The principal five 'Rs' of radiotherapy describe the characterised factors that modulate the relationship between dose and response: repair, redistribution, reoxygenation, repopulation, and radiosensitivity. Briefly, repair describes the capacity of the cellular mechanisms to repair DNA damage in any given tissue. Redistribution describes the reassortment of cells in response to damage to different phases of the cell cycle, as a result of cell cycle checkpoint activation. Reoxygenation describes the positive relationship between oxygenation state and biological response: the more hypoxic a tumour is, the fewer free radicals can be produced to generate indirect damage from IR (Horsman and Overgaard 2016). Repopulation describes the ability of the tissue to begin growth after damage and replace lost tissue. Radiosensitivity describes the intrinsic difference in sensitivity to radiation between different cell types and is traditionally described by the surviving fraction after a 2 Gy dose, or more recently by response to low dose rate (LDR)

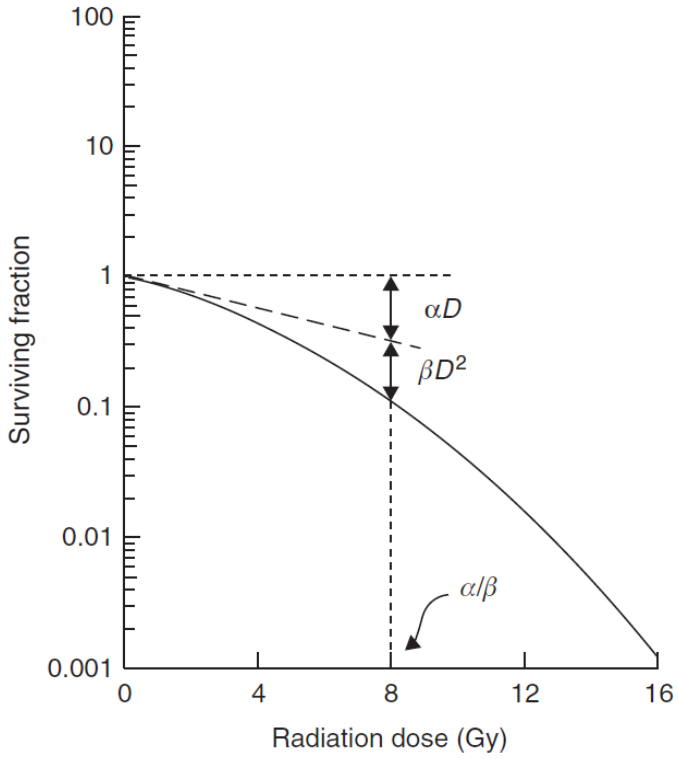

Figure 1.1 The Linear-Quadratic Model

The Linear-Quadratic Model of cell killing. S = e^(-αD-βD^2) where S is survival and D is dose. This example response has α/β ratio of 8Gy. (Adapted with permission from figure 4.5(b), page 34, Basic Clinical Radiobiology, Joiner and Kogel, CRC press, 2019).

radiation as well as more broadly by the parameters of the linear-quadratic model (Joiner and van der Kogel 2019), (McMillan, Peacock, and Steel 1989). For all five factors, radiobiological research looks to leverage any difference between a cancer response and the surrounding healthy tissue response to widen the therapeutic window. The work in this thesis primarily addresses repair, with the focus on determining how repair changes with fractionation of the dose. However, a broader definition of radiosensitivity that includes radiosensitisation across the linear-quadratic response is also touched upon.

1.2.2 The Linear Quadratic model and the *α/β* ratio

Descriptive mathematical models of the relationship between cell survival and dose have been proposed by comparing responses, a significant catalyst being those derived across tissues from small laboratory animals (Withers 1985, Thames et al. 1982). They provide an opportunity to consider the number of factors that could be at play and to test alterations that modify the expected response.

The most widely accepted descriptive model is the Linear-Quadratic (LQ) model that fits the response to a second-order polynomial (Figure 1.1). The curvature of the survival is determined by two components: a linear α and a quadratic β. The simplest mechanistic explanation of these factors is that the α component results from lethal damage arising along one ionisation track, whilst the β component results from the lethal interaction of two separate ionisation track events (Joiner and van der Kogel 2019, Loucas and Cornforth 2013). Supporting evidence for this explanation comes from the LQ fit of an increase of chromosome exchange aberrations with dose (M'Kacher et al. 2014). Additionally, if the temporal placement of ionisation events is sufficiently compressed by increasing the dose-rate (the time period within which a dose is absorbed), the survival curve straightens by flattening down. This reflects reaching a limit at which interaction potential is maximal for every ionisation event and therefore only the α component (the volume of damage) is affecting the dose-response. The α/β ratio is the dose at which the effect on survival of both the α and β component are equivalent. The LQ model is a purely mathematical model and is not without limitation. One notable limitation is the loss of fit at high dose ranges, whereby the measured relationship between

dose and response is more linear than predicted. Further models encompass a greater number of components: the lethal, potentially lethal (LPL) damage model proposed by Curtis (1986) and repair saturation models both integrate mechanistic proposals with mathematics and produce an improved fit to high dose-response. Additionally, the purely mathematical linear-quadratic-cubic (LQC) model, the LQ formulation with an additional term, has an improved fit and approximates well to the LPL model.

1.2.3 Fractionated Radiotherapy

Fractionation describes splitting the total radiation dose to be delivered into a schedule of smaller doses of specified size, separated by defined periods of time. In order to improve the difference between cancer and normal tissue response to IR, either the tumour effect needs to be increased or the side effects on healthy tissue decreased. Fractionation confers the latter by capitalising on a greater capacity for recovery between fractions for normal tissue than the cancer. As a substantial, but worthwhile generalisation, healthy tissue is sensitive to both the total dose and the fraction size (dose-limiting) whilst cancers respond comparatively more strongly to the overall dose and less so to the fraction size. Originally identified in the late 1920s by the successful sterilisation of Ram's testes without damage to the skin of the scrotum (Regaud and Ferroux 1927), fractionation schedules for radiotherapy evolved through clinical 'trial and error' to the establishment of once-daily fractions of 1.8-2.0Gy as optimal for cancer of the head and neck, cervix and skin. Randomised trials in the 1970s-2000s assessed reducing treatment time (accelerated fractionation) and giving multiple <2.0Gy fractions per day

(hyperfractionation) in head and neck and lung cancers (Hall and Giaccia 2012, Bernier, Hall, and Giaccia 2004). We currently have comprehensive guidelines for radiotherapy built upon decades of clinical practice, with careful considerations made for the total dose required to control or eradicate the tumour volume, the size and schedule of individual doses and dose constraints for the surrounding healthy tissue. The Royal College of Radiologists' Third edition of "Radiotherapy Dose Fractionation" contains guidance for 21 cancer types, further split by additional considerations including the staging of the cancer, concurrent treatment with other modalities, post-operative treatment and factoring the risk of recurrence (Hoskin 2019).

1.2.4 Fraction Size Sensitivity

For tissue to be considered fraction size sensitive, fractionation of the total dose over time should confer improved survival in comparison to a single dose. The greater the survival increase when the dose is split, the more fraction size sensitive the tissue is. For fraction size sensitive tissues, fewer chromosome type deletions and asymmetrical exchange aberrations occur with fractionation, directly implicating the fidelity of DNA damage repair to survival (Cornforth and Bedford 1987, Bedford and Cornforth 1987). Fraction size sensitivity can be argued to be an intrinsic property of any given tissue, with a consistent, measurable response under the same experimental conditions (Dasu and Toma-Dasu 2012). The α/β ratios determined for both normal tissue and cancers help to characterize the diversity in response to IR (Thames et al. 1990). Tissues are described as either early-reacting or late-reacting depending on the timeframe that responses to radiation manifest.

Early-reacting tissues, which are generally more proliferative, respond to IR damage in a few hours or days and have higher *α/β* ratios than late-reacting tissues. Late reacting tissues respond to damage months or years later and have lower *α/β* ratios (Withers 1985, Thames et al. 1982). The late-reacting tissues are more fraction size sensitive; their survival is spared more by decreasing the dose per fraction. Squamous carcinomas of the head and neck, skin and lung are the most commonly treated with curative radiotherapy and are fraction size insensitive with high *α/β* ratios, the surrounding healthy tissue is late-reacting with lower *α/β* ratios.

1.2.5 The Reclassification of Breast and Prostate Cancer *α/β*

A significant trigger for the renewed interest in fraction size sensitivity stems from recent clinical studies of the *α/β* ratio in breast and prostate cancer. Both were considered to be relatively insensitive to fraction size and followed standard 2 Gy per day fractionation regimen. However, recent clinical studies have determined that breast and prostate cancer are in fact more fraction size sensitive than previously thought, bringing their response closer to that of the surrounding late-reacting normal tissue dose courses (Fowler 2005, Bentzen et al. 2008). Larger fraction size courses >2 Gy (hypofractionation) are being demonstrated to be just as effective for these cancers without increasing toxicity. Hypofractionated courses are more convenient for the patient as they require fewer treatment sessions (Qi, White, and Li 2011, Catton et al. 2017). Comparatively, fraction sizes <2 Gy (hyperfractionation) bring a benefit to the treatment of head and neck cancers, where the difference between the *α/β* ratios of the cancer and healthy tissue are more substantial (Baujat et al.

2010). Discoveries such as these highlight the lack of a complete clinical understanding to fraction size sensitivity and the potential for improving radiotherapy regimen. There must be factors modulating the heterogeneity in fractionation sensitivity between normal tissues and between cancers.

1.3 DNA DSB repair

A great deal of progress has been made to elucidate the intricate mechanisms of DNA repair pathways. We now know how DNA damage is sensed, have determined the key genetic components of repair pathways and understand to a lesser extent how pathway choice is made (Chapman, Taylor, and Boulton 2012, Goodarzi and Jeggo 2013, Jackson 2002, Saini 2015). The aforementioned association between the sparing of chromosome exchange aberrations and improved survival with fractionation suggests that factors affecting the fidelity of DSB repair, whether by pathway choice or by directly impacting pathway fidelity, may determine fractionation sensitivity. We must, therefore, consider our current understanding of the identification, signalling and repair mechanisms of the primary DSB repair pathway before forming hypotheses.

1.3.1 DNA Damage Signalling

The Mre11/Rad50/Nbs1 (MRN) complex detects DSBs; upon binding, it activates the ataxia telangiectasia mutated (ATM) kinase. ATM phosphorylates histone variant H2AX and the resulting γ-H2AX initiates the assembly of DNA Damage Response proteins (DDR) (Goodarzi and Jeggo 2013). The DSB repair pathway choice is determined by the mediator actions of these DDR

proteins, as well as the nature and severity of the damage and the cell cycle stage. Pertinently, MDC1 binds to γ-H2AX and recruits the ubiquitin ligase RNF8. RNF8 ubiquitylates the linker Histone H1, recruiting RNF168 (Thorslund et al. 2015). RNF168 ubiquitylates histone H2A and this results in the formation of H2AK15Ub which drives further RNF8-dependent H2A ubiquitination. 53BP1 is recruited to damage by H2AK15Ub and histone H4 dimethylation (H4K20me2), which is effected in part by histone methyltransferase MMSET recruitment by MDC1 (Goodarzi and Jeggo 2013, Pei et al. 2011). Figure 1.2 depicts this initial response and assembly.

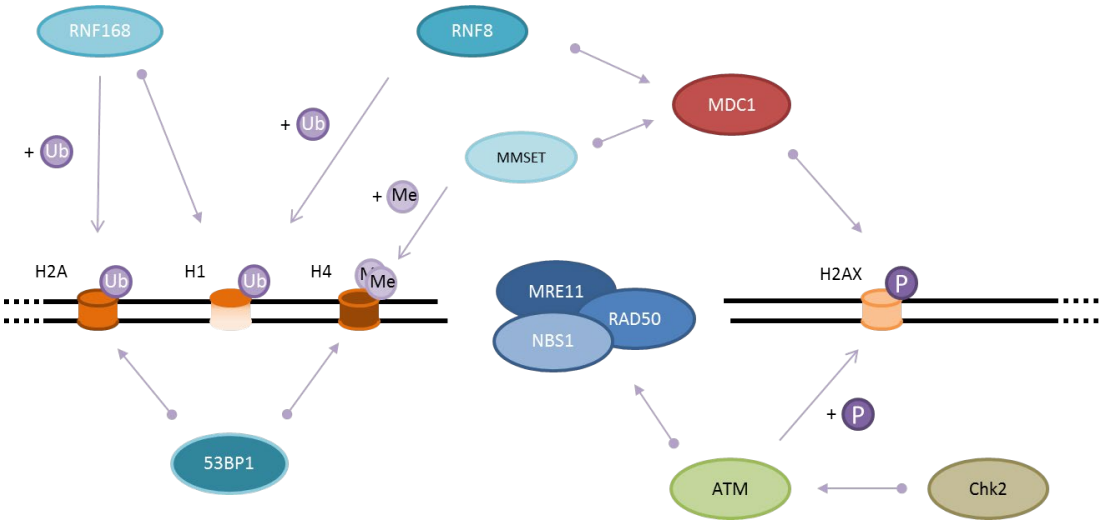

Figure 1.2 The Initial DNA Damage Response.

Schema depicting the initial stages of the DNA damage response. The MRN complex (centre) has identified the DNA DSB ends. Common arrows represent modification events, dot to the arrowhead lines represent recruitment of the protein at the dot end.

53BP1 recruits RIF1 which together inhibit DNA end resection, by facilitating binding by Shieldin, a four subunit protein complex with single-stranded DNA binding affinity (Setiaputra and Durocher 2019). This action

promotes the use of non-homologous end-joining (NHEJ), which can repair breaks without resection or with minor resection whilst impeding resection-dependent homologous recombination (HR) (Fradet-Turcotte et al. 2013). Importantly, DSB detection for NHEJ repair is independent of MRN, occurring via the Ku70/80 heterodimer.

In the late S and G_2 cell cycle phase, BRCA1 expression levels are greater and recruitment to damage is increased. Recruitment of BRCA1 is orchestrated by many proteins, the relative importance of each is as yet unclear; these include MRN, ATM, CDK9 and the BRCA1-A complex (Her et al. 2016, Nepomuceno et al. 2017). BRCA1 and its interacting partner CtIP promote end resection by relieving the 53BP1-Shielin dependent barrier, promoting the use of HR repair (Isono et al. 2017). The regulation of DNA resection arguably is the major mechanism by which repair pathway choice is determined (Panier and Boulton 2013).

Whilst ATM is primarily activated by DSBs, the ATM and Rad-3 related (ATR) kinase responds to a greater spectrum of DNA damage, because it is activated by single-stranded DNA (ssDNA), which is present as an intermediate structure during the processing of multiple forms of damage (Marechal and Zou 2013). It is therefore recruited to DSB damage following resection. Both ATM and ATR are effectors of Chk2 and Chk1, kinases which regulate the control of cell cycle stage checkpoints and therefore cell cycle progression. ATM primarily activates Chk2, affecting the G_1/S checkpoint whilst ATR primarily activates Chk1 (via TOPBP1), affecting the G_2/M phase checkpoint (Smith et al. 2010, Bartek and Lukas 2003). There is significant

crosstalk between the roles of ATM, ATR, Chk1 and Chk2, including the activation of p53 that influence cell cycle arrest, chromatin remodelling, DNA repair, transcription and cell fate.

Two further but less well understood signalling mechanisms are the bystander effect and induced radioresistance or adaptive response (AR). The bystander effect describes when un-irradiated cells proximal to irradiated cells exhibit effects of IR, including cell death. *In vitro* experiments have demonstrated that substituting the media of un-irradiated cells with the media from irradiated cells can result in cell death, suggesting the involvement of secreted signalling factors (Najafi et al. 2014, Matsumoto, Takahashi, and Ohnishi 2004). AR describes how a small radiation dose (generally <1 Gy) can increase radioresistance to a following higher dose (>1 Gy). One mechanistic proposal is the generation of reactive oxygen species (ROS) resulting in small scale DNA damage that may prime signalling (Wolff 1998, Bonner 2003).

1.3.2 Non-Homologous End-Joining

NHEJ is the predominant DSB repair mechanism in eukaryotic organisms and functions throughout the cell cycle (Burma, Chen, and Chen 2006). DSB ends are detected and bound by the Ku70/80 heterodimer which has a strong affinity across DNA double-stranded end structures. Ku70/80 forms a ring structure around the double-stranded DNA ends, forming contacts with the DNA backbone (Neal and Meek 2011). This structure recruits DNA-dependent protein kinase catalytic subunit (DNA-PKcs) forming the DNA-PK complex with Ku70/80 and the double-stranded DNA ends. DNA-PK forms a

bridge between the broken ends, which may aid structural support and alignment, whilst preventing degradation and misrepair (Pawelczak, Bennett, and Turchi 2011). DNA-PKcs has a number of phosphorylation substrates, including many proteins involved in NHEJ; however, only autophosphorylation is required for successful NHEJ (Neal and Meek 2011). Different autophosphorylation sites determine the accessibility of the broken ends, either permitting end-processing by polymerases/nucleases or protecting the ends from processing (Neal and Meek 2011).

In order for polymerisation and ligation of the DSB DNA ends to occur, the ends must have the requisite 5' phosphate and 3'OH ends (Goodarzi and Jeggo 2013). The majority of DSBs result in single-stranded overhang structures that require processing. The action and use of the nucleases (Artemis and polynucleotide kinase phosphatase (PNKP)) and polymerases (Pol λ, Pol μ and terminal deoxynucleotidyl transferase (Tdt)) depend on the extent and nature of the overhanging ssDNA at the damaged ends. NHEJ is able to utilise micro-homology mediated end-joining (MMEJ), using resection and small microhomology sequences (5-25 nucleotides) to process ends. This results in small deletions discussed later. Following appropriate processing, the ends are then able to be ligated by the DNA Ligase IV complex (Goodarzi and Jeggo 2013, Davis and Chen 2013). This complex contains the enzyme LigIV and X-ray repair cross-complementing protein 4 (XRCC4) in a ratio of 1:2. The XRCC4 is understood to increase the stability of LigIV and is suggested to form a bridge between broken DNA ends (Neal and Meek 2011). Further, recent studies have suggested that XRCC4 and XRCC4-like factor

(XLF), could form a stabilising filament sheath around the DSB (Mahaney et al. 2013, Roy, de Melo, Xu, Tadi, Négrel, et al. 2015, Brouwer et al. 2016). NHEJ is a very efficient form of repair, but the lack of a template to guide repair, predisposes a potential for misrejoining of incorrect break ends, leading to translocations or other large-scale rearrangements (Iliakis, Murmann, and Soni 2015). In humans, NHEJ is the primary pathway for the formation of translocations (Ghezraoui et al. 2014). Additionally, the processing of break ends prior to ligation can result in small deletions or insertions (Rodgers and McVey 2016). For these reasons, NHEJ has been conventionally described as error-prone and intrinsically mutagenic. However, some argue that the accuracy of NHEJ repair is determined more by DSB end-structure than mechanistic failures (Bétermier, Bertrand, and Lopez 2014). Finally, recent work has suggested that at actively transcribed genes, NHEJ is able to make use of nascent RNA as a template for increased accuracy of repair (Chakraborty et al. 2016). Figure 1.3 summarises the steps of NHEJ.

1.3.3 Homologous Recombination

HR requires a template for repair. Ideally, this is a sister chromatid and HR is therefore restricted to the S-G_2 phases of the cell cycle. Following break detection by the MRN complex and formation of the DDR proteins, as previously described, BRCA1 relieves the 53BP1 mediated Shieldin barrier to resection and ATM recruits the CtIP endonuclease, which works together with other nucleases such as EXO1 and EXD2 to initiate 5' to 3' resection (Isono et al. 2017). Replication protein A (RPA) coats resected ssDNA and BRCA2 acts

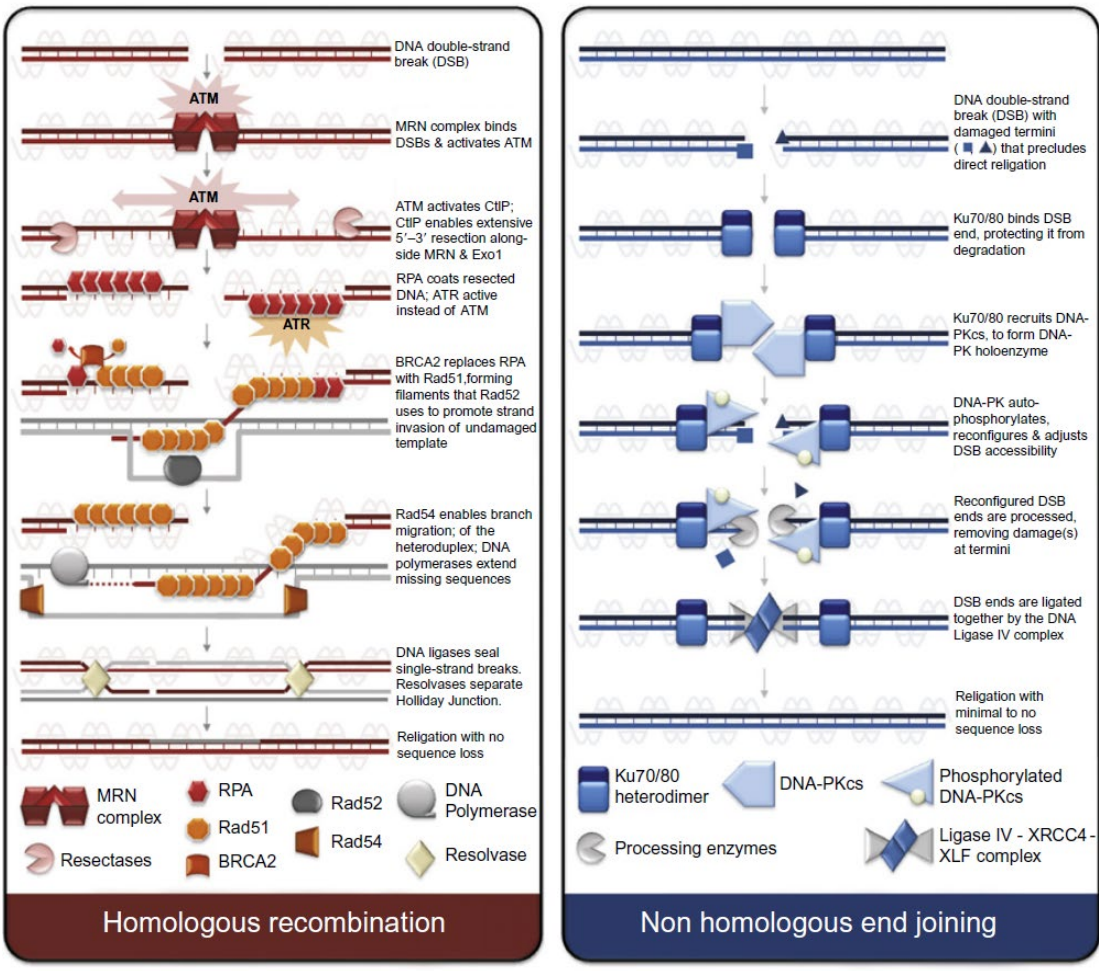

Figure 1.3 Homologous recombination and non-homologous end joining DSB repair pathways.

Illustration of the homologous recombination and canonical non-homologous end joining pathways. Both include the core genetic factors and commonly defined steps. Reprinted and minimally adapted from Goodarzi and Jeggo (2013) with permission from Elsevier.

as a mediator replacing RPA with Rad51, forming filaments; this completes the pre-synaptic stage (Jasin and Rothstein 2013). PALB2 (partner and localizer of BRCA2) interacts with BRCA1 to recruit BRCA2 to DSBs (Buisson and Masson 2012). The Rad51–ssDNA filament formed stretches the ssDNA, allowing for fast and efficient homology searching. Cohesin acts to keep sister chromatids in close proximity whilst Rad54 facilitates strand invasion between

the invading DNA substrate and homologous duplex DNA template (D-loop formation); this stage is termed synapsis (Litwin, Pilarczyk, and Wysocki 2018, Mazin et al. 2010). Post-synapsis Rad51 dissociates from dsDNA to expose the 3′-OH, permitting DNA synthesis (Krejci et al. 2012). Finally, ligases seal the single-strand breaks and the Holliday junction structure formed is resolved by either a resolvase or dissolved by the combined action of BLM DNA helicase with the type I topoisomerase TOPOIIIa (Li and Heyer 2008). In addition to these essential components of HR repair, 5 additional proteins, the Rad51 paralogs (RAD51B, RAD51C, RAD51D, XRCC2 and XRCC3), are essential to signal effector kinases and promote break repair (Suwaki, Klare, and Tarsounas 2011). An additional role of HR is the recovery of stalled replication forks, essential for cell proliferation (Willis et al. 2014). HR is also able to repair free DSB ends that arise from telomere erosion or replication fork collapse by strand invasion into homologous DNA followed by replication to the chromosome end (Llorente, Smith, and Symington 2008). Due to the use of homology guided repair, HR has a greater fidelity than NHEJ (Mao et al. 2008). Figure 1.3 summarises the steps of HR.

1.3.4 Micro-Homology Mediated End-Joining

MMEJ describes the rejoining of DSBs using small microhomology sequences (5-25 nucleotides), resulting in small deletions. Alt-NHEJ is one form of MMEJ and is a back-up pathway that can occur when progression through canonical NHEJ (c-NHEJ) is compromised, for example through the absence of a core c-NHEJ factor (Mansour, Rhein, and Dahm-Daphi 2010). Alt-NHEJ exploits microhomology and has been considered synonymous with

MMEJ. However, as explained previously, c-NHEJ can also exploit microhomology and alt-NHEJ is a distinct pathway with different genetic requirements. Recent studies have shown that Alt-NHEJ rarely occurs in human cells (only when Ku or 53BP1, which impacts pathway choice by preventing resection, are absent) and that most MMEJ in human cells occurs using resection-mediated c-NHEJ, requiring the Artemis nuclease (Ghezraoui et al. 2014, Löbrich and Jeggo 2017). This resection-mediated repair has been suggested to enhance the potential for translocation (Barton et al. 2014). Finally, the initial resection mechanism has been shown to be shared between resection-mediated c-NHEJ and HR (Truong et al. 2013). For these reasons, it is important to consider any repercussions to MMEJ pathway choice and repair fidelity from alterations to HR and c-NHEJ mechanisms.

1.3.5 Biphasic Kinetics of DSB Repair

Throughout the cell cycle in healthy cells, DSB repair occurs with biphasic kinetics, with a fast and a slow component (Figure 1.4) (Shibata et al. 2011, Wang et al. 2001). The fast process corresponds predominantly to c-NHEJ repair but the slow process occurs by different resection-mediated repair pathways depending on the cell cycle stage. In G_1, deficiencies in either Artemis or ATM signalling impact primarily on the slow component of repair and result in increased radiosensitivity, suggesting resection mediated NHEJ use (Goodarzi and Jeggo 2012, Martin et al. 2013, Riballo et al. 2004). In G_2, greater resection occurs due to the activity of CtIP; the use of HR predominates in the slow process (Löbrich and Jeggo 2017, Beucher et al. 2009).

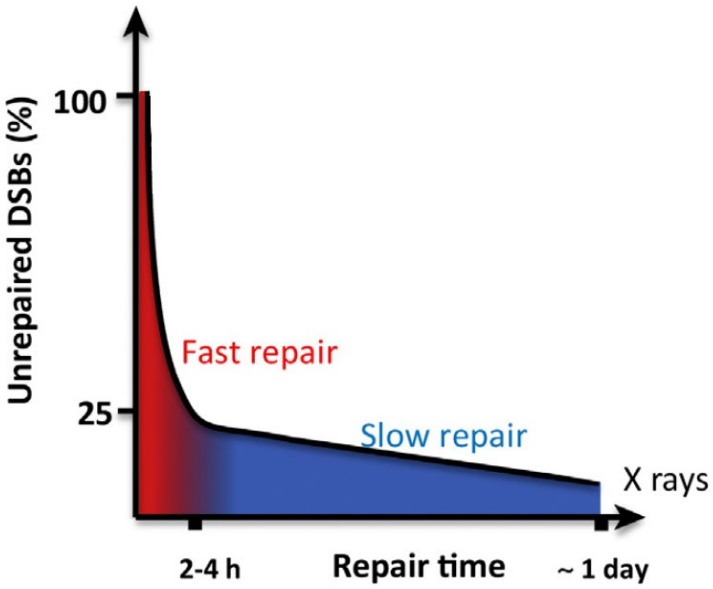

Figure 1.4 Biphasic kinetics of DSB repair.

Schema of DSB repair following X-ray irradiation (adapted from Löbrich and Jeggo (2017) under Creative Commons Attribution License (CC BY)). Red indicates period of fast repair, blue slow repair. In both G_1 and S/G_2 fast repair occurs via c-NHEJ. Slow repair occurs in both phases via resection mediated repair: HR in G_2/s and resection mediated NHEJ in G_1.

1.4 Investigating the Molecular Mechanisms of Fraction Size Sensitivity

Returning to the major question this thesis examines: what molecular mechanisms determine fraction size sensitivity? Now that a clinical and molecular background has been introduced, we can address unanswered questions that inhibit our ability to determine mechanistic insight and form hypotheses for testing. A mechanistic understanding of fraction size sensitivity is missing both across the heterogeneous responses of normal tissue and cancer types. The research presented in this thesis focuses on assessing normal tissue response. The intention is to target investigations to determine mechanistic insight in a normal model first, with the ability to then identify the altered regulation in cancer. However, in order to form hypotheses, the cancer

response both across cancer types and to matched normal tissue are considered. Below, we outline models that are relevant to the work carried out in this thesis. Broadly, they hypothesise that fraction size sensitivity is derived from the DSB repair response fidelity, thereby determining the extent of genome instability.

1.4.1 Cell Cycle Stage

The cell cycle stage determines the availability of DSB repair mechanisms and therefore impacts pathway choice (Figure 1.5). There is a strong inverse association between tissues with high-proliferative indices and fractionation sensitivity both for normal tissues and across cancers (Figure 1.6) (Somaiah, Rothkamm, and Yarnold 2015). Higher proliferation indices result in more cells in the S/G_2 cell cycle phase. It is therefore postulated that the increased availability of high fidelity HR repair results in an inverse association with fraction size sensitivity (Somaiah et al. 2013). It has been proposed that this is because HR facilitates higher-fidelity repair in the G_2 phase compared to resection-dependent NHEJ in G_1, resulting in a decrease in genome rearrangements (Somaiah et al. 2013). We hypothesise a significant decrease in the sparing effect of fractionation when lesions are repaired within G_2 compared to repair carried out during G_1. It has previously been demonstrated that misrepair damage can occur in G_2 from the formation of chromatid-type aberrations on one chromatid arm and that translocations occur in all cell cycle phases (Roukos et al. 2013, Revell 1974); it is, therefore, likely that c-NHEJ repair in G_2 would still result in misrepair translocations. The relative repair contribution of HR and c-NHEJ is therefore critical to the expected effect on

fraction size sensitivity.

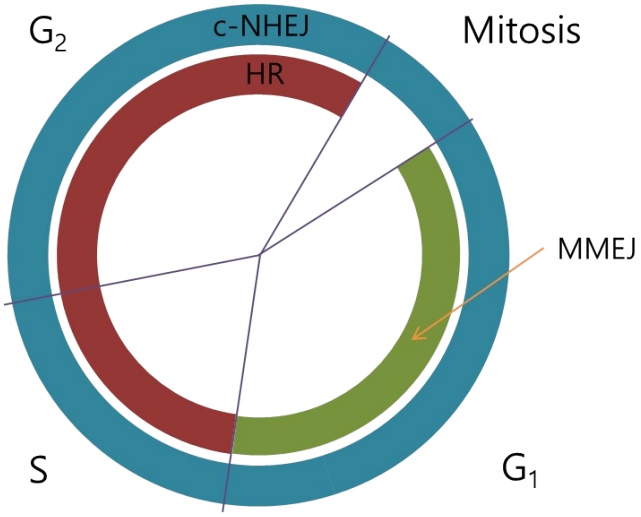

Figure 1.5 Cell cycle stage repair pathway specificity.

Schematic of the cell cycle demonstrating the DSB repair mechanisms available in each phase. DSB repair occurs with biphasic kinetics: the outer ring represents the fast repair process, whilst the inner ring represents the resection dependent slow processes of repair.

The basal epidermis is an early-reacting normal tissue with high proliferation indices. Biopsies across a 5-week course of breast radiotherapy demonstrated an arrest in G_2 following the first dose that continued throughout the duration of radiotherapy (Somaiah et al. 2012). This suggests that high-proliferative indices may also pre-dispose cells to a greater percentage of G_2 arrest, allowing more time for the relatively slow process of HR repair. A further study, performed in CHO cells, compared an HR-defective cell line that remained equally sensitive to fractionation despite G_2/S arrest with an NHEJ defective cell line which was fraction size insensitive (Somaiah et al. 2013). Rodent cells have significantly less Ku than human ones; additionally, translocations in rodent cells arise predominantly from alternative end-joining

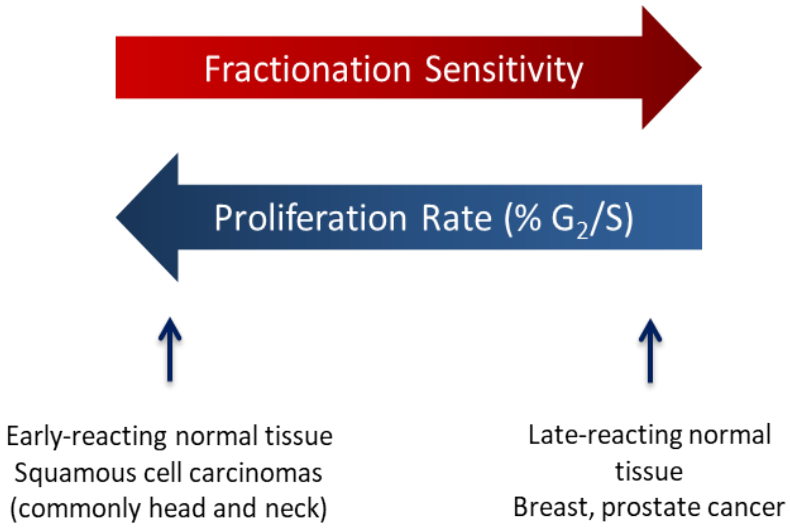

Figure 1.6 Inverse association between fractionation sensitivity and proliferation rate.

Schema demonstrating the inverse association between proliferation rate and fractionation sensitivity in both normal tissues and cancer. An increased rate of proliferation results in an increased proportion of cells in G_2/S phase.

rather than from NHEJ (Lorenzini et al. 2009, Ghezraoui et al. 2014). Despite these caveats, both studies could be interpreted to demonstrate either the reliance on NHEJ to fraction size sensitivity or HR to fractionation insensitivity (Somaiah et al. 2013). Together, these studies also highlight the importance of considering how cell cycle checkpoint activation could affect fractionation sensitivity.

The delayed plating effect, whereby cell survival is reduced if cells are seeded at low density immediately after irradiation when compared with a delay of a few hours before seeding, is believed to occur from effects of cell cycle progression in the presence of incomplete repair. This effect even occurs in cell cycle checkpoint proficient cells, where the signals to proliferate from immediate re-plating seemingly override checkpoint controls (Borgmann et al.

2004, Marchese, Zaider, and Hall 1987). Differences in cell cycle checkpoint stringency could, therefore, impact the fidelity of repair and subsequently fractionation sensitivity. From comparing classical cytogenetic aberration analysis to clonogenic survival in a normal fibroblast cell line, Borgmann et al. (2004) suggest that permanent G_1 arrest (where chromosome damage could not be seen) accounted for up to 50% of the lethal events. Further, in a p53-deficient LiFraumeni cell line, this contribution was lost; suggesting that small scale damage not visible at the cytogenetic level activates the G_1/S checkpoint in the normal cells, preventing progression through the cell cycle and development into visible chromosome aberrations. Therefore, in order to investigate the hypothesis that HR repair underlies fractionation insensitivity, we must be sure to control for the confounding variable of cell cycle progression.

1.4.2 Kinetics of DSB Repair

We understand the kinetics of DSB repair primarily through the formation and disappearance of irradiation-induced foci (IRIF) visualised by fluorescent labelling of repair proteins over time. The phosphorylation of the H2A-histone protein variant, H2AX, is a prime example. ATM/ATR/DNA-PKcs phosphorylates H2AX flanking DSB sites to produce γ-H2AX. γ-H2AX recruits DDR factors to amplify signalling (Jackson and Bartek 2009). A further method is the use of pulsed-field gel electrophoresis (PFGE) studies by studying the length of DNA fragments as DSBs are repaired (Löbrich et al. 2000).

Surprisingly, there has been very little work done to examine the kinetics

of repair following fractionated radiation using either PFGE or IRIF. A study by Mariotti et al. (2013) attempts to assess whether DSB induction or repair kinetics of γ-H2AX and 53BP1 foci is altered between the first and second fractionated dose. This is performed whilst altering the time between the doses and altering the amount of un-repaired damage interaction with the second dose. With a decreasing time between doses, they suggest that the kinetics of IRIF are slowed, both in induction and clearance. They do not reach a clear conclusion on whether the number of foci induced by a second dose was increased or decreased.

Understanding the kinetics of DSB repair following a fractionated dose would be enlightening to formulate appropriate hypotheses. For example, a decrease in the speed of formation and/or clearance of IRIF when the repair time between doses is decreased could indicate a limiting factor. As the level of damage requiring repair is increased above a threshold level, the limiting repair factor would delay efficient repair, potentially leading to the use of a lower fidelity pathway. Contrastingly, with the understanding that slow repair is believed to represent resection-mediated repair by HR or resection-mediated c-NHEJ, if we hypothesise that HR use in G_2 improves repair fidelity, we may expect to see an increase in the proportion of damage repaired in the slow component for G_2 cells for fraction size insensitive tissues. Finally, the extent to which repair is completed regardless of fidelity for single and fractionated doses has never been answered. The literature strongly suggests that misrepair is the crucial component determining survival, but any difference in the level of unrepaired breaks (a critical lesion) between a single and

fractionated dose course would require this to be reassessed.

1.4.3 The Chromatin Environment

DNA is packaged around histone octamers to form nucleosomes, which are in turn associated with linker histones. Further compaction via coiling creates higher-order chromatin structures. These structures are controlled by histone post-translational modifications, histone variants, and the activity of chromatin remodelling complexes. Compaction acts as a barrier to transcription and the genome is broadly organised into two domains; the more open and active euchromatic regions and more compact, inactive, heterochromatic regions.

The localisation of the DSBs within the chromatin architecture affects accessibility and repair pathway choice (Chiolo et al. 2013). Euchromatic domains are more sensitive to damage induction than heterochromatic domains; however repair within euchromatin is more efficient, most likely due to improved accessibility for repair machinery, notably c-NHEJ (Falk, Lukasova, and Kozubek 2008, 2010, Storch et al. 2010, Takata et al. 2013). Higher-order chromatin organisation also determines the spatial potential for DNA interaction. The more relaxed state of euchromatin is considered to increase the potential for misrepair by the joining of incorrect DSB ends.

Within euchromatin, actively transcribed genes are suggested to be particularly vulnerable regions to DSB misrepair (Osborne 2014). In particular, transcription factories could be especially vulnerable to misrepair due to the increased locality of DNA brought from different regions (Osborne 2014).

There is evidence to suggest from chromatin immunoprecipitation-sequencing (ChIP-seq) analysis that the more transcriptionally active a euchromatic region is, the greater the use of HR repair and that this preference occurs through an H3K36me3 histone mark dependent mechanism (Aymard et al. 2014). As heterochromatin is rich in H3K36me3, it is possible this mechanism could also promote HR use in heterochromatin (Aymard et al. 2014). Damage in heterochromatic regions has been demonstrated to require longer repair times than in euchromatin and suggested to represent HR use with a requirement for 53BP1 (Lorat et al. 2012, Watts 2016, Goodarzi, Jeggo, and Lobrich 2010, Kakarougkas et al. 2013). Heterochromatic regions contain repetitive regions whereby HR is potentially required to ensure repair fidelity. There is contrasting evidence in a Drosophila DSB reporter system that suggests HR and NHEJ frequency of use is the same in euchromatin and heterochromatin respectively (Janssen et al. 2016).

In response to a local DSB, transcription is rapidly repressed in cis (Shanbhag et al. 2010). This silencing is ATM dependent and requires the PBAF chromatin remodelling complex (Kakarougkas et al. 2014, Venkata Narayanan et al. 2017). The reason behind this damage-induced transcriptional repression (DITR) response has not been determined. It could be a protective measure to preclude further sensitivity to damage or to remove the transcription machinery impeding repair. Alternatively, the response may have evolved to prevent further indirect damage arising from transcription failure or aberrant transcriptional control resulting from damage. Meisenberg et al. (2019) demonstrate that when the DITR pathway is defective, an increase

in translocations occurs, indicating that the response prevents genome instability.

Although there are many shared traits to chromatin architecture, the chromatin environment can be substantially different between cell lines, as well as the response to damage (Zhu et al. 2013, Bolzer et al. 2005). It seems reasonable to consider that the chromatin environment and its response to damage could impact fractionation sensitivity by altering the potential for damage interaction, repair pathway choice and repair fidelity.

It is possible that alterations to the chromatin environment between fractionated doses could modulate fractionation sensitivity. One possibility is that after the first fraction, the DITR response could decrease the potential for misrepair by reducing the interaction potential of damage. Alternatively, the potential for derived damage through transcriptional failure may be lessened after the first fraction. Fraction size sensitive tissues might, therefore, have a strong DITR response. If the DITR response was defective or impaired, we would expect fractionation sensitivity to decrease.

1.4.4 Identifying the DNA misrepair events spared by Fractionation

Large scale genome rearrangement occurring from DSBs remains the focus of investigations into x-ray associated irradiation repair as the most deleterious consequence of irradiation. However, other forms of damage may also be influential, leading to misrepair events such as base changes, small insertions and deletions that are not identifiable using classic cytological approaches. Our understanding of misrepair of damage at this level across the

genome was, until recently, drawn from model organism work and deep sequencing of specific regions of interest in human cells. The use of next-generation whole-genome sequencing approaches is beginning to yield significant insights into the complete mutation signature associated with exposure to ionising radiation. Behjati et al. (2016) sequenced the genome of 12 radiation-associated secondary malignancies and found two common signatures: small scale deletions and balanced inversions. These were clonal samples and the signature will, therefore, encompass the confounding effects of cancer evolution. Adewoye et al. (2015) sequenced whole murine genomes of offspring irradiated whilst in the germline. This approach also results in selection prior to analysis. They demonstrated a significantly increased frequency of small-scale insertions/deletions and an altered spectrum of single-nucleotide variants in the offspring of exposed fathers. Kucab et al. (2019) present the most complete mutational signature for irradiation, on a whole-genome level in normal human cells. Their study of pluripotent stem cells demonstrates microhomology-mediated deletions as well as insertions, but no increase in substitutions. Large scale translocations were not found in their analysis. Stem cells have very stringent DNA damage control to ensure mutations do not occur to prevent catastrophic consequences to differentiated tissue. They are particularly prone to apoptosis when damage reaches a threshold, which has been shown to be lower than that of differentiated cells (Biechonski et al. 2018). It is possible, therefore, that large scale rearrangements were missed due to the isogenic methodology used, whereby only the cells able to proliferate following irradiation are analysed. It is clear that we do not yet have a complete picture of radiation induced mutational

signatures.

In addition to generating a more complete mutational signature for single radiation doses, it would be extremely beneficial to determine the complete subset of misrepair damage spared with a fractionated dose course. If the proportion of translocations is shown to decrease the most substantially with fractionation, then we would be able to more definitively narrow the focus of research to factors that influence the interaction of break ends and faithful end repair.

1.4.5 Limiting Factors to Fidelity of Repair

DNA repair pathways are dependent on having sufficient proteins to facilitate optimum identification, signalling and repair. In normal tissues, proteins of the DNA damage response and repair are abundant or rapidly upregulated (Craxton et al. 2015). This stems in part from the understanding that repair kinetics - and therefore efficiency - remains constant with increasing dose (Lobrich et al. 2000). Additionally, the most common proteins for DNA damage foci analysis, including γ-H2AX, 53BP1 and Rad51 demonstrate recruitment for a range of doses in repair proficient cells (Polo and Jackson 2011, Fernandez-Capetillo, Celeste, and Nussenzweig 2003). Crucially, while the kinetics of repair may remain constant, the fidelity of repair does not, resulting in the linear-quadratic increase in misrepair aberrations that inversely associate with survival. For large X-ray doses between 80-320Gy, Lobrich et al. (2000) demonstrate that the relative level of misrepair remains constant. When considered together, it raises the possibility that a threshold number of

DSBs could result in a signalling or repair component to become limiting to the fidelity of repair, if it was insufficiently abundant. This limitation could then be spared by splitting doses in time via fractionation. This hypothesis would also fit with the lack of fractionation sensitivity or improved survival seen when small overall doses are split, as this would be explained by sufficient protein abundance below a threshold of damage. It is important to consider that this limitation may not be of a protein, but rather the post-translational regulation of existing proteins (Tkach et al. 2012). A limiting factor has also been suggested in a dose-response modelling context by the repair saturation models, whereby the shoulder on cell survival curves is explained by reduced effectiveness of repair at higher doses (Joiner and van der Kogel 2019).

There is evidence in the literature for candidate- limiting factors. 53BP1 and its upstream recruitment to damage by RNF168 have been demonstrated to be potentially limiting to the fidelity of repair. Reduction of 53BP1 leads to hyper-resection and lower fidelity pathway choice by resection mediated NHEJ (Ochs et al. 2016, Bakr et al. 2016). Furthermore, Gudjonsson et al. (2012) show that the abundance of RNF168 is limiting to the recruitment of 53BP1. By knocking down TRIP12 and UBR5, ubiquitin ligases that regulate the abundance of RNF168, they increase the abundance of RNF168 and demonstrate an increase in the dose tolerated before a limitation in 53BP1 recruitment. These results also suggest the possibility that further proteins in this pathway, such as the abundance of ubiquitin and H1, could be rate-limiting.

Another possibility could be a limitation in complex formation between 2

or more proteins because of altered stoichiometry. XRCC4 forms a complex with Ligase IV to facilitate DNA binding for ligation in NHEJ. XRCC4 has been demonstrated to additionally interact with XLF, another NHEJ associated repair factor of similar structure, to form a filament sheath. This XRCC4/XLF sheath is suggested to be able to form rapidly, holding broken DNA ends together to facilitate repair (Brouwer et al. 2016, Mahaney et al. 2013, Roy, de Melo, Xu, Tadi, Negrel, et al. 2015). XLF is not required for NHEJ to function; however, if the formation of these filaments were to improve repair fidelity, a limitation of XLF in the formation of the sheath could be spared with fractionation. Whilst XLF abundance has not been experimentally tested, it is possibly an example of how non-critical factors influencing fidelity could impact fractionation sensitivity.

If the abundance of a repair factor is limiting, we would predict that its recruitment to chromatin with an increasing dose would plateau at a threshold dose. This prediction could also be made for limiting modifications of a repair factor. By manipulating the abundance of this factor or modification, we would also expect to be able to alter fractionation sensitivity.

1.4.6 Potential for Clinical Benefit

The aim of the research presented in this thesis is to increase our understanding of the mechanistic control of fraction size sensitivity, also referred to more simply as ‘fractionation sensitivity’ in the text. In the following chapters, we choose to undertake this in a human, normal late-responding and fraction size sensitive model. If we can identify the mechanisms that determine

fractionation sensitivity in normal cells, we will be able to apply this to understanding the responses seen across cancers. Determining the mechanistic basis of fractionation sensitivity could aid biomarker discovery to help reclassify the sensitivity status of cancers, as seen with the re-classification of breast and prostate cancer. If identified, biomarkers could also be utilised to stratify patients when response heterogeneity is observed for the same cancer type, to move away from a one size fits all approach to radiotherapy. Finally, defining drug targets that would increase the therapeutic window in fractionation sensitivity between healthy tissue and cancer would improve radiotherapy outcomes.

1.5 Aims & Hypotheses

1. Elucidate the contribution of the cell cycle stage that repair occurs within to fractionation sensitivity.

   Hypothesis: The use of the higher fidelity HR DSB repair pathway in S/G_2 phase decreases the incidence and interaction of misrepair, decreasing fraction size sensitivity.

2. Determine whether the kinetics of repair remain constant with dose fractionation.

   Hypothesis: Altered repair kinetics (induction or clearance) between fractions could indicate an adaptive response to damage from the first dose, decreasing the formation of misrepair.

3. Investigate the contribution of the chromatin environment to

fractionation sensitivity.

Hypothesis: Chromatin remodelling in response to a first fraction could alter either the accessibility of repair proteins and therefore pathway choice or the sensitivity of DNA to damage, both resulting in less misrepair.

4. Define a mutational signature of irradiation and determine whether this is altered by fractionation of the dose.

   Hypothesis: The mutational signature of fractionated dose courses will help determine the type and/or the location of the damage spared by fractionation.

5. Investigate whether there are limiting factors to the fidelity of repair that modulate fractionation sensitivity.

   Hypothesis: If the abundance of a protein becomes limiting to either repair pathway choice or directly to the fidelity of repair this would result in greater misrepair. This limitation could be spared by splitting the radiation doses in time, underlying fraction size sensitivity.

2 Materials & Methods

2.1 Materials

2.1.1 Plasmid

Cas9 Nickase (Cas9n) plasmid with mRuby was kindly gifted by Jon Pines' laboratory (3613 px466 2 x gRNA + Cas9 D10A T2A Ruby 2).

2.1.2 sgRNA and Primers

Two out of eighteen isoform transcripts of BRG1 begin at Exon 2 with the rest beginning at Exon1 of SMARCA4 as determined from the UCSC Genome Browser (Kent et al. 2002) (Figure 2.1). Therefore, guides were designed targeted to Exon 2 using the Atumbio CRISPR sgRNA Design tool

SMARCA4 Exon 2

UCSC Genome Browser location 5' – 3' >hg19_dna range=chr19:11093583-11095823 5'pad=0 3'pad=0 strand=+ repeatMasking=none

GTCCTGTTCTTTCTGTTAGGAAGATAAGCAAGTGGAGAGCAGTGTGAAGGGTAGACCAGCACCCCCTGAGACACCCTCTG
CCGTGATCAGGAATATGGCAGGAGCCCCTGAAGGCCCCTGTGGGGCAGTGCTTGTCTGTGAGCGTGGCCCACCCCTTCC
TGGGTAGACTGACTGATCTTGTGTGCCTGAGATGTAGGACTTCCTCTGAGAGTGATCATGGAGAAACGGTTTGGGTGGCT
GGTGGGGAAGGTACTGGCTTCCTGTGGGATGTAGATTCTGATGTGACCGTATGATTGTCCCTTGCTATCCCTGTCCTGCCT
CGCCCTTGGTCATGAACCCCAGACTGACCAGGACTGTCTTCCAGCAGGAG**GCCACTGTCTGCAGCTCCCGTG^AAGATG**
TCCACTCCAGACCCACCCCTG$_{v}$GGCGGAACTCCTCGGCCAGGTCCTTCCCCGGGCCCTGGCCCTTCCCCTGGAGCCAT
GCTGGGCCCTAGCCCGGGTCCCTCGCCGGGCTCCGCCCACAGCATGATGGGGCCCAGCCCAGGGCCGCCCTCAGCAG
GACACCCCATCCCCACCCAGGGGCCTGGAGGGTACCCTCAGGACAACATGCACCAGATGCACAAGGTAGGGATCCCTG
TGCCCGCCTCGCACCTGCGGCCTCTGCCCACTAGGGCTGCAGGCAGCCTCTGGACCGAGGGCCTTACTTGGAGGATGG
GGGGAAGCCTTCTTGTTGGAGGTGTCCTGCCTTGGCTCAGCCCCCTACCCCAGGGCCCACGGCCATGAACAGAAGGTTC
AGCTCGTCAGACCCCAGCCTGTGCTGGCGCATGATCTGGGCCCCGCGGGCACCTGCCCCACCGTTTCCCGCTCCCTTGC
TTTCTGCATGTGAAATTTGGGAATATCACTACAAAGTTTTCTTTTGGTAATGAAGAAAAACATCCAAATTCCTAAAAAGGCTTT

Figure 2.1 Genome region encompassing Exon 2 of SMARCA4.

Exon 2 in bold. sgRNA target sequences highlighted in yellow with $_{v}$ indicating sense nickase cut site and ^ antisense cut site. Primer sequences highlighted in green.

sgRNA	Insertion Sequence	Target Sequence
sgSMARCA4_ex2_1.1	accgCTGGGCGGAACTCCTCGGCC	CTGGGCGGAACTCCTCGGCC
sgSMARCA4_ex2_1.2	aaacGGCCGAGGAGTTCCGCCCAG	
sgSMARCA4_ex2_1.3	accgTCTGGAGTGGACATCTTCAC	TCTGGAGTGGACATCTTCAC
sgSMARCA4_ex2_1.4	aaacGTGAAGATGTCCACTCCAGA	

Figure 2.2 Two pairs of sgRNA guides used to guide Cas9n to SMARCA4 Exon 2.

accg and aac overhangs allow for cloning into plasmid.

and were cloned into the Cas9n plasmid. These steps along with primer design were performed by Federica Schiavoni (Downs' Laboratory).

Direction	Sequence 5' – 3'	Melting Point
Forward	GGCTTCCTGTGGGATGTAGA	58.3C
Reverse	ATCCTCCAAGTAAGGCCCTC	58.3C

Figure 2.3 Primers encompassing the sgRNA target region on SMARCA4 Exon 2.

2.1.3 Antibodies

Antibody	Dilution (Use)	Host	Source (Catalogue Number)
αTubulin	1/10000 (WB)	Mouse	Abcam (ab7291)
53BP1	1/100 (IF)	Rabbit	Abcam (175933)
BRG1 (G-7)	1/500 (WB)	Mouse	Santa Cruz (sc-28383)
H3	1/1000 (WB)	Rabbit	Abcam (ab1791)
H3 acetyl K9 + K14 + K18 + K23 + K27	1/500 (WB)	Rabbit	Abcam (ab47915)
H3K56ac	1/2500 (WB)	Rabbit	Active Motif (39281)
H3K9ac	1/10000 (WB)	Rabbit	Abcam (ab4441)
γH2AX (JBW301)	1/600 (IF)	Mouse	Millipore (05-636)
Anti-Rabbit HRP	1/5000 (WB)	Goat	Agilent (P044801-2)
Anti-Mouse HRP	1/5000 (WB)	Rabbit	Agilent (P026002-2)
Anti-Mouse FITC	1/300 (IF)	Goat	Sigma (F0257)
Anti-Rabbit Cy3	1/300 (IF)	Sheep	Sigma (C2036)
Anti-Mouse Alexa 488	1/2000 (IF)	Goat	Invitrogen (A-11001)
Anti-Rabbit Alexa 568	1/1000 (IF)	Goat	Invitrogen (A-11011)

Figure 2.4 Antibodies used in this research.

WB indicates dilution for western blot, IF indicates dilution for immunofluorescence.

2.1.4 Chemicals, DNA dyes and FISH probes.

Chemical	Source (Catalogue Number)
Calyculin A	Abcam (ab141784)
cDenHyb-1	Insitus Biotechnologies (D001)
StarFISH Human Chromosome Pan-Centromeric Probes	Cambio (1695-F-01)
Suberanilohydroxamic Acid	Sigma (SML0061)
SuperSignal West Pico PLUS Chemiluminescent Substrate	Thermo Scientific (34580)
Trichtostatin A	Sigma (T1952)
Vybrant DyeCycle Violet Stain	Invitrogen (V35003)
VECTASHIELD Antifade Mounting Medium with DAPI	Vector laboratories (H-1200)

Figure 2.5 Notable chemicals, DNA dyes and FISH probes used in this research.

2.1.5 Cell lines and tissue culture

1BR3, 1BR3 hTERT (human telomerase reverse transcriptase) and 1BR3 hTERT BRG1 mutant cell lines were grown in an in-house formulation of Dulbecco's Modified Eagle Medium (DMEM) prepared with antibiotics (Streptomycin Sulfate, Benzylpenicillin) supplemented with 10% FBS (Gibco) and grown in 37°C incubators with 5% CO2. 1BR3 and 1BR3 hTERT were kindly gifted from Penny Jeggo, GDSC, University of Sussex.

2.1.6 Radiation Sources

γ-rays were used for experiments at the GDSC, University of Sussex. The source is a Caesium-137 radioisotope (^{137}Cs 64 TBq – 1989). As this source decays over time, the reading as of January 2016 was 6.2 Gy min^{-1}.

X-rays were produced using an AGO HS MP1 X-ray unit (AGO X-Ray

Ltd) at 250 kV and at a dose rate of 0.6 Gy min^{-1}, as measured directly by a PTW UNIDOS E-digital dosimeter (PTW Freiburg GmbH).

2.2 Methods

2.2.1 SDS-PAGE - Western blotting

Whole cell extracts were prepared by removing media from cells, washing once with PBS, and scraping cells in ice-cold PBS. The cell suspension was then pelleted by centrifuge at 250 RCF for 5 minutes. Cell pellets were suspended in a Urea buffer (50mM Tris pH 7.9, 8 M Urea, 1% Chaps) and shaken for 30 minutes at 4ºC. The suspension was then centrifuged at maximum (16000) RCF and supernatant, containing the extracted protein, transferred to a new tube. Alternatively, extraction for histones analysis was performed using the Histone Extraction Kit from Abcam (ab113476).

Protein concentration was determined by the Bradford Protein Assay. Samples were prepared by adding 2 µl of whole cell extract to 798 µl ddH_20 and 200 µl Bradford reagent (Bio-Rad). The absorption of samples along with a set of BSA protein standards were measured at 595 nm using a spectrophotometer and used to determine protein concentration.

Acrylamide gels were either prepared in house or precast gels were used (4-20% Tris-Glycine, Invitrogen). NuPAGE lithium dodecyl sulfate (LDS) sample buffer (Novex, Thermofisher), freshly supplemented with 5% β-mercaptoethanol, was added to 20-40 µg of protein sample and ddH_2O to a final concentration of 1x in equal volumes for loading. Samples were denatured

at 95ºC for 5 minutes and briefly centrifuged to collect condensation. Samples and protein standards (Precision Plus Dual Colour, Bio-Rad) were loaded into gel wells submersed in 1x protein running buffer (5 mM Tris, pH8.3, 192 mM glycine, 0.1% SDS). Electrophoresis was performed at a constant 200 V until the dye front reached the bottom of the gel. Proteins were then transferred onto nitrocellulose membranes (0.45 µM pore size or 0.2 µM pore size for histones (Amersham Protran, GE Healthcare)) over 90 minutes at a constant 200 mA. Membranes were blocked for one hour in 3% milk / TBST (Tris-buffered saline and Tween 20) or 5% BSA / TBST for histones. Membranes were incubated with primary antibodies overnight at 4ºC with agitation. They were then washed thoroughly with TBST and incubated with a secondary antibody for 1 hour at room temperature with agitation. Following washing again with TBST, proteins were visualised using enhanced chemiluminescence (ECL) reagents and images were captured using a ChemiDoc Touch (Bio-Rad).

2.2.2 Plasmid transfection and clone selection

Cas9n plasmid containing the SMARCA4 Exon 2 sgRNA guides was transfected into 1BR3 hTERT using the Neon transfection system (Themo Fisher Scientific). 7 million cells were treated, 1 million cells in 9 ul of R buffer + 1 ul of plasmid to make 10 ul: the volume of the specialised electroporation pipette tips. Electroporation settings of 1100 V, 1 pulse, 30 ms were used and cells were dispensed into antibiotic free DMEM in 6 cm dishes and left overnight. The following morning, cells were collected and 24,000 single cells were sorted by fluorescence-activated cell sorting FACS for mRuby expression

(1% transfection rate was observed) into 96 well plates (Aria III, BD Biosciences). Clones were allowed to grow and selected by growth for expansion over 4 weeks.

2.2.3 PCR - Agarose gel electrophoresis

Genomic DNA extraction for polymerase chain reaction (PCR) was performed from cell pellets. Samples were resuspended in 100ul of DirectPCR lysis reagent (Viagen) with Proteinase K (New England BioLabs). This was incubated at 55ºC for 1 hour, 95ºC for 10 minutes and then held at 4ºC in a thermal cycler (T100, Bio-Rad). One µl of template DNA was then mixed with 0.5 µl Phusion polymerase (Thermo Scientific), 10 µl Phusion Buffer (Thermo Scientific), 1 µl dNTPs (Thermo Fisher), 20 µl primers and 35 µl ddH_2O. Thirty cycles of 98ºC for 2 minutes, 98ºC for 10 seconds, 59.5ºC for 30 seconds, 72ºC for 30 seconds were performed in the thermal cycler prior to holding at 10ºC.

Agarose gels for PCR product separation were made at 1% or 2% agarose in TAE plus 0.005% ethidium bromide. Two µl of each sample were loaded with 9 µl ddH_2O and 2 µl loading dye (New England Biolabs) into submerged wells in TAE plus 0.005% ethidium bromide. Gels were run at a constant 120 V and visualised on a Chemi-Doc Touch (Bio-Rad).

PCR product was sent to Genewiz (UK) for sequencing. BRG1 mutant 1 has a full sequence deletion between the target sites of the SMARCA4 Exon 2 sgRNA:

5’ AAGATGTCCACTCCAGACCCACCCCTG 3’.

2.2.4 Irradiation Dose Schedules

Fractionated courses were completed over an 8 hour period (Figure 2.6), except for experiments using daily fractions split by 24 hours. Where an 8 hour period was used, 24 hours were always given for repair from when the first fraction was delivered.

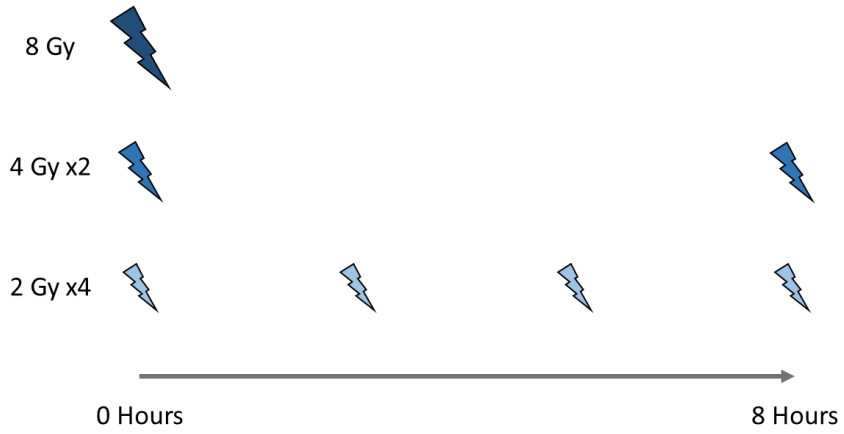

Figure 2.6 Schema demonstrating the separation of fractions over typical 8 hour fractionation schedules.

2.2.5 Cell cycle stage FACS sorting

Asynchronous 1BR3 hTERT human fibroblasts were pelleted and resuspended in 0.1% FCS media with Vybrant Dyecycle DNA dye (thermofisher), a cell permeable DNA dye , to the manufacturer's instructions and 150,000 G_1, S and G_2 cell cycle phase cells sorted in each condition by FACS (Aria III, BD Biosciences) over a 2 hour period. This provided sufficient numbers for subsequent clonogenic analysis (Figure 2.7).

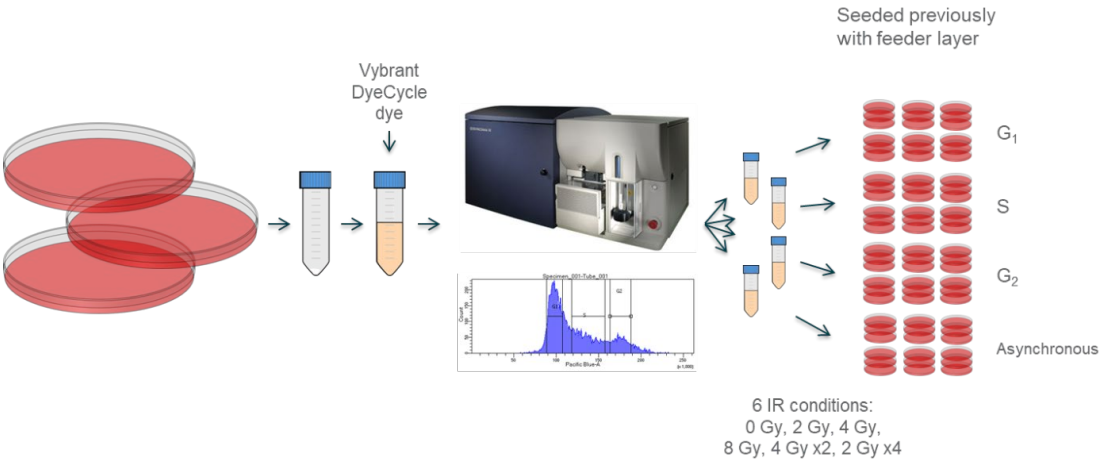

Figure 2.7 Schema illustrating cell cycle phase-specific sorting for clonogenic analysis. FACS insert demonstrates cut off boundaries.

2.2.6 Clonogenic Survival Analysis

Clonogenic survival analyses were performed in 6 cm dishes. For both 1BR3 and 1BR3 hTERT cells, a feeder layer was first made with the same cell line by irradiating 30,000 cells per dish with 35 Gy in suspension, seeding and allowing cells to adhere overnight. For cell cycle stage FACS sorted clonogenic assays, cells were seeded and immediately irradiated whilst still in suspension to ensure no cell cycle phase progression. For G_0/G_1 and matched asynchronous clonogenic analysis, cells were grown to confluence over a period of 7 days to enrich a G_0/G_1 population. Subsequently, IR courses were delivered followed by 24 hours for repair. Finally, cells were split and seeded onto the feeder plates. For all other clonogenic analysis, asynchronous cells were seeded on feeder layers 4 hours prior to IR to allow cells to adhere. Typical seeding is shown in Figure 2.8. Standard 10% FBS in DMEM was used and clones were scored by eye after 18 days growth with the aid of a colony counter.

Dose	Cells Seeded
0 Gy	100
2 Gy	350
4 Gy	2000
8 Gy	24000
4 Gy x2	12000

Figure 2.8 Typical clonogenic seeding used for 1BR3 hTERT.

2.2.7 Premature Chromatin Condensation

For analysis of repair in G_1 by cytogenetic analysis, cells were serum starved in 0.1% FCS media for 72 hours prior to irradiation. Following a 24 hour period for repair, the plates were split and given fresh 10% FCS media to permit synchronised progression to G_2. Following timeframes determined by previous analysis of EdU incorporation, the 0 Gy sample was taken 24 hours after splitting and the IR treated cells were taken 32 hours after splitting. For G_2 analysis, asynchronous cells were pelleted and resuspended in Vybrant Dyecycle DNA dye (Thermofisher) to the manufacturer's instructions and

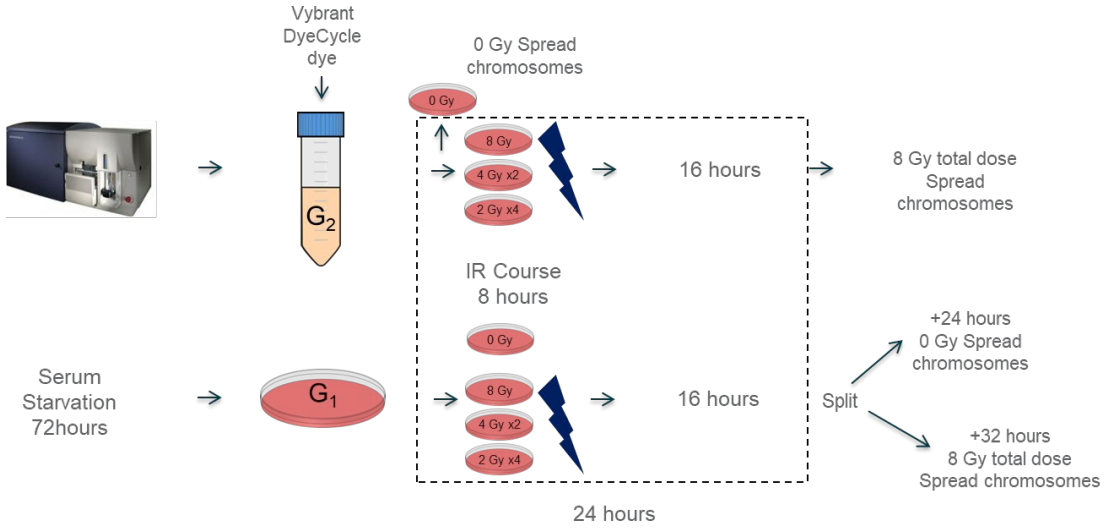

Figure 2.9 Schema illustrating cell cycle stage enrichment for G_1 and G_2, IR dose course and timecourse for sample collection prior to G_2 PCC for cytogenetic analysis.

sorted in G_2. The 0 Gy sample was taken immediately after sorting, whilst the IR courses were plated and given IR. After a 24 hour period of repair, the IR samples were taken (Figure 2.9).

G_2 premature chromatin condensation was then performed using a protocol adapted from Gotoh and Durante (2006). Briefly, 100 ng/ml Calyculin A was added to the media for 30 minutes at 37ºC, which resulted in the cells rounding up and releasing into suspension. The cells were then collected by centrifuge at 200 RCF for 5 minutes and the supernatant removed. Five ml of 37ºC 0.075 M KCl was then added dropwise to resuspend the cells with continuous gentle agitation by flicking with soft side of the index finger. Following a 20 minute incubation at 37ºC to swell the cells, 5 ml of 4ºC Carnoy's fixative (3:1 methanol / acetic acid) was added dropwise with gentle agitation before pelleting at 200 RCF for 5 minutes at 4ºC. Following careful resuspension twice more in 5 ml of Carnoy's, after the final centrifugation cycle cells were resuspended in 200 µl of Carnoy's fixative and could then be stored at -20ºC. To create spreads, 20-40 µl of cell suspension was released from above head height to fall onto microscope slides. The slides were suspended over a vessel containing warm wet tissue paper and allowed to dry.

Pan-centromeric chromosome FISH paints (StarFISH, Cambio) were hybridised according to the manufacturer's instructions with the following exceptions. The optional slide pre-treatment steps were not performed and the probes were diluted 1:3 in cDenHyb-1 (Insitus Biotechnologies) for use with 22 x 40 mm coverslips, 22.7ul of diluted probe per slide. Slides were sealed with vulcanising rubber glue during hybridisation. DAPI antifade (Vectorlabs) was

used to mount coverslips for imaging.

2.2.8 Chromosome aberration analysis

Chromosome spreads were captured using an advanced spinning disk confocal microscope at 63x magnification. A 9 segment z-stack was used at optimum size split and nearest neighbours deconvolution performed and projected used to create the final image (3i, Intelligent Imaging Solutions). Spreads were scored using an updated methodology from Cornforth and Bedford (1987) to include the use of pan-centromeric FISH probes. Folders were designated randomly assorted numbers to blind score. The total number of chromosomes and excess fragments were counted by eye with the aid of a custom made script in ImageJ. Dicentrics and centric rings (very rare) were scored by appearance aided by the pan-centromere FISH probes: 2 centromeres per a chromosome for dicentrics and a clear hole seen for a circular chromosome. For each dicentric or ring aberration, an acentric chromosome was attributed. The remaining fragments without a centromere were then counted as terminal deletions with the exception of clear interstitial deletions, which were generally less than the width of one chromatid arm in size. Chromatid breaks were scored based on the appearance of gaps in chromatid arms or clear orientation change of the chromatid arm to its partner with no observable chromatid continuation. Complex chromatid exchanges where scored as any aberration containing 2 or more centromeres with independently adjoined chromatid arms. Without the aid of whole chromosome FISH probes, the complexity of the misrepair in chromatid exchanges frequently makes it difficult to determine the number of exchange partners.

Therefore complex chromatid exchange aberrations were each only considered as one count.

2.2.9 Live cell growth analysis

An IncuCyte S3 live-cell analysis system (Essen Biosciences) was housed in an incubator and set to capture images of 96 well plates seeded with 2500 cells per well with varying drug concentrations. Images were taken at 10x magnification every 4 hours and % confluence in the field determined by IncuCyte software with customised thresholding.

2.2.10 Foci analysis

Cells were seeded onto coverslips in 6 cm dishes and once adherent were given the desired IR course. At time-points of interest, coverslips were removed with a scalpel and transferred to a 6-well plate. They were then washed twice with PBS prior to fixation with 1 ml 4% paraformaldehyde for 12 minutes. Following two further PBS washes the coverslips were left submerged in PBS and stored at 4ºC prior to antibody staining. When all slides were fixed ready for staining, the PBS was removed and cells permeabilised in 1 ml of PBS + 0.2% Triton for 3 minutes. Following two PBS washes the primary antibodies were hybridised at 4ºC overnight in 800 µl PBS + 2% weight/volume BSA. Following three PBS washes, the secondary antibodies were hybridised at room temperature for 1 hour in 800 µl PBS + 2% weight/volume BSA. Following a final three PBS washes the coverslips were

mounted with DAPI antifade (Vector Laboratories) and sealed with nail polish.

Foci were counted by two different methods. For early experiments (as

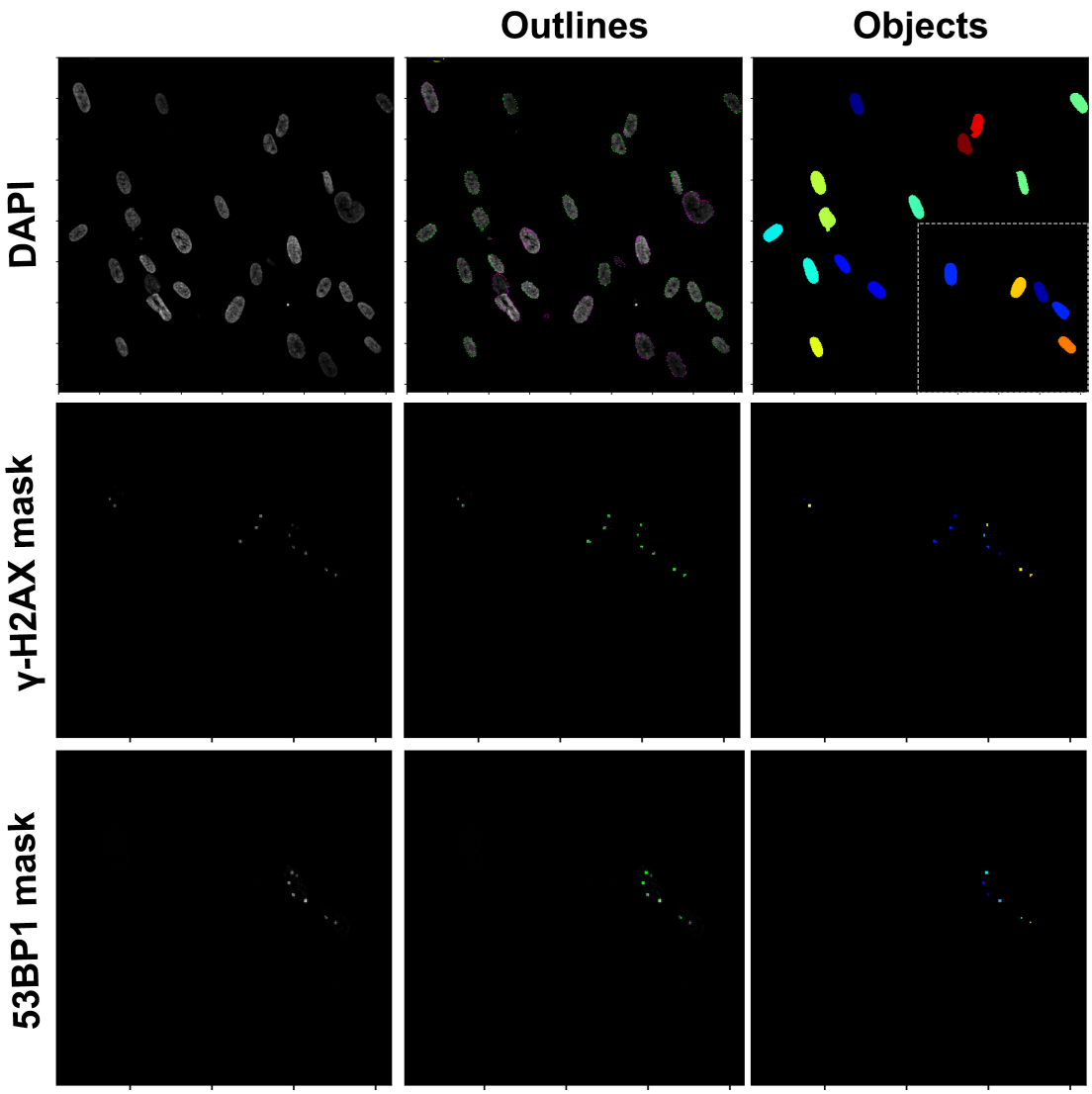

Figure 2.10 Cell Profiler object identification.

The top panel demonstrates nuclei selection based on size. Top centre: Green outlines pass the size selection, purple outlines fail. Top right: pass nuclei are coloured for identification and their area used subsequently as a mask for foci channels. The dashed area represents the area magnified for the foci images. Middle left and bottom left: After masking by nuclei area, speckle enhancement is performed to isolate foci from γ-H2AX and 53BP1 channels respectively. Middle centre and bottom centre: foci outlines pass or fail size selection. Right centre and right bottom: identified foci.

marked in the text), microscope slides were blanked with tape and given a

randomly generated number to blind score by eye. Scoring was performed on an upright fluorescent microscope (Olympus) at 63x with moving focus to ensure capture of all foci in the nucleus. For the later analysis, nuclei were captured at 40x on an advanced spinning disk confocal microscope. An 11 segment z-stack was used at optimum size split and nearest neighbours deconvolution performed and a projection made to create the final 2D images (3i, Intelligent Imaging Solutions). A customised cell profiler pipeline v3.1.9 was made using cell profiler stock speckle counting and colocalisation pipelines as a starting point. All images were scored using the same thresholding to identify foci and colocalisation. G_1 nuclei were selected within this analysis by nuclei area.

2.2.11 Genomic DNA extraction

After collecting a cell pellet, the pellet was resuspended in 500 µl of tail buffer (1% SDS, 0.1 M NaCl, 0.1 M EDTA, 50 mM Tris pH 8) and vortexed. In a fume hood, 500 µl of Phenol/Chloroform/Isoamyl (25:24:1) was added and the solution agitated at 4ºC for 10 minutes to form a white emulsion. The sample was then centrifuged at 16000 RCF for 5 minutes. The top layer was carefully transferred to a new Eppendorf and 200 µl of 5M NaCl added. The Eppendorf was then wrapped with parafilm and secured to a vortex for 5 minutes at medium speed followed by centrifugation for 10 minutes at 16000 RCF. The supernatant was poured into a new Eppendorf and 700µl isopropanol added and mixed by inversion. Following a 10 minute 16000 RCF spin the isopropanol was gently removed with a pipette and 1 ml of 70% ethanol added without disturbing the pellet and was left at room temperature

for 1 minute. The sample was then centrifuged for 5 minutes at 16000. The ethanol was then carefully removed with a pipette and pellet left to air dry for a minimum of 20 minutes. A matched volume to the pellet size of ssH_2O was added and left for at least 10 minutes. The DNA was then quantified on a NanoDrop (Thermo Scientific) and the A260/280 and A260/230 measured to determine whether the sample was free from contaminants. A DNA electrophoresis gel was also run to check gDNA integrity.

2.2.12 Single cell DNA extraction and amplification

Following cell sorting, the Ampli1 WGA kit (Menarini Silicon Biosystems) was used following the manufacturer's instructions. The Ampli1 QC kit was then used following the manufacturer's instructions. This kit utilizes a PCR-based assay to establish DNA integrity. By testing for the presence of four DNA fragments from different locations in the genome, the quality of the DNA can be tested. The highest quality DNA typically produces four PCR bands, while DNA with unbalanced amplification or degradation will show fewer QC bands. five single cells (25 in total) per condition were amplified and QC tested, of which seven demonstrated poor DNA quality (Appendix Figure 1). Three high quality samples per a condition were selected. The Ampli1 ReAmp/ds kit was then performed to remove single stranded DNA and aid accurate DNA quantification. The Ampli1 WGA adapter was then removed by digestion with MseI followed by DNA bead purification (AMPure XP, Beckman Coulter) performed according to the manufacturer's instructions. A final DNA quantification was performed using a Bioanalyzer High Sensitivity DNA chip (Agilent) (Appendix Figure 2). The samples were then sent to Genewiz (USA)

for sonication using a Covaris machine to even sizes and library preparation performed (NEBNext Ultra, New England BioLabs) with a size selection for 300-400 bp. The sample was then sequenced (HiSeq, Illumina).

2.2.13 Whole population sequencing analysis

A simulation was performed in the R v3.4.0 statistical computing environment designed and run by James Campbell with the following assumptions: number of cells $4x10^6$, genomes per cell 2, genome size $3x10^9$, fragment size 400bp and 30x depth across a range of potential number of misrepair events.

FASTQ files received from BGI (China) were checked using FastQC for quality control (Babraham Bioinformatics). Alignment to the human reference genome hg19 was performed by BGI using the Burrows-Wheeler Aligner V0.7.12 (Li and Durbin 2010) with Samtools v1.5 to produce sorted and indexed BAM (binary alignment map) files. BAM files were then uploaded into the ICR high performance computing (HPC) environment where all analysis steps were performed. Small variants were then called using the Haplotype caller v3.3.0 (GATK, Broad Institute) and large variants by Delly v0.7.7 (McKenna, Hanna et al. 2010, Rausch, Zichner et al. 2012), both in the germline mode, with post call filtering performed using R v3.4.0 and svprops (Delly v0.7.7) to remove shared calls found between samples. These steps were all performed with the guidance and assistance of James Campbell (ICR).

2.2.14 Single cell sequencing analysis

FASTQ files received from Genewiz (USA) were checked using FastQC for quality control. This analysis identified a large percentage of duplicate reads, which were expected from the PCR based Ampli1 amplification. Alignment was performed to the human reference genome GRCh38 along with post alignment QC using the HiSeq Analysis Software v2.1 (HAS) (Illumina) pipeline performed by Genewiz. The post alignment QC also demonstrated duplicate alignments but these were flagged as part of the HAS pipeline to prevent them being used in variant calling. Small variant calling was performed during HAS by the Strelka Germline Variant Caller in the germline mode for all samples. Variant filtering by R v3.6.0 was performed by Alice Gao (ICR) to remove all calls from the 0 Gy samples that were present in any of the irradiated samples as well as any variant calls that were shared between the IR samples.

Following BAM file upload to the HPC, large scale variants were called using Manta (Illumina). This was performed in two stages; first, the 0 Gy sample variants were called in the germline mode in the joined setting to produce one normal dataset. The irradiated samples were aligned in the somatic mode with the tumour only option. Post variant call filtering was performed using R v3.6.0 to remove variants found in the 0 Gy dataset from the IR samples. These steps were performed by Alice Gao. Ordinarily, somatic analysis is used to compare a single normal sample to multiple tumour samples. Because we have three single cell control genomes, the germline analysis performed compares each of these to the reference to create a joint data set. The somatic analysis is performed for the IR samples. Finally, the

filtering step removes any called variants (false positives) that are in the joint control. Ideally our small variant calling would also be run using this methodology, and consequently, this process is ongoing using Mutect2 variant calling software.

2.2.15 Statistical Analysis

All statistical analysis was performed in Graphpad Prism 8.2.0 (435), with relevant methodology given within each figure legend.

3 Cell Cycle Stage and Fraction Size Sensitivity

3.1 Repair-proficient healthy tissue model demonstrates fractionation sensitivity

3.1.1 Selecting a tissue model for investigating fractionation sensitivity

In order to examine the molecular mechanisms that control fraction size sensitivity, we made the decision to focus on a fraction-size sensitive model. The cancers most commonly treated with fractionated radiotherapy are fraction size insensitive whilst the surrounding healthy tissue is fraction size sensitive. A healthy tissue model with a measurable sensitivity to fraction size would therefore give us the starting point from which to manipulate sensitivity with a clear read out. Additionally, normal healthy tissues are DNA repair and cell cycle checkpoint proficient, allowing us to first consider what governs sensitivity across normal tissues, an important prerequisite to understanding the distinct responses of cancer cells. To replicate the response to IR in a normal late-reacting tissue, the human dermal fibroblast primary cell line 1BR3 was initially chosen. Derived from a skin biopsy from a healthy male volunteer, previous research demonstrated that 1BR3 is radiosensitive (Arlett et al. 1988) and shows split-dose recovery (Alsbeih et al. 1996). 1BR3 is repair pathway proficient and has normal p53 expression with intact cell cycle checkpoints (Green and Almouzni 2003, Flinterman et al. 2003, Riballo et al. 2004).

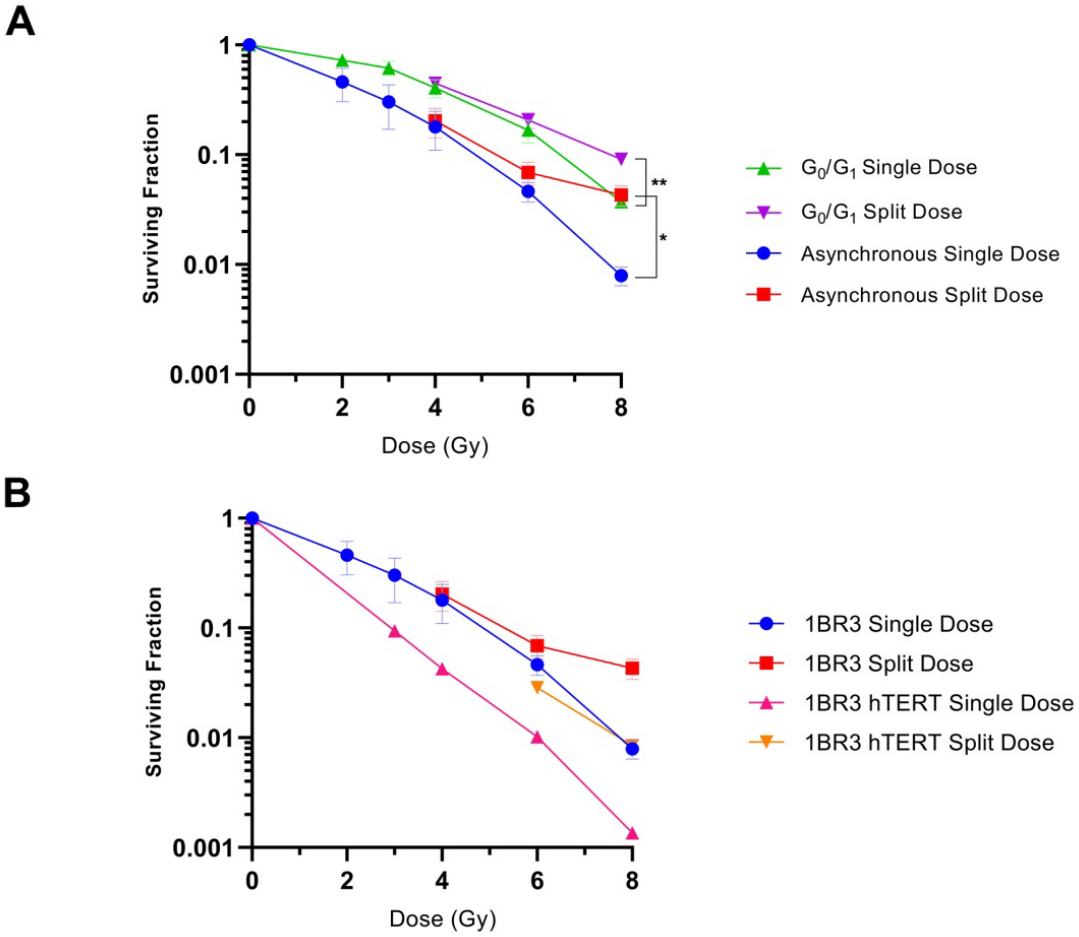

Figure 3.1 1BR3 is fraction size sensitive providing a suitable model for late responding normal tissue.

A) *Clonogenic survival data obtained from exponential phase 1BR3 (n=3) and G_0/G_1 phase (following 7 day confluence arrest) 1BR3 cells (n=3). 24 hour repair period given from the first dose, with second dose given after 8 hours. Error bars represent Standard Error of the Mean (SEM). Student's t-test (two tailed, equal variance) significance between 8 Gy and split dose 4 Gy x2. * ≤ 0.05, ** ≤ 0.01. Recovery factor for 8 Gy vs split dose for exponential phase and G_0/G_1 phase cells is 5.42 and 2.43, respectively.* ***B)*** *Additional comparison of 1BR3 result from A to n=1 result for asynchronous 1BR3 hTERT. Further experiments examined 1BR3 hTERT survival with multiple repeats (such as* ***Figure 3.2****).*

3.1.2 1BR3 is fraction size sensitive.

To validate the fractionation sensitivity of 1BR3 in our test conditions, clonogenic assays were performed with single and split-doses of high dose rate γ-rays to assess survival. Clonogenic assays are the gold standard for measuring radiosensitivity as they give a read-out of clonogenicity following damage that does not discriminate between senescence, necrosis or apoptosis. A “split-dose” describes splitting the total dose into two doses of equal size and offers the simplest test of cellular recovery in the interval between exposures. Asynchronous 1BR3 showed a split-dose recovery within our experimental conditions that becomes visible between 6 Gy vs 3 Gy x2 and reaches t-test significance at 8 Gy vs 4 Gy x2 (Figure 3.1 A). Based on these data, a fractionated course of no less than an 8 Gy total dose was used for all further experiments to ensure significant sparing was reached.

The 1BR3 radiosensitivity can be used to calculate an α/β ratio of 6.55 Gy, however as elucidated by Garcia, Wilkins, and Raaphorst (2007) there is a dose range dependency on this calculation. Because the dose range used here only reaches to 8 Gy (as higher doses preclude suitable seeding for accurate survival assays), it is insufficient to accurately calculate the α/β ratio. Instead of the α/β ratio, we can use the recovery factor (RF) as a measure of fractionation sensitivity. The RF factor is calculated by dividing the surviving fraction of the fractionated course by the surviving fraction from the single total dose. The RF (also referred to as the recovery ratio) has been utilised in the literature to examine how external factors such as the dose rate, repair time and temperature (hypothermia) affect split-dose recovery (Steel et al. 1987, Ryan, Seymour, and Mothersill 2009, Raaphorst 1992, Chapman, Taylor, and

Boulton 2012). Our primary interest in validating the model is to ensure a significant sparing of survival with fractionation within a measurable dose range for the clonogenic assay. As such, we are looking for a robust recovery factor that clearly demonstrates recovery: the RF 5.42 (4 Gy x2 / 8 Gy) achieves this.

3.1.3 1BR3 arrested In the G_0/G_1 phase is fraction size sensitive and less radiosensitive than asynchronous 1BR3

Previous work by Alsbeih et al. (1996) performed in confluence arrested and exponential phase 1BR3 demonstrated a decrease in radiosensitivity with confluence arrest. We wanted to confirm this finding in our experimental conditions whilst also examining whether there was an effect on fraction size sensitivity. We find that 1BR3 cells arrested in G_0/G_1 demonstrate a split dose recovery within our experimental conditions that is visible at 6 Gy vs 3 Gy x2 and reaches t-test significance at 8 Gy vs 4 Gyx2 (Figure 3.1 A). Additionally, the G_0/G_1 arrested populations are significantly less radiosensitive than the asynchronous cells, with t-test significance between all conditions at 6 Gy and 8 Gy (Figure 3.1 A). The calculated RF of 2.43 (4 Gy x2 / 8 Gy) is lower than the RF in the similarly treated asynchronous cells.

3.1.4 1BR3 hTERT is more radiosensitive than 1BR3 primary cells

Primary cell cultures are challenging to work with due to their limited window of cell growth combined with sensitivity to alterations in serum lot and potential for differentiation. The 1BR3 cell line has been immortalised, and this cell line, termed 1BR3 hTERT, could provide a more practical system for these

studies. We therefore investigated the characteristics of 1BR-hTERT cells and found that asynchronous populations demonstrate recovery with a split dose **(**Figure 3.1 B). The RF at 4 Gy x2 / 8 Gy was 1.875. In addition, the asynchronous immortalised cells are more radiosensitive than the 1BR3 primary cells (Figure 3.1 B). Moreover, the 1BR-hTERT cell line has been well characterised in the literature for DNA repair and damage responses and retains normal p53 expression with intact cell cycle checkpoints (Shibata et al. 2014, Alagoz et al. 2015, Tomimatsu, Mukherjee, and Burma 2009). Therefore, because 1BR3 hTERT also showed split-dose recovery, further experiments were performed in this cell line.

3.2 Clonogenic survival demonstrates fraction size sensitivity in the G_1, S and G_2 cell cycle phases

As discussed within the introduction, we hypothesise that the availability of HR repair in S and G_2 phases imparts fractionation insensitivity as a consequence of the higher fidelity of HR repair. In order to test this possibility, we set out to assess whether the cell cycle stage that DSB repair occurs within impacts fractionation sensitivity. To do this, an asynchronous population of 1BR3 hTERT were sorted by gated FACS analysis into the G_1, S and G_2 phases of the cell cycle. The sorted cells were then irradiated with single or fractionated dose courses, and clonogenic analyses were performed.

For this experiment, we wanted to ensure that the cells remained within the cell cycle stage of interest to avoid confounding the results in any way. In this way, survival was not impacted by cell cycle progression. Figure 3.2 A

A

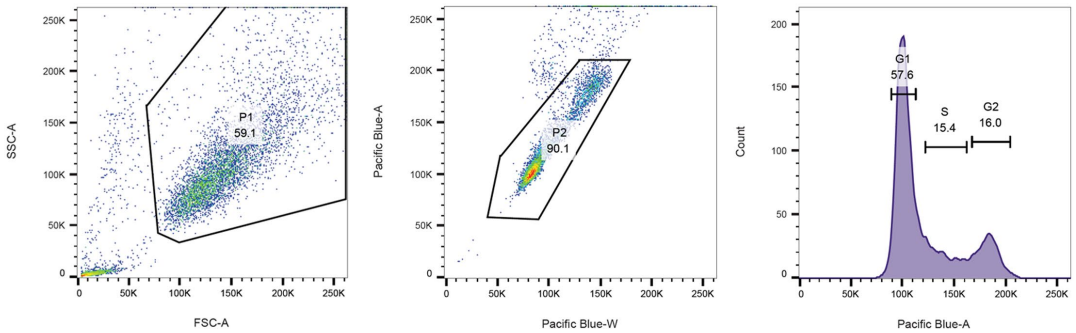

B

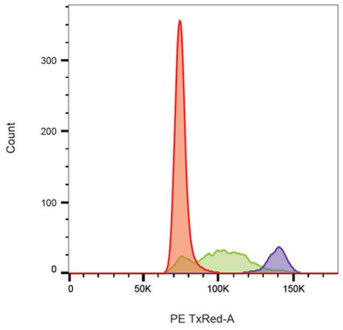

C

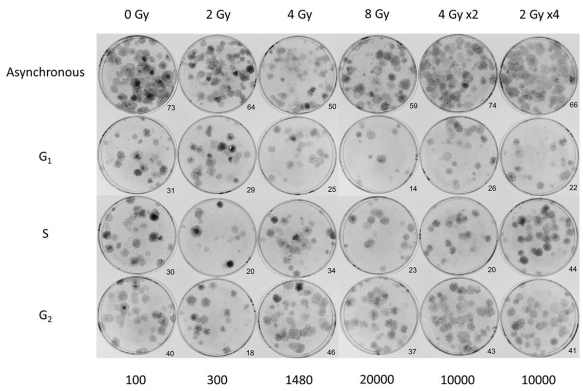

D

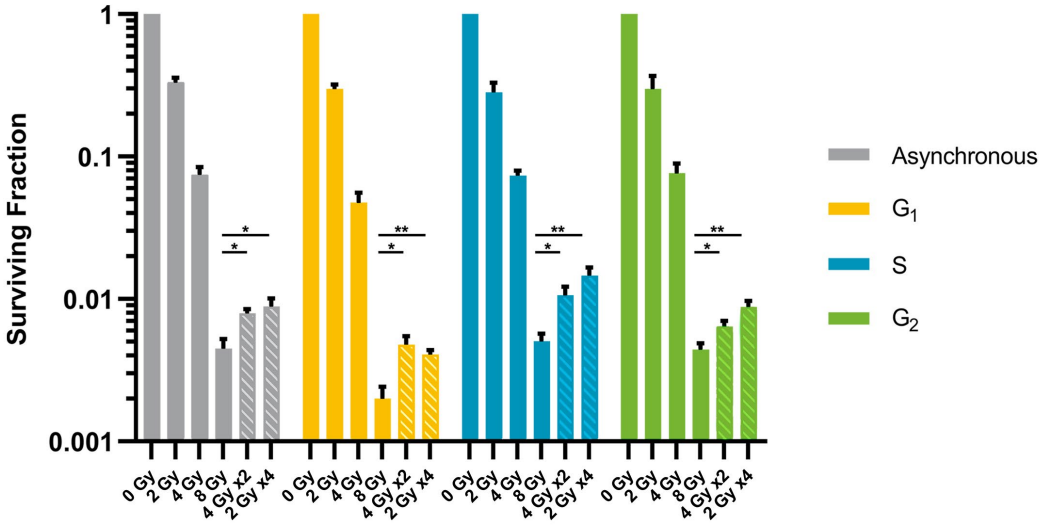

E

	Plating Efficiency	RF 4 Gy x2 / 8 Gy	RF 2 Gy x4 / 8 Gy
Asynchronous	0.48	1.78	1.99
G_1	0.30	2.40	2.05
S	0.22	2.11	2.91
G_2	0.31	1.45	2.00

Figure 3.2 Clonogenic survival assays following FACS cell cycle sorting demonstrate fraction size sensitivity in G_1, S and G_2.

Asynchronous 1BR3 hTERT was FACS sorted into G_1, S and G_2 phases of the cell cycle using DyeCycle DNA dye. Cells were seeded onto feeder layer plates and irradiated with single or fractionated dose courses, with fractionated courses within 8 hours. Surviving clones were grown out and counted. ***A)*** *Example gating for FACS selection of cell cycle phase using Vibrant DyeCycle dye. The left panel is forwards scatter (FSC-A) against side scatter (SSC-A) with gating to remove cellular debris. The middle panel is Pacific Blue Width against Pacific Blue Area with gating for single cell selection. The right panel is a histogram of the single cell Pacific Blue Area with gating used to sort by cell cycle.* ***B)*** *G_1 (red),S (green) and G_2 (purple) sorted populations were reanalysed by FACS using propidium iodide stain 1 hour after sorting to monitor for cell cycle progression.* ***C)*** *Representative clonogenic assay dishes. The number along the bottom of the panel refers to the number of cells seeded, and clone counts are given at the bottom right of each dish.* ***D)*** *Survival results plotted as a bar graph, dashed bars represent fractionated courses. t-test (two tailed, equal variance) significance was found between the single and fractionated dose courses for each cell cycle condition. * ≤ 0.05, ** ≤ 0.01, error bars SEM, n=4. Hashed bars demonstrate fractionated courses.* ***E)*** *Table of calculated plating efficiencies and recovery factors.*

demonstrates example FACS analysis to select single cells along with the gating used to sort cells into the G_1, S and G_2 cell cycle phases. A separation was left between gates to reduce the possibility of isolating cells from neighbouring cell cycle phases. To ensure that progression through the cell cycle had not occurred during the sorting process, samples from an independent biological repeat were stained with propidium iodide and reanalysed one hour after the initial sorting process (Figure 3.2 B). The G_1 and G_2 populations showed distinct peaks, demonstrating that they had not progressed into another cell cycle phase. The S phase sample was less distinct, with a small peak in G_1. It is not clear whether some of the S phase sorted cells progressed through G_2 to G_1 or whether there was another

explanation for this population. Because the G_2 phase sorted cells did not progress, it is unlikely the S phase sorted cells progressed through G_2 into G_1. Therefore, we are confident that the cells can be used to analyse the relative response to single and split dose irradiation.

When clonogenic survival analyses were performed, the asynchronous control (grey bars) displayed a decrease in radiosensitivity compared to the earlier initial experiment (Figure 3.1 B) and a significant sparing of survival with both the fractionated dose courses (Figure 3.2 D). This decrease in radiosensitivity coincided with a move in laboratory facilities and altered methodology and is not considered a concern. In addition to a split dose of 4 Gy x2, a further course with four fractions of 2 Gy (2 Gy x4) was utilised to attempt to increase sparing. However, the asynchronous control was not significantly more spared in survival by the more fractionated course.

The G_1 (yellow bars), S (blue bars) and G_2 (green bars) phase cell populations all demonstrated a significant sparing of survival when fractionated dose courses (4 Gy x 2, 2 Gy x4) were used when compared to the single dose (8 Gy). The more fractionated course (2 Gy x4) appeared to result in increased survival compared to the split dose (4 Gy x 2) in G_2 and S phase, but this was not statistically significant. Notably, the recovery factors did not deviate by more than 1 between all conditions for the same fractionation course and there was no consistent pattern between the differences or order of greatest to lowest recovery between the two fractionated courses (Figure 3.2 E). This suggests that the ability of cells to benefit from fractionation exists in all phases of the cell cycle, including those where HR is available for repair. This could

be further confirmed by performing the experiment again with an HR-deficient cell line.

3.2.1 Cell cycle phase radiosensitivity

At 8 Gy, the survival of 1BR3 hTERT cells irradiated in G_1 is significantly lower than the asynchronous, S or G_2 cell population survival (two-tailed, equal variance t-test at 8 Gy, G_1 vs asynchronous 0.03, G_1 vs S: 0.01, G_1 vs G_2: 0.01). Relative cell cycle stage radio-sensitivity based on the literature is discussed later. The FACS clonogenic assay developed here is the first to utilise DyeCycle dye to live-cell sort by cell cycle phase for clonogenic analysis in response to radiation. DyeCycle is described by the manufacturer to be of low toxicity throughout the cell cycle and was recently demonstrated to show no toxicity to stem cells (Boesch, Wolf, and Sopper 2016). The asynchronous control was also treated with DyeCycle and demonstrated similar survival to untreated samples in other experiments (such as Figure 5.3 and Figure 5.5) . The difference in plating efficiency seen in Figure 3.2 E can, therefore, be considered to be due to induced stress from single-cell sorting alone.

3.3 Chromosome aberration analysis of cells irradiated in G_1 or G_2

The cell cycle phase sorted survival data suggests that cells irradiated in both G_1 or G_2 phase are equally spared by splitting the dose. Because there is evidence to suggest that survival rates correlate with the number of chromosome exchange aberrations, a prediction from this result is that there are fewer exchange aberrations after treatment with a fractionated dose when compared with a single dose. Therefore, to determine how the sparing seen in

both G_1 and G_2 related to the fidelity of repair, chromosome spreads were generated following irradiation and time for repair in G_1 or G_2 using the same fractionation schedules as the clonogenic survival. G_2 premature chromatin condensation (PCC) was utilised, resulting in chromatin condensation into visible chromosomes that can be fixed and spread for analysis (Gotoh, Asakawa, and Kosaka 1995). During PCC a chemical inhibitor of type 1 and type 2A protein serine/threonine phosphatases is added to the media, which induces chromatin condensation via an unclear mechanism (Gotoh and Durante 2006). Okadaic acid, Colcemid and Calyculin A can all be utilised for this purpose (either individually or together) however following optimisation we use Calyculin A solely as it resulted in the aesthetically pleasing chromosomes to facilitate accurate scoring..

3.3.1 Chromosome type exchange aberrations are spared with fractionation during repair in G_1

In order to assess aberrations following repair in G_1, serum arrest was utilised in order to enrich a G_0/G_1 population. The G_0/G_1 cells were given a fractionated or single-dose course (fractionated course over 8 hours) followed by a 24 hour period of repair after the first dose. Following this repair period, the media was replaced with serum rich media to allow cells to progress into G_2 phase and PCC was performed (the timeframe for G_2 enrichment was determined by EdU incorporation, not shown). Serum starvation was chosen instead of the FACS sorting performed previously in order to allow synchronous passage into G_2, which was necessary for sufficient G_2 PCC yield. The number of chromosome aberrations (Interstitial deletions, terminal deletions, dicentrics, chromatid

A

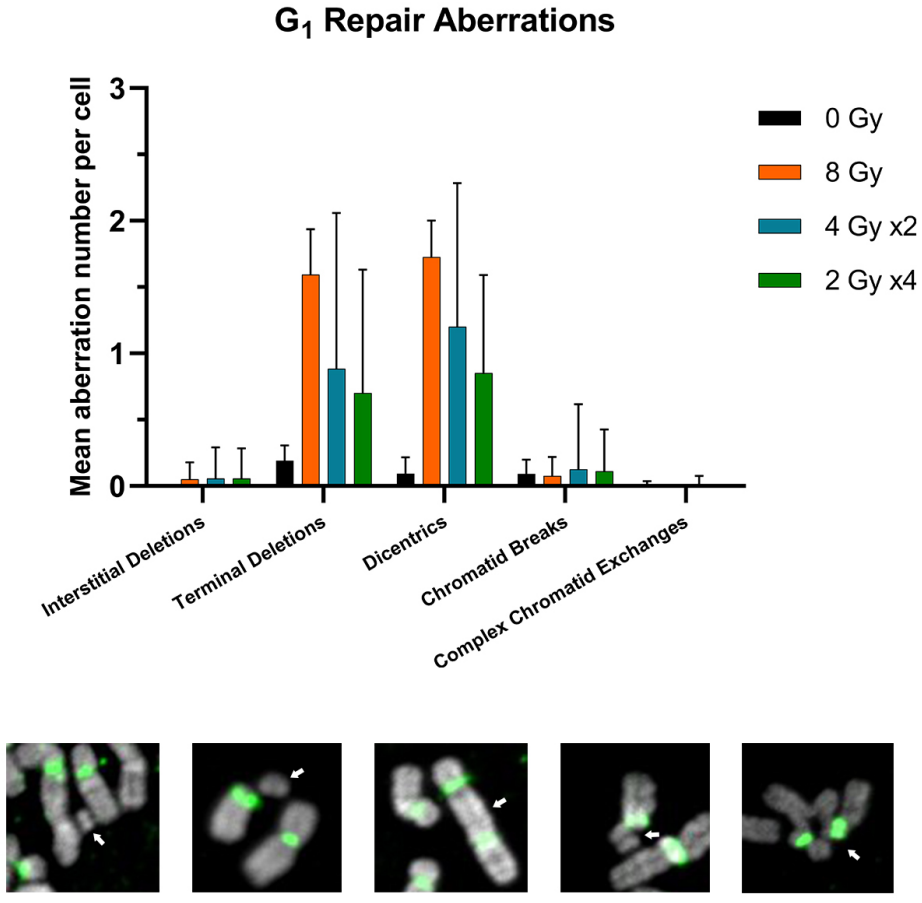
G1 Repair Aberrations
Mean aberration number per cell
3
2
1
0
0 Gy
8 Gy
4 Gy x2
2 Gy x4
Interstitial Deletions
Terminal Deletions
Dicentrics
Chromatid Breaks
Complex Chromatid Exchanges

B

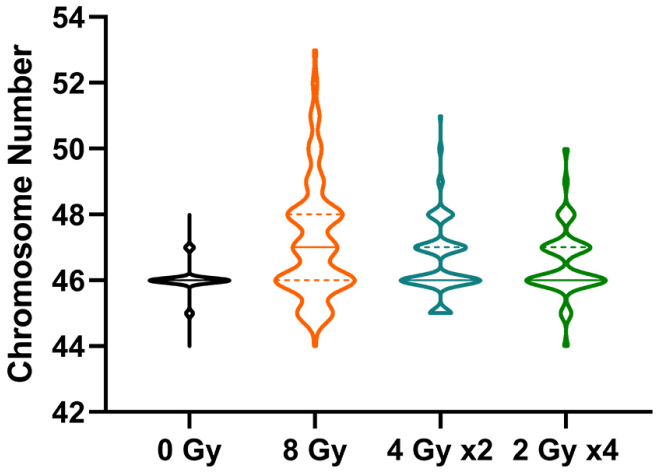
Chromosome Number
54
52
50
48
46
44
42
0 Gy
8 Gy
4 Gy x2
2 Gy x4

Figure 3.3 Chromosome aberrations by G_2 PCC following G_1 repair.

A) *1BR3 hTERT was held in G_1 by serum arrest, irradiated with either single or fractionated dose courses, with a total dose of 8 Gy. Fractionated courses were complete within 8 hours and a 24 hour period for repair from the first dose was given. Serum arrested cells were then given 10% serum media to progress to G_2 and treated with Calyculin A to induce premature chromatin condensation. Chromosome spreads were fixed and scored for chromosome aberrations with the aid of a centromeric FISH probe. 706 spreads analysed from two separate biological experiments (0 Gy 336, 8 Gy 119, 4 Gy x2 203, 2 Gy x4 48). Examples of aberrations scored given in corresponding order below the bar graph. White arrows indicate aberration.* ***B)*** *Violin plot of the number of chromosome fragments per spread. Tukey's test significance of <0.0001 between 8 Gy and 4 Gy x2 and 0.0021 significance between 8 Gy and 2 Gy x4.*

breaks and complex chromatid exchanges) were scored for chromosome spreads generated after irradiation and repair in G_1 (Figure 3.3 A). A representative image of each aberration type is given underneath. Following 8 Gy (orange plot) there is a marked increase in chromosome number (a count of the total number of chromosome fragments), which decreases with fractionation (blue and green plots) (Figure 3.3 B). This is concordant with the number of terminal deletions observed, which also decrease significantly with fractionation, indicative of un-repaired breaks (Tukey's test <0.0001 between 8 Gy vs 4 Gy x2 and 8 Gy vs 2 Gy x4).

Chromosome aberrations can be classified as chromosome or chromatid type aberrations dependent on the cell cycle stage that the repair occurs in. Chromatid breaks and complex chromatid exchanges only occur on one chromatid arm from repair in G_2 (Figure 3.6 A). As expected for repair occurring in G_1, very few chromatid breaks and complex chromatid exchanges

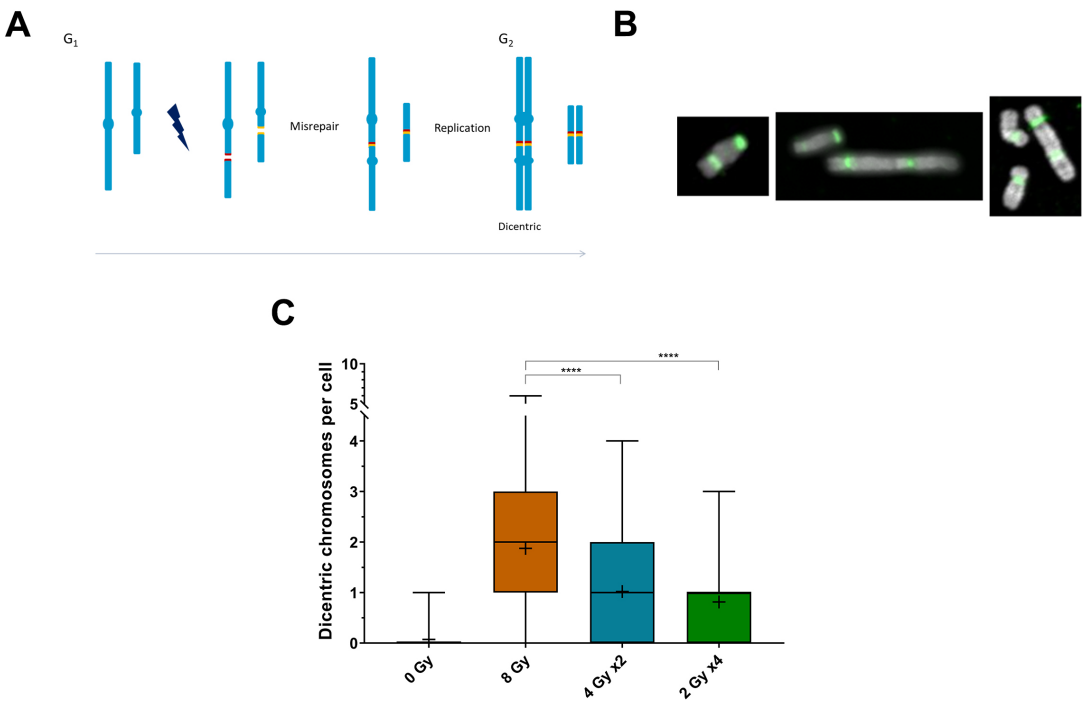

Figure 3.4 Dicentric chromosome exchange aberration formation is spared with fractionation during repair in G_0.

A) *Generation of chromosome type aberration, a dicentric chromosome and a acentric partner, as a result of repair in G_1 and subsequent progression through S phase replication to G_2.* ***B)*** *Representative dicentric chromosomes with centromeric FISH probes utilised to aid quantification.* ***C)*** *Box and whiskers plot of the number of dicentric chromosomes formed from repair in G_1 per spread. Dicentric chromosomes formed from repair in G_1 are spared with fractionation, with significance determined by Tukey's test **** ≤0.0001.*

were observed. Chromosome type aberrations occur when misrepaired damage in G_1 is replicated during S phase so that it appears on both chromatid arms, dicentric chromosomes are the primary example of this (Figure 3.4 A). Dicentric chromosomes were observed in significant numbers following repair in G_1. The formation of dicentric chromosomes was significantly spared with fractionation, which is consistent with the analysis performed by Bedford and Cornforth (1987) (Figure 3.4 C). These data demonstrate that chromosome

aberrations caused by misrepair of DNA DSBs following irradiation of G_1 cells are spared by fractionation.

3.3.2 Chromatid type exchange aberrations are spared with fractionation during repair in G_2

In order to assess aberrations following repair in G_2, FACS based sorting was performed to isolate a population of cells in G_2. G_2 cells were given a fractionated or single-dose course (fractionated course over 8 hours) followed by 24 hours after the first dose for repair prior to PCC. We first determined using FACS analysis that G_2/M checkpoint responses to irradiation prevent progression through the cell cycle in this timescale. Moreover, any cells that did progress would not be picked up by G_2 PCC. Therefore, only cells that were irradiated in G_2 and that remained in G_2 until PCC were scored. Figure 3.5 A demonstrates the number of aberrations (Interstitial deletions, terminal deletions, dicentrics, chromatid breaks and complex chromatid exchanges) scored for spreads generated after repair in G_2. Representative images of each aberration type are given underneath. Figure 3.5 B: following 8 Gy (orange plot) the range in the number of chromosomes/fragments increases compared to the 0 Gy control. An increase in the number indicates more unrepaired fragments, whilst a decrease could occur as a result of complex chromatid exchange formation (discussed in more detail below). Terminal deletions are observed with all IR courses and are not spared with a fractionated dose course (Figure 3.5 A).

A

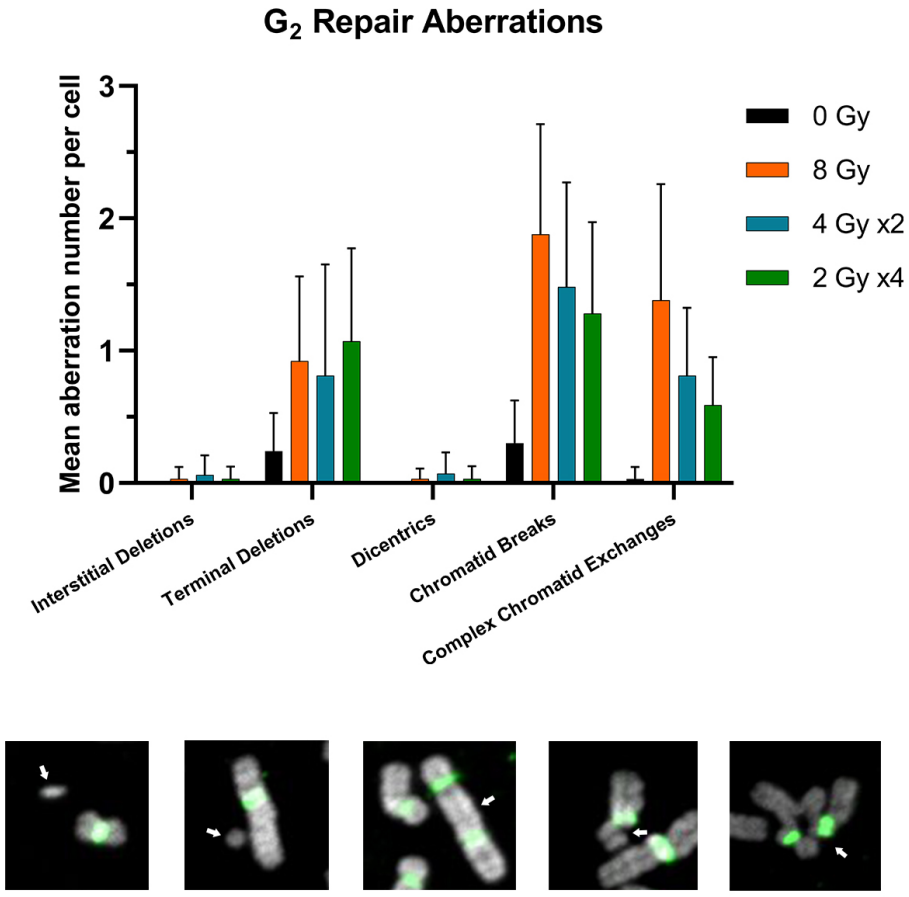
G2 Repair Aberrations
Mean aberration number per cell
3
2
1
0
0 Gy
8 Gy
4 Gy x2
2 Gy x4
Interstitial Deletions
Terminal Deletions
Dicentrics
Chromatid Breaks
Complex Chromatid Exchanges

B

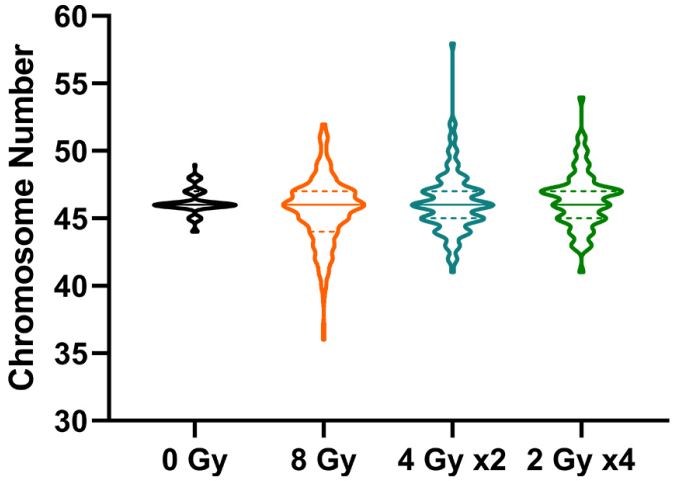
Chromosome Number
60
55
50
45
40
35
30
0 Gy
8 Gy
4 Gy x2
2 Gy x4

Figure 3.5 Chromosome aberrations by G_2 PCC following G_2 repair.

A) *G2 cells were sorted by FACS and irradiated following the same single and fractionated dose courses. Spreads were scored following 24 hours of repair from the first dose and G_2 PCC performed. Chromosome spreads were fixed and scored for chromosome aberrations with the aid of a centromeric FISH probe. 463 spreads analysed from four separate biological experiments (0 Gy 72, 8 Gy 206, 4 Gy x2 111, 2 Gy x4 74)* ***B)*** *Violin plot of the number of chromosome fragments per spread. Tukey's test significance of 0.046 between 8 Gy and 2 Gy x4, no significance between 8 Gy and 4 Gy x2.*

Dicentric chromosomes are not observed in substantial number following repair in G_2, which is as expected since they should only be generated from repair in G_1. Chromatid breaks were generated in significant numbers, with an observable but statistically insignificant decrease seen with fractionated courses. Notably, however, the formation of complex chromatid exchange aberrations during G_2 repair was significantly spared with fractionation (Figure 3.6 C). This result is novel and has not previously been reported in the literature. Unlike the dicentric aberrations formed during G_1 repair that result from two translocation events, G_2 phase complex chromatid exchange chromosomes can form as a result of multiple translocation events. The complexity of these exchange chromosomes makes it challenging to precisely determine how many exchange events occurred. Complex chromosomes were therefore each scored as one individual aberration and it is possible that further sparing may exist (i.e. a decreasing complexity with fractionation). This complexity also prevents an interpretation of terminal deletions: it is not clear if these fragments originate from original un-repaired DSBs or from complex chromosome formation.

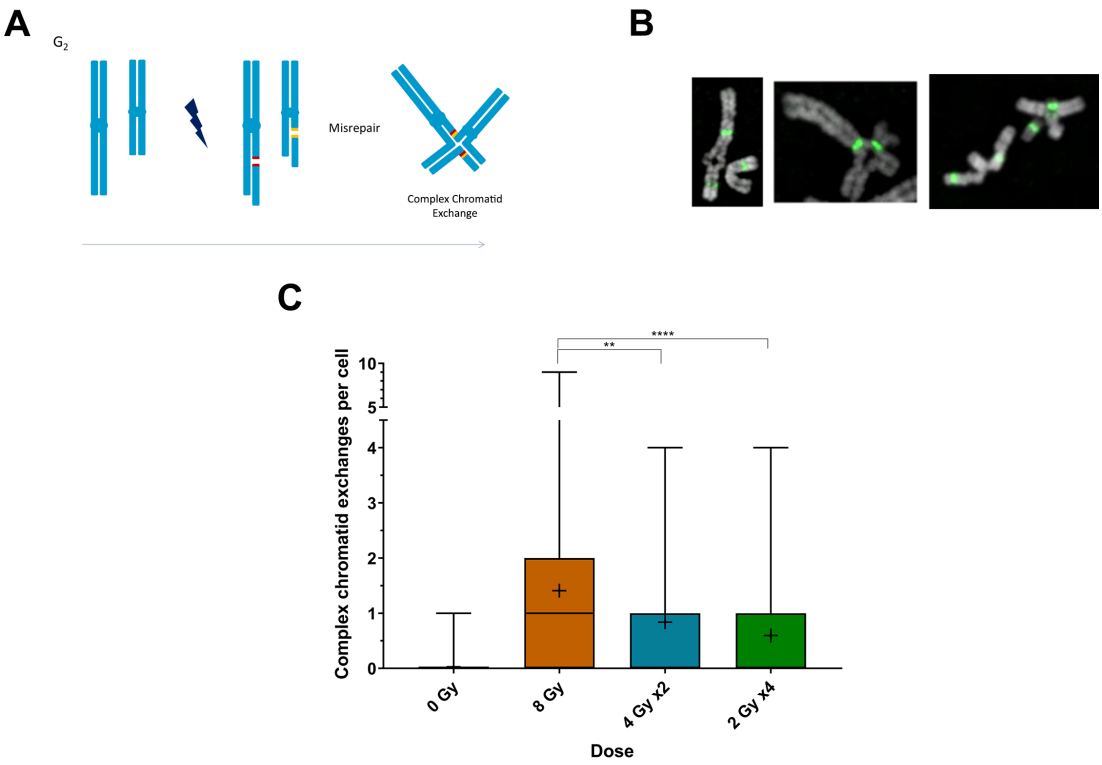

Figure 3.6 Complex chromatid exchange aberration formation are spared with fractionation during repair in G_2

A) *Generation of chromatid type aberration, complex chromatid exchanges, as a result of repair in G_2.* ***B)*** *Exemplar complex chromatid exchange chromosomes with centromeric FISH probes to aid identification.* ***C)*** *Box and whiskers plot of the number of complex chromatid exchange chromosomes formed from repair in G_2 per spread. Complex chromatid exchanges are spared with fractionation, with significance determined by Tukey's test (two-tailed), ** ≤0.01 **** ≤0.0001.*

3.4 Discussion

3.4.1 Interpreting repair fidelity

Kinetic analysis of the clearance of γ-H2AX foci suggests that with 24 hours of repair following 8 Gy, repair will be close to completion. Complete in this context does not mean that repair has been faithful, but that all DSBs that are going to be repaired (or misrepaired) have been, resulting in a constant

and close to background remaining number of γ-H2AX foci.. The chromosome spread analysis following irradiation in either G_1 or G_2 phase cells allows us to examine a different read out of the fidelity of repair.

From the G_1 chromosomal analyses, we find that the fidelity of repair increases with fractionation, with a decrease in translocations (by dicentric aberration occurrence). The extent of repair is difficult to consider as the number of terminal deletions and/or terminal fragments cannot be purely attributed to un-repaired breaks directly occurring from IR. In our analysis, following the identification of all chromosomes with centromeres and the removal of acentric fragments assumed to be generated 1:1 with dicentrics, the remaining fragments were classified as either an interstitial deletion or a terminal deletion. Derived DSBs, generated from replication across misrepair damage in S phase could contribute to the number of terminal fragments seen. Consequently, it is not possible to infer the relative contribution of lack of repair or misrepair of irradiation-induced DSBs to the decrease in chromosome number and terminal deletions observed with fractionation. We can however suggest that the decrease seen with fractionation is either due to an improvement in repair fidelity with fractionation that prevents derived break occurrence or an improvement in repair extent.

For G_2 irradiated cells, similarly to spreads from G_1 repair, the fidelity of repair increases with fractionation, demonstrated by the decreased formation of translocations (measured by complex chromatid exchange aberrations). The number of chromosomes and chromosome fragments per spread is a more complex picture than from the G_1 derived spreads. Specifically, following

8 Gy, the range of the number of chromosomes and fragments per a spread increases (wider vioin plot) compared to the control (Figure 3.4 B). An increase in the number indicates more unrepaired chromatid fragments (lost from cohesion with the sister arm), whilst a decrease occurs as a result of complex chromatid exchange formation. For illustration, with the exemplar quadradial formation shown in Figure 3.6 C, the number of chromosomes that would be counted decreases from two at the beginning to one at the endpoint. The reduction of the lower end of the distribution in the fractionated samples, therefore, suggests improved repair fidelity. Finally, the observation of chromatid breaks following G_2 repair (Figure 3.4 A), whereby the broken chromatid arm is held in place by cohesin, can be considered a partial readout of the number of DSBs remaining. Statistical significance is not found for a decrease in chromatid breaks with fractionation, but the remaining unrepaired numbers are significant lesions as discussed in the chapter on repair kinetics. G_2 specific foci analysis indicates the timeframe for repair given should be sufficient for close to complete repair (Geuting, Reul, and Lobrich 2013, Löbrich et al. 2010). However, it is possible that within the experimental timeframe these lesions represent a small proportion of repair yet to be completed, presumably by the slow process of HR. An alternative interpretation is that a proportion of these chromatid breaks may form from mechanical stress due to the compaction of complex chromatid exchange chromosomes during the PCC, which would explain their decrease with fractionation as a function of decreased complex chromatid exchange formation. Crucially, the fidelity of DSB repair measured by translocation events is improved with fractionation in both G_1 and G_2 repair.

3.4.2 Cell cycle stage radiosensitivity

The data from the survival assays performed from cells sorted by cell cycle phase suggests that cells in the G_1 phase of the cell cycle are more radiosensitive than cells from S, G_2 or the asynchronous control at 8 Gy. The common perception within the field of radiobiology is that the most radiosensitive stages of the cell cycle are the G_2 and M phases, followed in decreasing sensitivity by the G_1 phase and finally the S phase. This understanding is drawn from the seminal work of Sinclair and Morton (1966), Terasima and Tolmach (1963), Sinclair and Morton (1965). Since then, these findings have been challenged in different species, normal cell lines and cancer cell lines by numerous methodologies including radioisotope labelling, synchronisation and recently using the fluorescent ubiquitination-based cell-cycle indicator system, each with their own caveats (Otani et al. 2016, Pawlik and Keyomarsi 2004). The majority of these studies agree that mitosis is the most sensitive cell cycle phase and that within S–phase radio-sensitivity decreases from early to late S (Pawlik and Keyomarsi 2004). However, this literature, combined with further analysis by the seminal authors, together demonstrate that the comparative radiosensitivity of all the cell cycle phases can differ between species, cell types and cancer cells (Djordjevic and Tolmach 1967, Sinclair 1968). Therefore, our analysis could reflect the properties of the cell line used. Alternatively, it is possible that the intrinsic differences in radiosensitivity during each cell cycle phase are influenced by variables such as media, handling, or methodologies used.

3.4.3 Availability of HR in 1BR3 hTERT does not significantly impact on

fractionation sensitivity

By comparing two different endpoints of exchange aberrations and clonogenic survival following repair in G_1 –we can consider the effect of fractionation on the G_1 pre-eminent DSB repair pathway: NHEJ. The sparing of exchange aberrations and increase in clonogenic survival with fractionation demonstrate that NHEJ has inherent misrepair that is spared with fractionation and that this misrepair correlates with survival respectively. This correlation likely underlies fractionation sensitivity.

The G_2 repair derived sparing of clonogenic survival demonstrates that the availability of HR repair in our normal cell line is insufficient to cause a marked loss of fractionation sensitivity. Furthermore, the G_2 derived spread analysis also shows a sparing of exchange aberration formation that correlates to survival, again likely underlying sensitivity.

3.4.4 The relative contribution of HR vs NHEJ

Whether the fidelity of HR repair itself is spared by fractionation cannot be examined from our analysis due to the concurrent use of NHEJ in G_2. As a result, it is pertinent to consider the relative usage of HR vs NHEJ in G_2.

HR deficient cells have been used to suggest HR is the dominant repair pathway in both S and G_2, but these studies were performed in either mouse or chicken cells (Rothkamm et al. 2003, Takata et al. 1998). As previously discussed, mouse cells have low levels of the Ku heterodimer, and have been shown to utilise alt-NHEJ at higher levels than human cells. The DT40 chicken

cell line has significantly greater usage of HR relative to most other cell line systems (Buerstedde and Takeda 2006). A study in the human osteosarcoma U2OS cell line suggests that the use of HR peaks at mid-S phase - when DNA replication is at its peak - and continues trailing off throughout G_2 (Karanam et al. 2012). However, the most relevant study to our normal human fibroblast cell line, performed predominantly in primary human fibroblast lines, demonstrate that NHEJ is the dominant repair pathway in G_2 and that HR usage is confined to 15% of DSBs, which pertain to the slow component of repair. A BRCA2-deficient primary human fibroblast (HSC62) was shown to have identical repair kinetics to a normal line in G_1 but a deficiency in late G_2 repair that accounted for 15% of the DNA DSBs (Beucher et al. 2009). If we assume that this 15% of repair is indiscriminate to severity of damage or the location of damage in the genome then it would seem unlikely HR usage would have a substantial effect on the overall fidelity of repair. NHEJ has a greater propensity for misrepair, but is still a precise repair process that would faithfully repair the majority of this 15%. However, if this 15% of repair by HR was in transcriptionally active regions alone, the effect could be significant. Indeed recent studies suggest that the slow process of repair in G_2 may account for a greater percentage of the repair than in G_1 due to HR repair at transcriptionally associated DSBs (Shibata and Jeggo 2019). It is possible that the level of unrepaired chromatid DSB breaks we see following G_2 repair represent some of these slow repair breaks still persisting after 24 hours and therefore the benefit of their accurate repair has not yet occurred. Regardless of this, the fidelity of repair which has occurred and the survival in G_2 cells were both fraction size sensitive.

It is possible that increased usage of HR in early-reacting normal tissue or cancer cells could result in the decreased fraction size sensitivity seen in these systems. Somaiah et al. (2012) applied coimmunostain in breast skin biopsies of the basal epidermis, a self-renewal and early reacting normal tissue, demonstrating an increase S/G_2 phase %, proliferation (Ki67), p21 activation and RAD51 foci between the first and final fraction (25 fractions of 2 Gy). A ten-fold increase in basal epidermal RAD51 foci by the end of breast radiotherapy and data consistent with a complete G_2/M arrest was postulated to explain the low fractionation sensitivity of human early skin reactions, a mechanism not supported by the results presented in this chapter. In cancer, there is evidence for an increase in HR use in some breast cancers (Mao et al. 2009) but is complicated by the recent reclassification of breast cancer fractionation sensitivity. Additionally, many cancers are deficient in HR repair.

Substantial differences between recovery factors are easy to interpret but subtle differences are not, and these are potentially relevant at a clinical endpoint. The RF factors calculated in our data (Figure 3.2 E) are close between phases and do not show a clear pattern between the two fractionated courses. We therefore have no evidence of cell cycle stage-specific difference in fractionation sensitivity and conclude that this is not a major factor in determining fraction sensitivity in this model system.

3.4.5 Association with proliferation revisited

As discussed previously, fractionation sensitivity negatively correlates with proliferation rate across both normal tissue and cancer (Thames et al.

1982, Wilson 2007, Somaiah, Rothkamm, and Yarnold 2015). In our analysis, we were therefore careful to ensure that proliferation was excluded from the experimental design. This allowed us to assess the effect of repair completion within one cell cycle phase, without damage progression through the cell cycle acting as a confounding effect. The data presented rejects the hypothesis that an increased percentage of cells undertaking repair in S/G_2 alone facilitate an HR dependent decrease in sensitivity. We must consider alternative hypotheses as to causal factors behind the association to proliferation speed, if they do indeed exist. To do so, it is beneficial to consider the situation in both insensitive early-reacting normal tissue and cancer.

Replication and mitosis are the stages where DSBs are the most dangerous. Perhaps fractionation sensitivity is primarily dependent on having a sufficient amount of time within G_1 or G_2 to facilitate repair in order to prevent progression of damage into replication/mitosis. Fast-growing tissues have stronger signalling for proliferation and spend less time in G_1. It is likely this same pressure is placed upon both DNA damage checkpoints at G_1/S and G_2/M. It would be beneficial to determine the strength of DNA damage checkpoint arrest across a range of early and late-responding normal models. Our 1BR3 hTERT late-reacting model has intact checkpoint control, resulting in accumulation in the G_1 and G_2 phases post irradiation, imparting time for repair. The most substantial difference in fractionation sensitivity comes from the comparison between the two fractionated courses in S phase (Figure 3.2 E), in which the 2 Gy x4 split course compared to the 4 Gy x2 course has a recovery factor increase from 2.107 to 2.906, respectively. Perhaps the

increased fractionation of the dose is benefitting survival through S phase as more DNA is undergoing replication prior to IR delivery. Early-reacting tissue, due to a greater proliferation rate, can be considered to be under more signalling pressure to move through the cell cycle, potentially giving insufficient time to derive a benefit from fractionation. However, as previously mentioned Somaiah et al. (2012) demonstrate an increase in proliferation alongside an increase in the percentage of cells in S/G_2 phase from the first to the final fraction in biopsies of the basal epidermis. Furthermore, there is no increase in the mitotic marker phospho-Histone H3 in this period, which suggests G_2 arrest (Turesson et al. 2010). It would therefore seem that the G_2 checkpoint is robust in their model, preventing progression with damage within the timeframe of irradiation. In this example, a relatively fraction size-insensitive tissue becomes further insensitive following 4 weeks of treatment. Somaiah et al. (2012) present the hypothesis that an increase in the S/G_2 phase % facilitates HR usage for a higher fidelity of repair. Our data would suggest that availability of HR alone is insufficient to impact fractionation sensitivity, assuming 15% of repair is facilitated by HR, but an increase in usage between fractions could be sufficient and is suggested by the demonstrated increase in RAD51 foci. It is also possible that the G_2 arrest, whilst robust between fractions and re-invigorated by each additional fraction could leak following treatment completion, allowing damage to enter mitosis to such an extent that there is no remaining benefit to be gained from fractionation.

A lack of time for accurate and complete repair could also be more pronounced for fractionation insensitive cancer cells, which commonly lose

P53 and cell cycle checkpoint control. Additionally, a hallmark of cancer is the ability to tolerate genome instability (Hanahan and Weinberg 2011). Cancer cells are capable of preventing cell death pathways from becoming triggered by damage. To highlight this, LIGIV deficient mice embryos die during development but p53 negative LIGIV deficient embryos survive to birth, underlining the role of p53 in determining damaged cell fate (Frank et al. 2000). These two factors together could prevent fractionation sparing survival in cancer.

We conclude that the availability of HR repair in our normal late-reacting tissue model does not impact fractionation sensitivity when proliferation is controlled for. It remains to be discovered whether either upregulation of HR usage or a greater pressure to proliferate with damage could result in fraction size insensitivity and give a causal explanation to the negative association between proliferation rate and fractionation sensitivity. Ideally, our next step would be to examine HR use in proficient cancer cell lines and adapt our assays for analysis of these cell lines with the addition of HR inhibition. Alternatively we could utilise our normal cell line model and allow cell cycle progression during repair with a range of proliferative pressures by manipulating cell cycle control to examine the effect on fractionation sensitivity.

4 Kinetics of DSB Repair with Fractionation

As previously described, there has been limited analysis performed on the kinetics of DSB repair following fractionation. However, a greater understanding of the induction, efficiency of clearance, and the number of breaks that are misrepaired or unrepaired could give vital insight towards determining the mechanistic basis of fractionation sensitivity. In our 1BR3 hTERT model, we questioned whether the induction of damage is altered between the initial dose and following fraction. A lower induction of damage with a following fraction could suggest alterations take place between doses that decrease radiosensitivity, priming the cell to future damage. Similarly, this analysis would indicate whether the kinetics of repair remain constant between initial doses and subsequent fractions. A more efficient repair of damage with a second dose would suggest alterations between doses that increase the capacity to repair damage. Finally, given the known correlation between misrepair and survival, we asked whether the proportion of damage that remains un-repaired is, as expected, the same between single and fractionated dose courses. In order to do this, we utilised γ-H2AX foci analysis as a sensitive surrogate biomarker for DSBs.

4.1 γ-H2AX foci induction and repair kinetics are constant between fractions

In order to examine DSB repair over time, 1BR3 hTERT cells were seeded on coverslips in dishes and allowed to grow to confluence arrest to enrich a G_0/G_1 population and remove potential analysis of S/G_2 cells. This

A

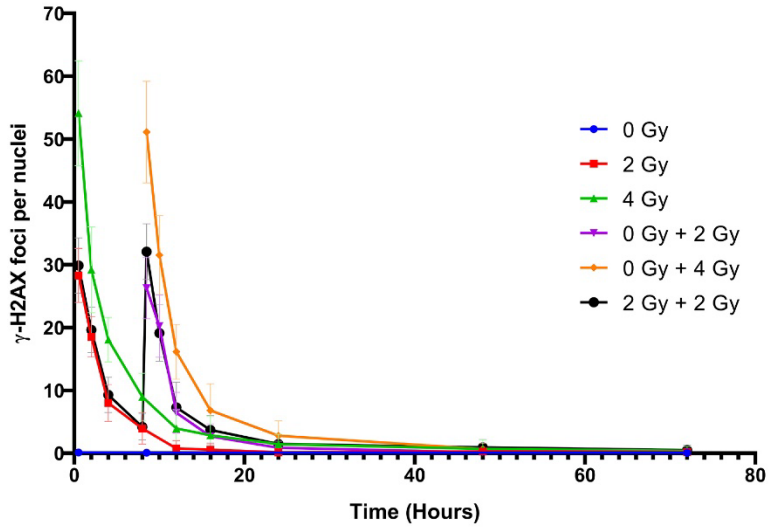

B

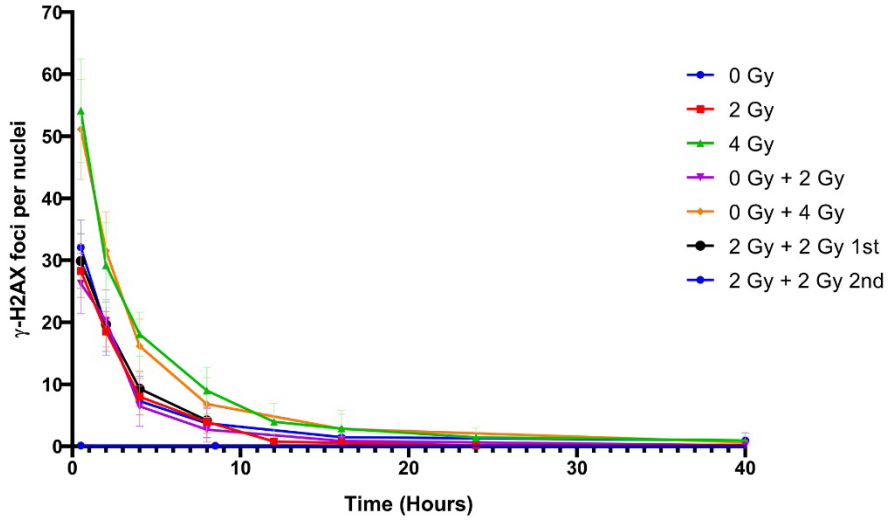

Figure 4.1 Rate of DSB repair by γ-H2AX foci analysis following single and split fractionation dosage in 1BR3 hTERT.

A) *Fractionated (split dose) and delayed doses were given 8 hours after first fraction in confluence arrested 1BR3 hTERT. The first time-point following IR (single dose and fractions) were fixed 30 minutes after delivery. Induction of breaks after second 2 Gy fraction is cumulative on top of the un-repaired foci from the first dose. 40 nuclei per condition, error bars SD, n=1.* ***B)*** *Initial, delayed and fractionated doses are overlaid such that they start at the same time to aid visual comparison.*

A

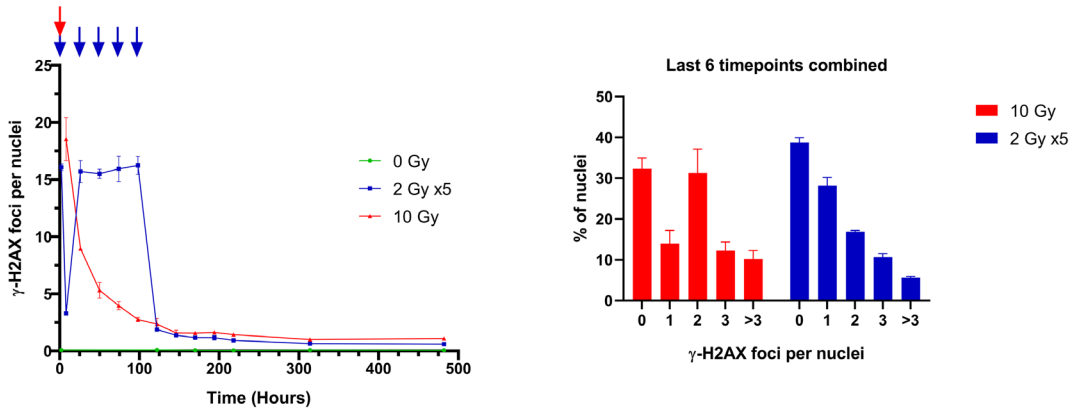

B

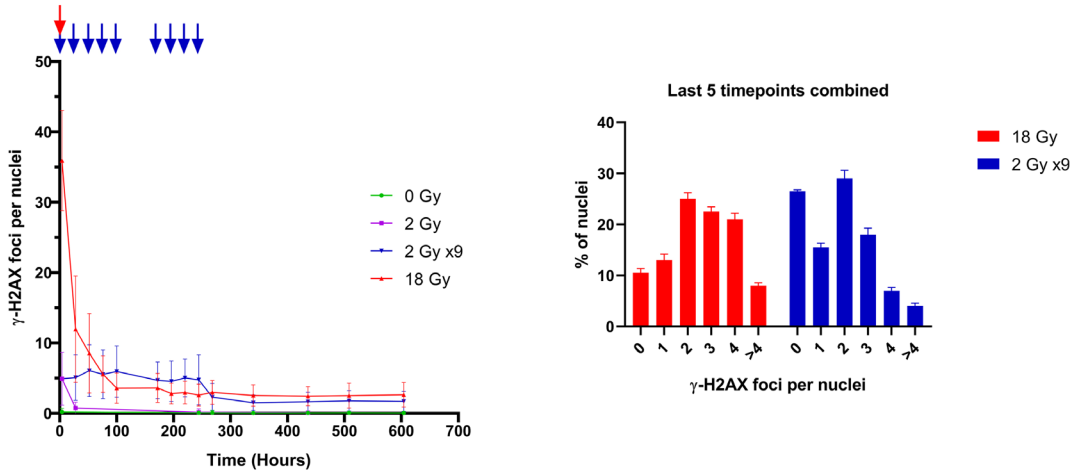

C

	Final timepoint γ-H2AX per nuclei
0 Gy	0.06
10 Gy	1.10
2 Gy x5	0.61
0 Gy	0.05
2 Gy	0.27
18 Gy	2.65
2 Gy x9	1.7

Figure 4.2 Large IR doses and long repair times reveal an un-repaired DSB component measured by γ-H2AX foci which are spared with fractionation.

A) *Left: Confluence arrested 1BR3 hTERT were irradiated with a single dose of 10 Gy or 2 Gy fractions x5 with 24 hours between fractions. The first time-point following IR (single dose and fractions) were fixed 2 hours after delivery, arrows indicate dose delivery. Right: Histogram of the distribution of γ-H2AX foci per nuclei averaged between the last 6 time-points. 40 nuclei per condition, error bars SD between repeats, n=2.* ***B)*** *Left: Confluence arrested 1BR3 hTERT were irradiated with a single dose of 18 Gy, 2 Gy or 2 Gy fractions x9 with 24 hours between fractions, with the exception of between the 5th and 6th fraction of 72 hours. The first time-point following IR (single dose and fractions) were fixed 4 hours after delivery, arrows indicate dose delivery. Right: Histogram of the distribution of γ-H2AX foci per nuclei averaged between the last 5 time-points. 40 nuclei per condition, error bars SD, n=1.*

was done to ensure a robust scoring of foci by eye, removing the need to determine between G_1 and G_2 cells, since G_2 cells have double the DNA content and number of foci. Cells were irradiated with single or fractionated doses and cells were fixed at varying time-points thereafter. Because γ-H2AX foci formation is delayed after irradiation and higher doses lead to a large number of foci that are hard to accurately quantify, we chose small doses for these experiments. Using 2 Gy doses delivered 8 hours apart; we measured the kinetics of repair of both the initial dose and the second fraction. We found that there was no change in DSB induction levels with the second fraction when the existing un-repaired damage was accounted for (Figure 4.1 A). Additionally, a 24 hour period between multiple 2 Gy doses was used, which is sufficient for complete repair, the same result was found (Figure 4.2 A&B). Moreover, the efficiency of repair did not observably change in either the fast or slow repair component between the initial dose and the second fraction (Figure 4.1 B). Together, these results suggest that the cumulative number of DSBs induced by a second fraction is similar to an equivalent total dose and that the efficiency of repair following the first dose is similar to that of the subsequent dose.

4.2 Fractionation results in fewer late γ-H2AX per nuclei

We wanted to extend these analyses to larger total doses and to the use of multiple fractions to more closely reflect clinical conditions. Therefore, following single large doses (10 Gy or 18 Gy) or the same total dose delivered in 2 Gy daily fractions, the kinetics of DSB γ-H2AX were again measured (Figure 4.2 A&B Left). Surprisingly, the level of un-repaired DSBs as measured

by persistent g-H2AX foci seemed to decrease with fractionation and this difference was greater with the larger total dose (Figure 4.2 C).

To further explore this sparing effect, we analysed the distribution of the DSB numbers per cell in each condition for time-points at which the repair process should be complete (Figure 4.2 A&B Right). This demonstrated a distribution difference between the fractionated and single dose IR courses, with a shift towards fewer or no foci per nuclei in cells treated with fractionated doses. This supports the idea that the average number of un-repaired breaks presented in Figure 4.2 C was not due to outliers in either population. This result suggests that fractionating the dose results in more complete repair of DNA DSBs. Nevertheless, this was a small and subtle difference in foci number, so we used a more robust and independent approach to examine whether this difference was significant. An asynchronous population of 1BR3 hTERT were given a single 4 Gy dose, 8 Gy dose, or two 4 Gy fractions separated by 8 hours. Six days after the initial dose, the presence of unrepaired DNA DSBs was analysed using both γ-H2AX foci and 53BP1 foci that were analysed by a customised cell profiler pipeline. The number of γ-H2AX foci at this late time point was found to be significantly spared by the fractionated dose course compared to the single dose (Figure 4.3 B). The distribution of the breaks again indicated a shift towards lower breaks per cell in the fractionated sample, but no clear increase of the nuclei with no foci (Figure 4.3C). Contrastingly, 53BP1 foci were not spared with fractionation when examining either mean number or distribution (Figure 4.4 A&B). The implications of these findings are discussed later.

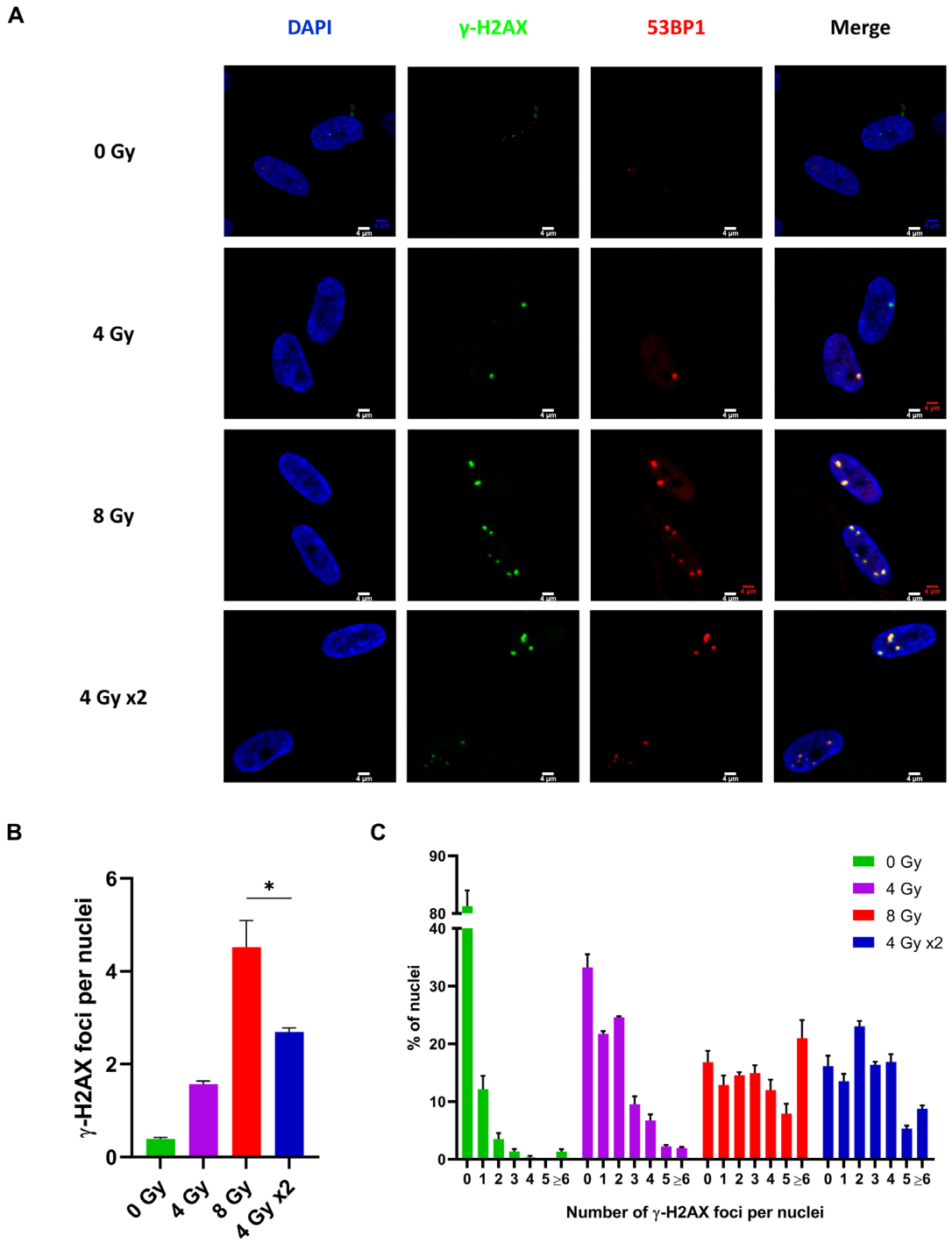

Figure 4.3 Sparing of γ-H2AX foci is found between 8 Gy vs 4 Gy x2 after 6 days of repair in 1BR3 hTERT.

A) *Asynchronous 1BR3 hTERT was irradiated with a single 8 Gy, single 4 Gy or 4 Gy x2 fractions, with the second fraction delivered after 8 hours, cells were fixed after 144 hours. Example images of DAPI, γ-H2AX, 53BP1 antibody guided immunofluorescence microscopy at 40x magnification.* ***B)*** *γ-H2AX foci analysed by cell profiler pipeline. A minimum 138 nuclei examined per biological repeat, p = 0.033 (t-test, two tailed, equal variance), error bars SEM, n=3. Mean values: 0 Gy 0.388, 4 Gy 1.57, 8 Gy 4.52, 4 Gy x2 2.69.* ***C)*** *Histogram of the distribution of γ-H2AX foci per nuclei in all conditions, error bars SEM.*

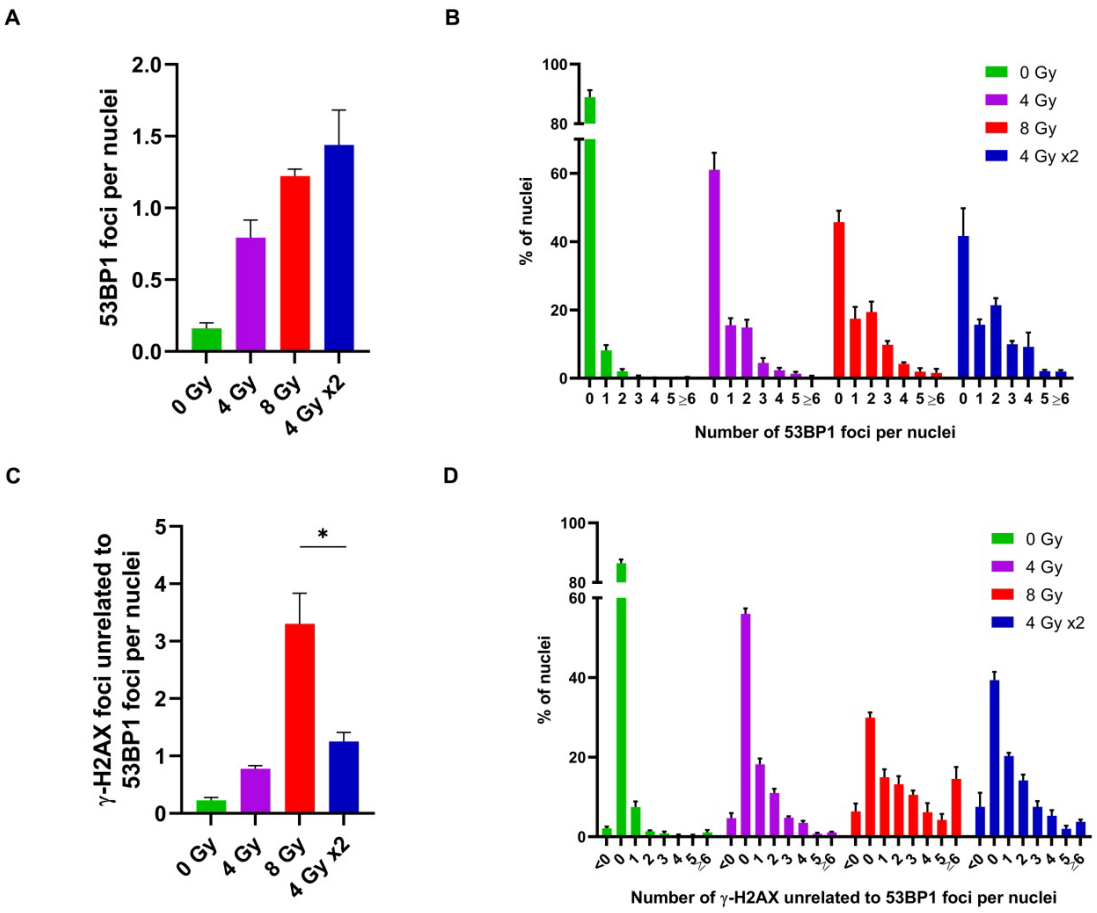

Figure 4.4 53BP1 foci are not spared, γ-H2AX foci unassociated with 53BP1 are spared by 8 Gy vs 4 Gy x2 after 6 days of repair in 1BR3 hTERT.

A) *Asynchronous 1BR3 hTERT was irradiated with a single 8 Gy, single 4 Gy or 4 Gy x2 fractions, with the second fraction delivered after 8 hours, cells were fixed after 144 hours. 53BP1 foci analysed by cell profiler pipeline. A minimum 138 nuclei examined per biological repeat, error bars SEM, n=3.* ***B)*** *Histogram of the distribution of 53BP1 foci per nuclei in all conditions, error bars SEM.* ***C)*** *53BP1 foci were almost all co-localised with γ-H2AX foci. γ-H2AX foci number independent of 53BP1 foci were analysed by cell profiler pipeline, p = 0.021.* ***D)*** *Histogram of the distribution of γ-H2AX foci per nuclei in all conditions, <0 indicates instances of unassociated 53BP1 foci, error bars SEM.*

4.2.1 Spared un-repaired γ-H2AX foci are not associated with 53BP1 foci

There were fewer 53BP1 foci than g-H2AX foci, and the 53BP1 foci were almost all co-localised with γ-H2AX foci. We therefore examined the mean and distribution of γ-H2AX foci that were not associated with 53BP1 and demonstrate that this subset of foci seems to account for the foci spared with fractionation. Further, there is a decreasing ratio of 53BP1 foci to γ-H2AX foci with dose that is lessened with fractionation (4 Gy 0.51:1, 8 Gy 0.27:1, 4 Gy x2 0.53:1).

4.3 Discussion

4.3.1 Controlling foci analysis

Discovery of γ-H2AX foci has provided a novel surrogate biomarker for DSBs and a convenient means to assess DSB repair (Kuo and Yang 2008). Although a useful surrogate for DSBs, IRIF use has its limitations. For example, the number of IRIF induced do not reach the expected numbers of DSBs measured by pulsed-field gel electrophoresis (PFGE) studies. PFGE studies suggest that DSB repair occurs exponentially immediately following damage induction; however, IRIF appearance is delayed with induction peaking between 30 minutes to 1 hour after damage. IRIF have also been suggested to appear faster as dose increases and persist for longer (Neumaier et al. 2012). Finally, IRIF experiments must be carefully designed to remove the confounding variable of proliferation. G_2 cells, if counted, contain double the number of foci due to their 2N DNA content, whilst S phase cells demonstrate pan-nuclear staining that can skew results (Beucher et al. 2009). Further, indirect damage from IR through processing stalled or collapsed replication forks can occur in replicating cells. Finally, the formation of IRIF is

entirely dependent upon DNA damage sensing and signalling, this must be considered in experimental analysis, especially for signalling differences between cell cycle stages. Despite these issues, IRIF analysis can still be a useful surrogate to the progression of repair and has been instrumental in identifying repair defective tissue (Martin et al. 2013).

In order to ensure accuracy within our analysis we were careful to only examine cells within the same cell cycle stage. This was achieved by either G_0/G_1 arrest (Figure 4.1 & Figure 4.2) where cells were held in G_0/G_1 throughout or by nuclear size gating (Figure 4.3 & Figure 4.4). There can also be differences in response between cell cycle phase, in the latter experiments we cannot be sure of the cell cycle phase that the cell was irradiated was in but are able to demonstrate that the G_2 nuclei at the 6-day time-point had the same result (not shown). γ-H2AX foci act as a surrogate for DSBs, but it is possible that they can persist after repair has completed, and it is not possible to determine whether this has occurred from the IF data. In addition to this issue, IRIF do not always correspond to damage induced directly by IR. They can also be induced by derived damage, such as through transcriptional failure, especially in the context of misrepaired damage in the genome and could still therefore be classified as a consequence of misrepair. There is a greater potential for derived damage in the latter experiments where the cell cycle is not arrested and therefore cells with damage may enter replication or mitosis. Finally, there is the potential for substantially different numbers of foci to be determined based on the conditions used and the analysis method (including thresholding set). The initial 18 Gy and 10 Gy experiments were

scored by eye with attempts made to ensure the entirety of the 3D nucleus was examined. However, it is difficult to identify smaller foci from the background by eye; comparatively, the confocal microscopy performed over z-stacked layers with deconvolution and projection gives a much more accurate representation of the number of foci. The background of foci identified in the 0 Gy is higher too. Our figures in both regards complement the work of Ruprecht et al. (2019) who use 3D nuclei reconstruction with confocal microscopy in comparison to foci scored in 2D. As previously mentioned the potential for derived breaks with replication or proliferation could also result in an increase between experiments. This is important to understanding our own results and in comparison from others (Löbrich et al. 2010).

4.3.2 γ-H2AX Induction between fractions

Mariotti et al. (2013) suggest that in the AG01522 primary fibroblast that a <5-hour gap between 1 Gy fractions results in a decrease in γ-H2AX induction of up to ~13 foci that is lost with a 12-hour gap between 1Gy fractions (timeframe for complete repair). However, this result does not correspond with their own clonogenic survival data, which they cannot explain. Additionally, the second fraction is suggested to have slower kinetics of repair. Despite using a higher dose (2 Gy), we don't see evidence of either result in our system. Instead, induction following 2 Gy fractions remains consistent both when existing damage is accounted for (8 hours between fractions) or not (24 hours between fractions). Additionally, repair kinetics of the second dose are not slowed. The difference in response between these analyses could be due to a difference in cell line response but are more likely to be explained by technical

differences in the analysis resulting from the discussed limitations to foci analysis. We consider our analysis to be more robust, primarily as our analysis was independently scored by computational analysis compared to by eye by one operator. We therefore conclude that there is no difference in induction or repair kinetics between identical fractions in 1BR3 hTERT. This suggests that for 2 Gy doses there doesn't seem to be a considerable effect of any adaptive response from the first 'priming' fraction. Additionally, the lack of a difference in induction and kinetics supports a misrepair hypothesis as the fidelity of repair is not assessable and therefore hidden. This consideration is made possible as an addition to the evidence of decreased aberration formation and increased survival with fractionation.

4.3.3 Unrepaired vs misrepaired

The extent to which repair is completed for either single or fractionated doses has never been definitively answered. Some proposed models suggest a role of un-repaired breaks in the ability of fractionation to result in sparing of cellular survival. The target theory model suggests that the shoulder on cell survival curves results from the number of unrepaired lesions per cell (Chadwick and Leenhouts 1973). However, the literature is strongly weighted towards misrepair being the crucial component determining the survival fit to the LQ model. One reason for this is that the LQ increase in misrepair aberrations in cytogenetic analysis correlate well with dose, and unrepaired aberrations are relatively rare after long repair times (Savage 2004, Bedford and Cornforth 1987). The existence of an un-repaired component of damage with irradiation following complete repair is therefore a topic of controversy in

the field that has been reopened in recent years.

Moving away from classical cytogenetic analysis, Löbrich et al. (2000) demonstrated by a PFGE approach with very large doses that after 80 Gy in normal human fibroblasts essentially all damage is repaired (0-2% unrepaired) but that AT homozygous cells have 10% of DNA breaks left unrepaired. Riballo et al. (2004) demonstrate using γ-H2AX analysis that both ATM and Artemis deficient cell lines show a 10% proportion of damage left unrepaired 3 days after damage with 2 Gy. Further, LIG4 removal results in the vast majority of breaks remaining un-repaired. Loucas and Cornforth (2013) demonstrate with mFISH chromosomal analysis a 5% level of unrepaired breaks from γ rays and *α* particles and, despite high LET similar to *α* particles, a 14% level following Fe ion IR. They demonstrate that this increase is due to an increase in incomplete exchanges and hypothesise that there must be an increasing tendency for incompleteness as the number of breaks potentially involved in exchange increases. In particular, they suggest that this is a spatial effect, which reflects the maximum distance over which breaks can interact. It would seem therefore that there is clear evidence of a substantial unrepaired component in certain circumstances.

Identifying unrepaired breaks in the order of 0-5% in normal repair proficient cell lines is difficult and this can affect the conclusions reached in the studies most relevant to our own analysis that utilised IRIF. The senescent growth arrest of fibroblasts has been central to this. The long term viability of fibroblasts, which enter growth arrest in response to IR, allows for repair to be examined at time points beyond the point where apoptotic death would limit

this analysis in other cell lineages. However, studies have suggested that the persistent foci seen in fibroblast cell lines drive a stress dependent senescent response. Rodier et al. (2011) argue that persistent foci are DNA segments with chromatin alterations reinforcing senescence (DNA-SCARS) with an altered (larger and brighter) morphology to transient breaks. To support this they highlight an association with PML (promyelocytic leukaemia) nuclear bodies (a stress associated response) and a lack of RPA and RAD51 foci. Additionally, when they deplete H2AX this did not deplete 53BP1 at the foci but did decrease MDC1 presence, CHK2 activation and p53-dependent growth arrest. They therefore suggest that the foci form as a stress response. They do not explicitly comment on whether the damage to initiate formation remains un-repaired, i.e. if the DNA-SCAR precludes repair or persists after repair. However, the suggestion of a different mechanism or type of foci development calls into question whether they can be used as a surrogate for DSBs.

Ultrastructural analysis using transmission electron microscopy utilising gold conjugate beads attempted to address whether persistent foci relate to unrepaired damage. Lorat, Schanz, and Rübe (2016) demonstrate that with repeated low-dose IR in mouse cortical neurons there was an increase of persisting foci with cumulative doses and that these differences were most pronounced in repair deficient mice. In wt mice, 53BP1 was shown to locate to these foci but not Ku. Persistent foci in the repair deficient mice had a much greater association with Ku. As Ku is a sensitive detector of DSBs they suggest the foci in the wt mice do not relate to unrepaired breaks, but reflect alterations in heterochromatin.

Finally, Noda et al. (2012) argue that persistent foci in their human normal fibroblast model do represent unrepaired breaks and that their formation is linearly correlative with dose. To support this, they demonstrate that almost all recognised DNA damage foci accumulate at persistent foci and that phosphorylated DNA-PKcs, essential for the onset of NHEJ, accumulates at persistent foci. They also demonstrate an increase of persistent foci with LIG4 inhibition and knockdown. Most interestingly, with an ATM inhibitor treatment persistent foci were not formed, but following removal of the inhibitor at late time points the foci would then form. This suggests that the foci are dependent on an ongoing signalling response. Finally, they use histogram distributions to suggest that persistent foci tend to exist in pairs, suggesting that this could be both ends of an unrepaired break (or two breaks if from incomplete exchanges). This seems extremely unlikely due to the weight of evidence demonstrating DSB break ends are kept in close proximity by the chromatin architecture and scaffold action of repair proteins (Jain, Sugawara, and Haber 2016, Lobachev et al. 2004).

Taking this knowledge together, we can consider our own data. We certainly have persistent foci that increase with dose. Noda et al. (2012) suggest that in their system 3.2 Gy is required to generate 1 unrepaired focus. At 4 Gy and 8 Gy they predict ~1.25 and ~2.9 persistent foci respectively. We see 1.58 and 4.52 respectively. Therefore despite being able to judge relative foci size or intensity without our own earlier point of comparison, it would seem we are seeing the same structures. However, they do not suggest, as we see, that there is an increasing proportion of these foci which do not co-localise with

53BP1. They do not determine between kinetics for different foci, with most figures attributed to IRIF broadly rather than a specific protein. It is likely that their analysis is based on γ-H2AX analysis (as the most prevalent foci used for foci analysis) and there is evidence of unrelated γ-H2AX foci to other foci in their exemplar persistent foci images. They do however suggest that 53BP1 accumulation at persistent breaks requires continuous ubiquitylation of substrates, as inhibition of polyubiquitylation results in the rapid disappearance of 53BP1 foci at late time-points. This could suggest that we are seeing a ubiquitylation based limiting factor response to the localisation of 53BP1 with dose. Finally, our histogram distributions seem to partly demonstrate pairs of persistent foci. With 8 Gy (single or 4 Gy fractions) 53BP1 foci both show an overrepresented proportion of 2 foci per nuclei compared to a Poisson distribution. Total γ-H2AX demonstrates this at both 2 and 4 foci per nuclei but only with fractionation, correspondingly 4 Gy shows a 2 foci overrepresentation and the unassociated γ-H2AX foci show no overrepresentation with or without fractionation. We have no viable explanation to give for the phenomena.

If these persistent foci do truly represent un-repaired breaks, then this would suggest the target theory is supported, in relation to a role for unrepaired damage to impact on survival. Even if they are not, then the senescence associated growth arrest suggested to result from them could clearly impact survival, especially with bystander effects. More work is required to understand the response we are seeing and the implications for fractionation sensitivity.

5 The Chromatin Environment and Fraction Size Sensitivity

As previously described, the locality of DSB damage within the chromatin environment affects the choice of repair pathway. Additionally, the chromatin environment has been demonstrated to respond to damage; one example of this is damage induced transcriptional repression. We wanted to more broadly investigate whether alterations within the chromatin environment following a first fraction of irradiation benefit the repair of damage induced by further fractions, therefore modulating fractionation sensitivity. In order to test this, we took two approaches using clonogenic survival analyses as the endpoint.

5.1 Histone deacetylase inhibition by SAHA does not modulate fraction size sensitivity

The first approach taken was to target the action of histone deacetylases (HDACs), which control the acetylation status of lysine residues in core histones within nucleosomes. HDACs are a major factor in determining both chromatin compaction state and gene regulation. In the absence of acetylation, the positively charged histones interact with the negatively charged DNA phosphate groups. Acetylation decreases the positive charge of the histone, weakening this interaction with DNA, which can result in a more relaxed chromatin environment. In addition, acetyl groups on the histone proteins can form binding platforms for proteins that regulate chromatin compaction and/or gene expression. Acetylation state is controlled by histone acetyltransferase (HAT) and histone deacetylase enzyme activities. By targeting the action of

HDACs with chemical inhibition, we can examine whether a significant alteration of the global chromatin compaction status impacts fractionation sensitivity.

Suberanilohydroxamic acid (SAHA), also known as Vorinostat, is a broad HDAC inhibitor which acts on class I, II and IV HDACs (Kim and Bae 2011). SAHA has been demonstrated to suppress the growth of cells and cause cell death via apoptosis at high concentrations (Butler et al. 2000, Hrzenjak et al. 2010, Kumagai et al. 2007, Huang and Pardee 2000) but does not cause cell cycle redistribution (Singh et al. 2010). In order to use SAHA within clonogenic survival analyses, we had to first ascertain a tolerable SAHA concentration that would not substantially decrease cell proliferation, hindering the identification of clones derived from surviving cells. Additionally, SAHA has been demonstrated to radiosensitise normal cell lines at higher concentrations (Purrucker et al. 2010, Frame et al. 2013). Whilst the RF factor gives a relative read out of any difference seen in survival with fractionation, where possible we want to avoid radiosensitisation, which would make any specific effect on fractionation more difficult to delineate.

5.1.1 Determining SAHA treatment conditions

In order to establish experimental conditions, the growth of cell populations treated with a range of SAHA concentrations was measured using live cell microscopy over a period of 4 days. We found a decrease in the growth of 1BR3 hTERT with increasing concentrations of SAHA between 0.1 – 0.5 μM (Figure 5.1 A). Additionally, we examined the acetylation status

of H3 following treatment with varying concentrations of SAHA for 0, 4 or 24 hours (Figure 5.2 A & B). This demonstrated an increase in acetylation with

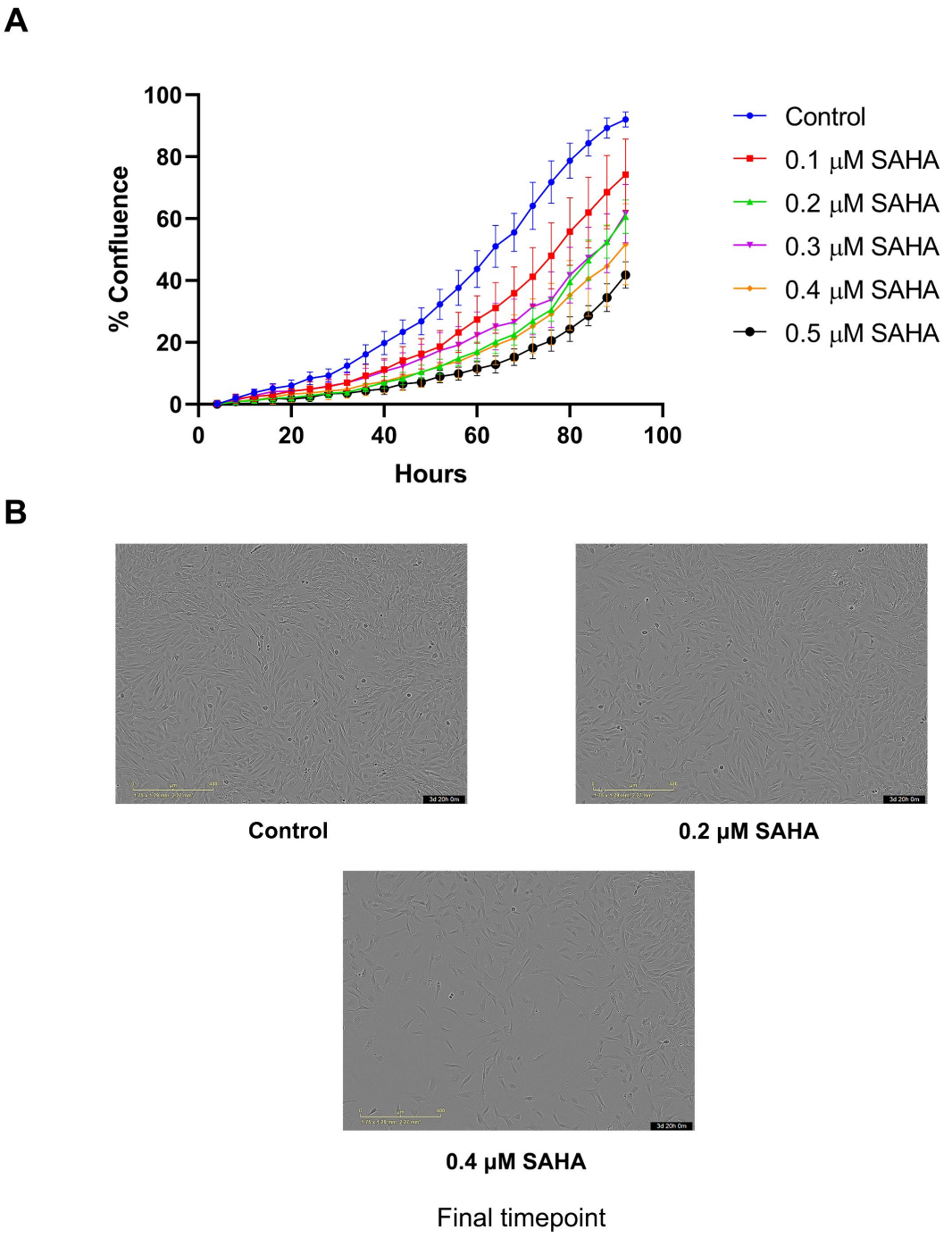

Figure 5.1 SAHA causes a growth defect in 1BR3 hTERT.

A) *Incucyte analysis of cell growth over 4 days determined by % area covered by cells (confluence), starting confluence normalised to 0, error bars are SEM.* ***B)*** *Incucyte images taken from the final time-point of analysis.*

A

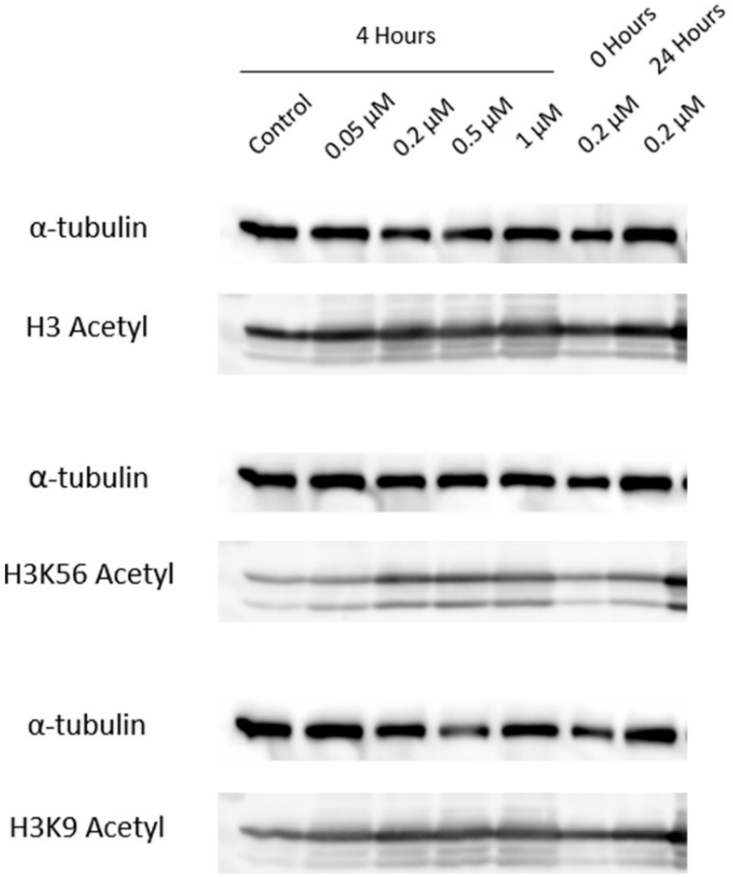

B

		4 Hours				0 Hours	24 Hours
	Control	0.05 µM SAHA	0.2 µM SAHA	0.5 µM SAHA	1 µM SAHA	0.2 µM SAHA	0.2 µM SAHA
H3 Acetyl	1.00	1.35	2.36	2.00	1.65	1.66	1.24
H3K56 Acetyl	1.00	1.07	2.55	2.31	2.48	1.82	1.43
H3K9 Acetyl	1.00	1.30	1.98	2.96	1.75	2.73	1.45

Figure 5.2 HDAC inhibition by SAHA increases H3 acetylation in 1BR3 hTERT.

A) *Western Blot analysis of acetylation state of H3 with SAHA treatments. H3 Acetyl antibody is specific to acetyl K9, K14, K18, K23, K27.* ***B)*** *Relative expression of acetylation after controlling by tubulin loading for SAHA treatments.*

both the multiple target antibody (labelled H3 Acetyl) and the H3K9ac and H3K56 specific antibodies. Of the exposure times investigated, 4 hours caused the greatest increase in acetylation. Based on these findings, we chose 0.2 μM SAHA for use in all future assays, since this had the optimal balance between the effect on growth and acetylation.

5.1.2 Clonogenic survival analysis demonstrates treatment with SAHA does not alter fractionation sensitivity

Clonogenic survival assays were done with cells treated with 0.2 μM SAHA added either 0 hours (immediately prior to irradiation), 4 hours or 24 hours prior to irradiation. SAHA remained in the media throughout colony growth. No significant radiosensitising of 1BR3 hTERT following a 0 or 4 hour treatment at 0.2 μM SAHA prior to IR was observed (Figure 5.3 A). However, treatment with 0.2 μM SAHA for 24h prior to IR did radiosensitise 1BR3 hTERT with a significant decrease in survival against the control at 4 Gy (T-test, two-tailed, equal variance, p= 0.00003 ***) and 8 Gy (T-test, two-tailed, equal variance, p= 0.00032 ***) (Figure 5.1 B).

In addition, treatment with SAHA was used to examine whether the extent of chromatin relaxation could modulate fractionation sensitivity by irradiating cells with split doses. Here, we found that the 0 hour and 4 hour treatments did not alter the fractionation sensitivity, as seen by the similar RF factors and significant sparing of survival in Figure 5.3 C. Interestingly, the 24 hour pre-treatment did cause an increase in the RF factor from 1.73 to 3.40 (Figure 5.3 B & C). This shows an increase in fractionation sensitivity but is

difficult to interpret due to the radiosensitisation by SAHA under these

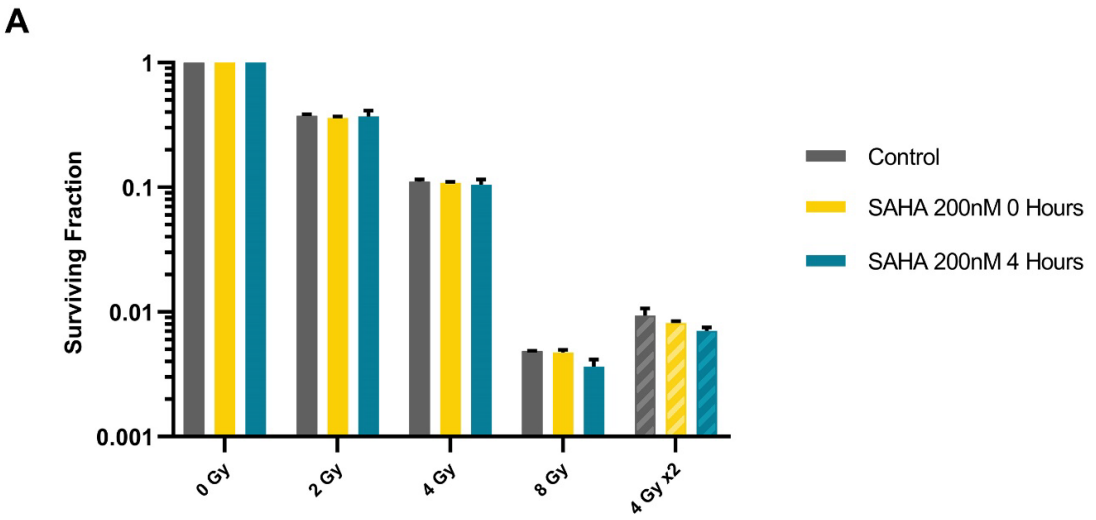

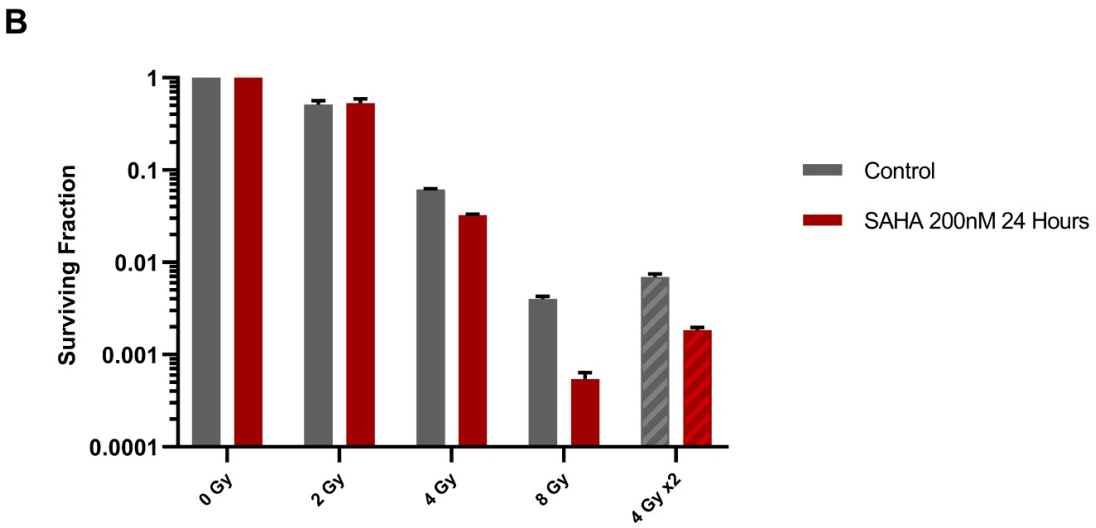

C

	RF 4 Gy x2/8 Gy	P value 4 Gy x2 vs 8 Gy	
Control	1.93	0.0274	*
SAHA 200nM 0 Hours	1.73	0.0007	***
SAHA 200nM 4 Hours	1.93	0.0085	**
Control	1.73	0.0092	**
SAHA 200nm 24 Hours	3.40	0.0014	**

Figure 5.3 Clonogenic survival analysis demonstrates SAHA treatment does not substantially alter fractionation sensitivity.

*Asynchronous 1BR3 hTERT were treated with SAHA 0.2 μM either immediately prior to irradiation (0 hours), for 4 hours or for 24 hours before being given single or fractionated dose courses, with the second split 4 Gy fraction given after 8 hours. A) Clonogenic survival following 0 and 4 hour treatment and B) 24 hour treatment. Results are plotted as bar graphs, dashed lines representing fractionated courses, error bars SEM, n=3. C) Table of the calculated recovery factors and t-test (two tailed, equal variance) results between the single and fractionated dose courses for each condition, * ≤ 0.05, ** ≤ 0.01, *** ≤ 0.001.*

conditions as discussed later.

5.2 BRG1 mutant cell lines remain fraction size sensitive.

Our second approach was to focus on BRG1, the catalytic ATPase of the PBAF and BAF SWI/SNF chromatin remodelling complexes. SWI/SNF functions as a tumour repressor and genes encoding subunits of SWI/SNF are mutated in 19% of cancer (Shain and Pollack 2013). PBAF is required for the DNA damage induced transcriptional repression (DITR) response to DNA double strand breaks (Kakarougkas et al. 2014). We set out to test the role of BRG1 in the cellular response to fractionation.

5.2.1 Generation of 1BR3 hTERT-based BRG1 mutant cell lines

To test the contribution of BRG1 to fraction sensitivity, we decided to create a knockout of the SMARCA4 gene (encoding BRG1) using CRISPR-Cas9 nickase technology in the 1BR3-hTERT cell line. Therefore, two gRNA guides specific to exon 2 of SMARCA4 were cloned into a plasmid containing Cas9n and mRuby (Figure 5.4). The resulting plasmid clone was transfected into 1BR3 hTERT via the Neon transfection system. 24000 cells were single cell sorted by FACS analysis for mRuby expression and grown separately. Those that formed colonies were then analysed for BRG1 expression by western blot and sequence alterations by PCR sequencing.

Despite substantial efforts, no clones were identified that completely lacked BRG1 expression. One possibility was that loss of function mutants were not produced. Alternatively, the growth of complete BRG1 knockout

A

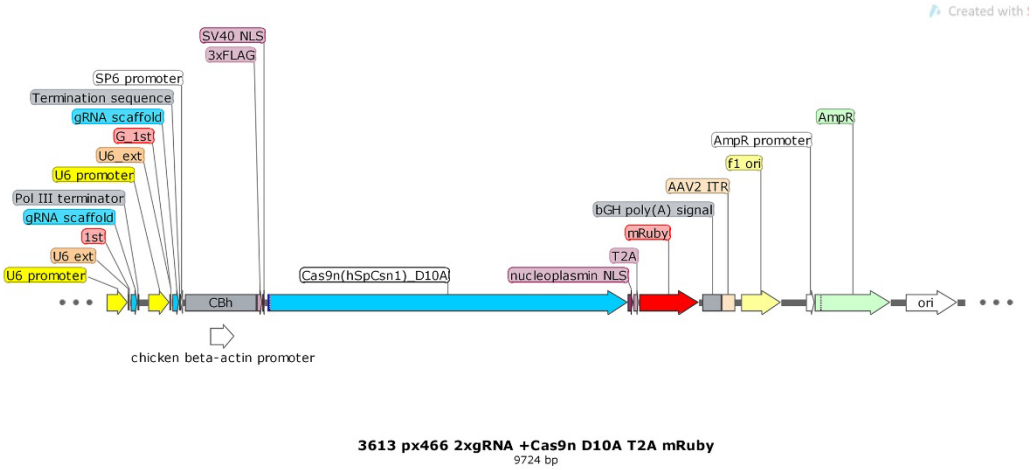

B

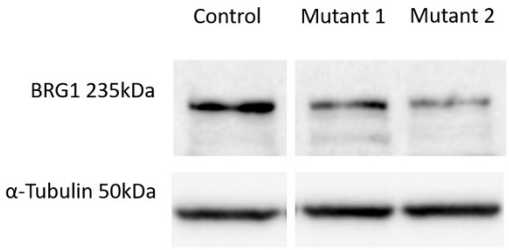

	BRG1 Relative expression
Mutant Clone 1	48%
Mutant Clone 2	19%

C

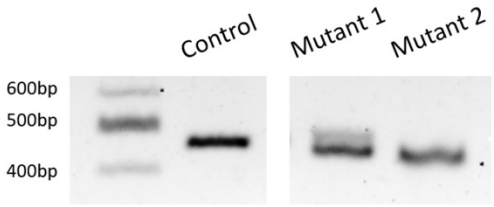

Figure 5.4 Validation of two BRG1 mutant 1BR3 hTERT clones generated by CRISPR-Cas9 nickase.

A) *Straightened map of the Cas9n plasmid backbone utilised to insert gRNA guides to target exon 2 of SMARCA4 (listed in methods).* ***B)*** *Western blot of BRG1 expression alongside table giving the relative expression of BRG1 to the 1BR3 hTERT control as measured by BRG1 band volume and relative loading controlled by α-tubulin volume.* ***C.*** *PCR product length for region encompassing gRNA target sites, mutant 2 demonstrated a single shortened product that facilitated sequencing, mutant 1 demonstrated two products, one shorter and one longer but the proximity prevented successful extraction for sequencing. PCR primer sequences and product sequence given in methods.*

A

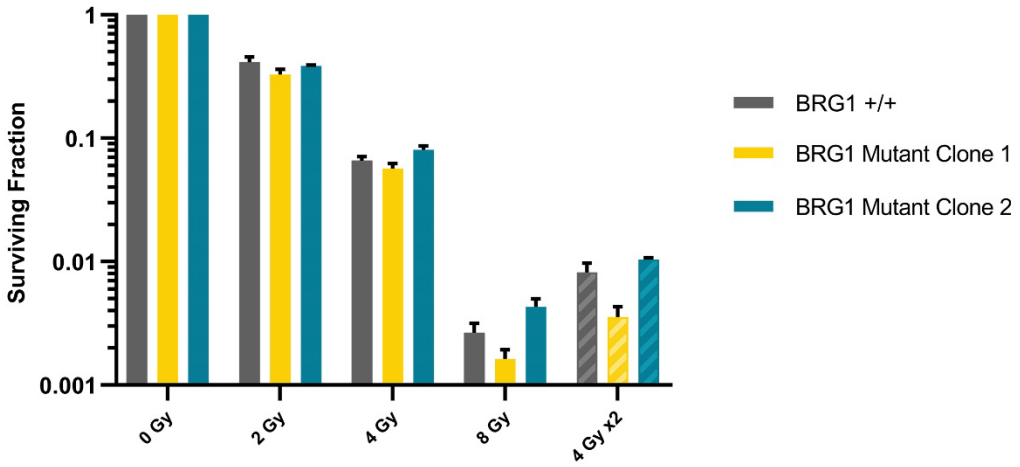

B

	RF 4 Gy x2/8 Gy	P value 4 Gy x2 vs 8 Gy	
Control	3.09	0.028	*
BRG1 Mutant Clone 1	2.19	0.076	
BRG1 Mutant Clone 2	2.41	0.002	**

Figure 5.5 Clonogenic survival analysis demonstrates that 1BR3 hTERT derived BRG1 mutant clones do not differ in fractionation sensitivity.

A) *Asynchronous cell lines were given single or fractionated dose courses, with the second 4 Gy fraction given after 8 hours. Survival results are plotted as bar graphs, dashed lines represent fractionated courses, error bars SEM, n=3.* ***B)*** *Table of the calculated recovery factors and t-test (two tailed, equal variance) results between the single and fractionated dose courses for each condition, * ≤ 0.05, ** ≤ 0.01.*

cells was severely impacted or BRG1 expression could be essential in the 1BR3 hTERT cell line.

However, we identified two clones with a significant decrease in BRG1 expression compared with the parental cell line (Figure 5.4 B). Primers flanking the gRNA target region were used to amplify the targeted region of the gene.

This demonstrated an altered sequence length in both mutants (Figure 5.4 C). The presence of two bands in clone 1 suggests that there is a CRISPR-Cas9 mediated deletion of one of the two SMARCA4 alleles. The remaining allele, if intact, could be responsible for the residual BRG1 expression in this cell line (Figure 5.4 B). Sequencing of the PCR product for mutant clone 2 revealed a 27bp site removal, which corresponds to the entire range between the target sequences. This deletion, presumably present in both alleles according to the single band in the PCR amplification, would result in an in frame deletion of amino acid residues (AAGATGTCCACTCCAGACCCACCCCTG). From the reduced expression of the protein, this suggests the loss of this region leads to unstable BRG1 expression.

While we were unable to produce cell lines that lack BRG1 expression entirely, we have created two cell lines with altered BRG1 expression, which could lead to changes in DNA damage responses, including fraction size sensitivity.

5.2.2 Sensitivity of BRG1 mutant cell lines to irradiation

Clonogenic survival analysis with fractionation was performed for both BRG1 deficient clones (Figure 5.5 A). Surprisingly, there was a significant difference in the radiosensitivity when comparing between the two clones for survival at 8 Gy (T-test, two-tailed, equal variance, p= 0.025 *). Clone 1 showed increased sensitivity relative to the parental line, which could suggest that the reduction of BRG1 expression leads to defective DNA repair following irradiation. In contrast, clone 2 appeared to be less radiosensitive than the

parental cell line (Figure 5.5 A). This could reflect the impact of the specific BRG1 mutation function in this cell line. However, more work is needed to determine whether this is the case.

Notably, although the difference between the two BRG1 mutant clones was significant, neither mutant clone was significantly different in radiosensitivity compared to the parental 1BR-hTERT cell line (Figure 5.5). Significant sparing with fractionation was found for mutant clone 2 but not for clone 1 with a p-value of 0.076 (Figure 5.5 B). However, the proximity of the RF factors suggest that with further biological repeats, both clones would demonstrate statistically significant sparing following fractionation (Figure 5.5 B).

5.3 Discussion

5.3.1 Delineating cellular clonogenicity response to radiation and fraction size sensitivity.

It is important to understand how at the clonogenic assay endpoint the cellular response to single radiation doses and fraction size sensitivity with multiple fractions can be delineated. Both are a response to the amount of damage caused and reflect the ability to repair that damage. Radiosensitivity as a cellular property classically defined by a response to 2 Gy and is therefore attributed to the linear α-component of damage. Often however, radiosensitivity or more specifically radiosensitisation is used to describe the cellular response across the linear-quadratic model. The differences described as radiosensitising in this chapter, seen between clonogenicity responses with

greater doses are reflective of changes to the β-component, reflecting repair capacity. This may occur alongside changes to the β-component with the addition of fractionation making the two effects indistinguishable.

Clonogenic analysis allows us to consider an effect on survival, but only up to the point where survival is quantifiable. Beyond the dose where this occurs, DSB repair can still be measured as a method to interrogate cellular responses to radiation. Cytogenetic analysis allows for this, but underrepresents the extent of repair or misrepair. Pulse field electrophoresis assays such as the FAR assays (similar to the comet assay) and the extension developed by Löbrich, Rydberg, and Cooper (1995) which utilises DNA probes for NotI restriction fragments to determine repair extent and misrepair extent by correct fragment size reconstitution, pushes the resolution further. In Löbrich et al. (2000), they utilise their NotI fragment probe system to consider the rejoining of breaks following a single 80 Gy dose and a range of fractionated courses up to an 80 Gy total dose in normal fibroblasts and Ataxia–telangiectasia cells. AT cells have a defective ATM gene and are highly radiosensitive. Löbrich demonstrates that induction of DSBs is the same between both cell lines and that for single doses between 80 Gy and 320 Gy misrepair remains constant (50%). However, with an increasing level of fractionation (smaller doses, with each dose separated by 24 hours) the misrejoining of damage decreases for the normal cells. Crucially, in the AT cells the decrease is less pronounced, resulting in a substantially greater amount of misrepair comparatively at the smallest fractionated courses. This context is important as it suggests that part of the radiosensitivity and the

fractionation sensitivity (in break repair) seen in these AT cells are both a consequence of misrepair. It also highlights how sparing of misrepair with fractionation continues well past the dose range where survival can be ascertained.

In clonogenic assays, there is a threshold dose above which, fraction size sensitivity cannot be seen in survival due to the extent of misrepair. Alterations to radiosensitivity can move this threshold. Applying this to our results, when radiosensitivity is altered, if it is due to an impact on misrepair this will also affect the level of sparing seen with fractionation. In our analysis in this chapter, an increase in radiosensitivity co-occurs with an increase in recovery factor with 24-hours 0.2 μM SAHA treatment (**Figure 5.3**In addition, treatment with SAHA was used to examine whether the extent of chromatin relaxation could modulate fractionation sensitivity by irradiating cells with split doses. Here, we found that the 0 hour and 4 hour treatments did not alter the fractionation sensitivity, as seen by the similar RF factors and significant sparing of survival in **Figure 5.3** C. Interestingly, the 24 hour pre-treatment did cause an increase in the RF factor from 1.73 to 3.40 (**Figure 5.3** B & C). This shows an increase in fractionation sensitivity but is difficult to interpret due to the radiosensitisation by SAHA under these B & C) and a loss of t-test significance to sparing in one BRG1 mutant (Figure 5.5 A & B). In light of the discussion above, it is important not to overly interpret these results, especially as they occur at the end of the dose range where survival is readily quantifiable. Alternative end point analysis, such as cytogenetics, would also be hindered by the confounding variable of radiosensitisation in this regard.

There is no clear option other than to apply fractionation within dose and treatment ranges that allow for sufficient survival.

5.3.2 Changes to the chromatin environment caused by either SAHA or BRG1 dysregulation do not alter fractionation sensitivity

Singh et al. (2010) use a single break IPCR approach in cancer cell lines, and argue that the radiosensitisation seen with 0.5 μM SAHA treatment occurs as a result of both an increased induction of DSBs in the more open chromatin regions following acetylation as well as an increase in the potential for rearrangements. This is suggested to occur via NHEJ, a decrease in microhomology is shown for sequences at an induced site specific DSB with SAHA treatment. If there is an increase in the potential for rearrangements, it may explain the subtle decrease in fractionation sensitivity seen with a 24-hour exposure, but their analysis is very site specific. That said, the global changes to acetylation levels after 4 hours of exposure that we see with 0.2 μM are the most substantial. It is therefore surprising that no effect would be visible at a cell survival level in either radiosensitivity or fractionation sensitivity.

A lack of impact on fraction size sensitivity with global chromatin acetylation changes or BRG1 dysregulation does not rule out an effect of more specific changes. It would be beneficial in particular to more carefully consider the role of DITR, whereby actively transcribed regions might become more condensed. In addition, chromatin compaction proteins are known to play a role in response to all DNA DSBs. In particular, HDAC1 and HDAC2 have been implicated in the DDR (Miller et al. 2010). These responses could in

theory be counteracted by SAHA treatment yet in this context we don't see a decrease in fractionation sensitivity.

PBAF has identified roles in DNA repair, chromatin topology and organisation as well as on transcription. However, although our two BRG1 clones have substantially decreased expression of mutant BRG1 forms, we do not know their effect on these activities, including DITR. The effect on radiosensitisation observed in the BRG1 deficient cell lines suggests that there are alterations to the actions of PBAF that are impacting pathways leading to changes in DNA damage signalling and repair. It would therefore be beneficial to examine known activities of BRG1 in these clones, in particular in relation to DITR and whether there are any alterations to sister chromatid cohesion through cohesion (Brownlee et al. 2014, Meisenberg et al. 2019).

In conclusion, exploratory clonogenic assays did not elucidate a clear role for global histone acetylation levels or BRG1 activity to affect fractionation sensitivity. It remains to be seen whether more targeted approaches on the role of transcriptional repression could modulate fractionation sensitivity.

6 Mutational Signature of Irradiation and Fraction Size Sensitivity

As discussed previously, Kucab et al. (2019) present the most complete mutational signature for irradiation, on a whole-genome level in normal human cells. However, their study was performed in pluripotent stem cells that have stringent DNA damage responses resulting in high levels of apoptosis following irradiation. The clonal selection methodology employed will therefore result in apoptotic cells being lost, along with the most deleterious mutations. Additionally, clonal selection will naturally lead to the fittest cells outgrowing the population, so that even viable cells with deleterious misrepair events, will be lost. To gain a more thorough understanding of the misrepair events following irradiation, we wanted to assess the feasibility of using a whole genome sequencing (WGS) approach in 1BR3 hTERT. This approach capitalises on the senescent fibroblast response to IR so that the full spread of IR induced mutations can be captured, including those that result in cell lethality in other model systems. Further, the fraction size sensitivity of 1BR3 hTERT provides the opportunity to investigate how the mutational signature changes with fractionation and therefore determine whether there are specific forms of damage that are spared by fractionation. In the following research, with the exception of library preparation and sequencing which were performed out of house, all wet lab work was performed by myself. Data analysis pipelines were designed through collaboration between bioinformaticians James Campbell (ICR) an Alice Gao (ICR) and myself. Pipeline implementation was

predominantly performed by James Campbell and Alice Gao within the ICR HPC clusters.

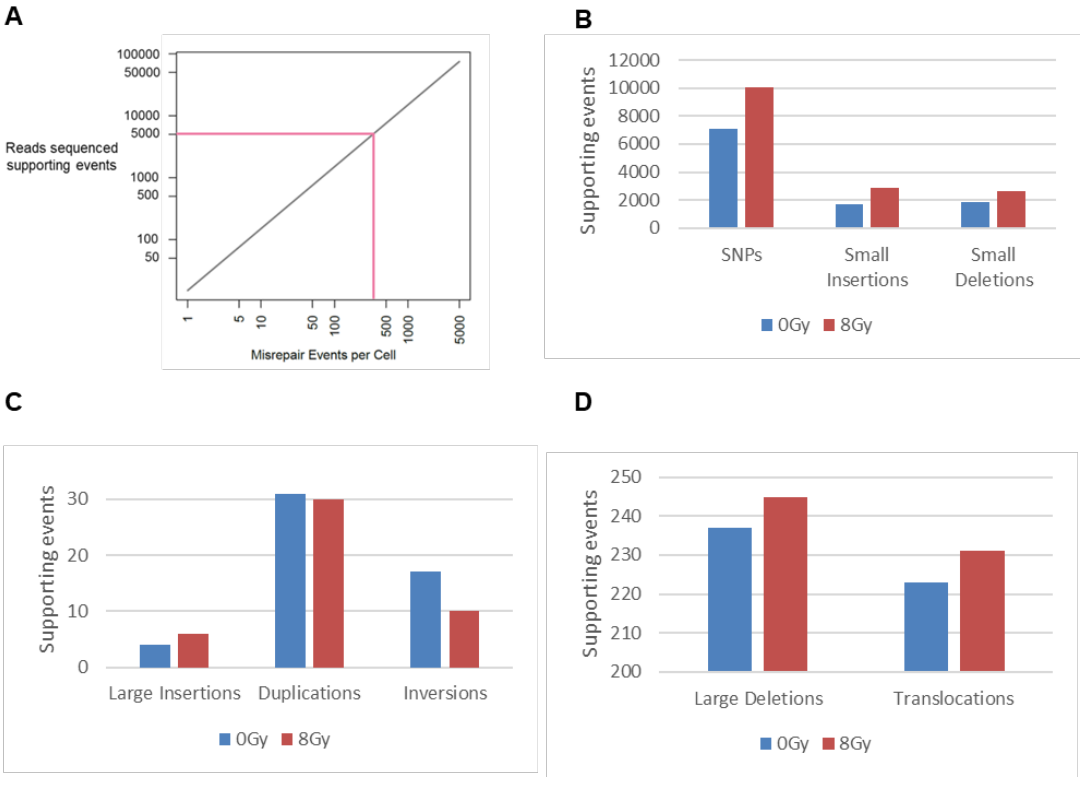

E

Type	SNPs	Small Insertions	Small Deletions	Large Insertions	Large Deletions	Duplications	Inversions	Translocations
0 Gy	7122	1704	1871	4	237	31	17	223
8 Gy	10037	2899	2659	6	245	30	10	231
Difference	2915	1195	788	2	8	-1	-7	8

Figure 6.1 Whole genome sequencing analysis of mutations in a population of cells following IR.

Asynchronous 1BR3 hTERT human fibroblasts were given an 8Gy dose of irradiation followed by 24 hours for DSB repair, prior to gDNA extraction for sequencing alongside an unirradiated (0 Gy) control. ***A)*** *Simulation of the number of supporting reads expected at 30x whole genome sequencing for a range of 1 to 5000 DSB misrepair events per cell. Pink line indicates the number of unique 8 Gy reads (subtracting the 0 Gy background) that supported a mutation and the corresponding predicted number of misrepair events.* ***B)*** *Unique small mutations called by Haplotype caller (<100bp)* ***C & D)*** *Unique large scale mutations called by DELLY.* ***E)*** *Mutation calls for both samples.*

6.1 Mutational signature of irradiation

6.1.1 A Mutational signature of irradiation in a population of cells

We first investigated the mutational profile following irradiation in a population of cells. To do this, we made a simulation to estimate the likelihood of observing a random misrepair event by whole genome sequencing at 30x depth. This resulted in a level of identifiable hits, suggesting that this approach would yield sufficient information (Figure 6.1 A). We then used asynchronously growing cells irradiated with 0 Gy or 8 Gy that were given a 24 hour period for repair prior to DNA extraction and whole genome sequencing using the BGISEQ-500 platform (Huang et al. 2017). After aligning both sequence samples to the human reference genome (BWA/GATK, Broad Institute) (Li and Durbin 2010), small variants were called by Haplotype caller in germline mode and large variants were identified using Delly in germline mode (McKenna et al. 2010, Rausch et al. 2012). Post call filtering was performed to remove shared calls found in both samples leaving unique variants called for the 0 Gy and 8 Gy treated samples. These steps were all performed in collaboration with James Campbell (ICR).

We found an increase in small (<100bp) deletions, insertions and single nucleotide polymorphisms along with more moderate increases in large (>300bp) deletions and translocations with irradiation. The unique variants identified in the unirradiated sequencing data are a product of heterogeneity between cells in the population in the 1BR3 hTERT sample, the sequencing depth and the germline methodology used and can therefore be considered

‘background’ variants, i.e. not induced by irradiation. This background will by definition also be in the 8 Gy sample. Therefore, the data could be presented alternatively as the difference between samples with the background removed. Considering our further analysis we have chosen to include this background, but the calculated differences are given in Figure 6.1 E. These differences together accounted for almost 5000 supporting reads in the 8 Gy cells. By entering this figure back into our simulation, this equates to approximately 450 misrepair events across a single genome following 8 Gy.

6.1.2 A mutational signature of irradiation and fraction size sensitivity by single cell sequencing

In order to be able to more accurately call misrepair damage resulting from IR and remove the background such that differences with fractionation could be seen we decided to employ a single cell approach. Moreover, we produced a clonally derived parental population of 1BR hTERT from single cell sorting in order to ensure as homogenous a sample of 1BR3 hTERT as possible. Cells were then irradiated with 0 Gy, a single 8 Gy dose, a single 16 Gy dose, or split 8 Gy or 16 Gy doses delivered in two fractions (4 Gy x2 or 8 Gy x2) with the second fractions given after eight hours. All cells were given 24 hours from the initial dose for repair. Populations were then sorted into single cells and single cell whole genome amplification performed. Three cells per condition were subjected to whole genome sequencing using a HiSeq X system (Illumina). Alignment and small variant calling was

A

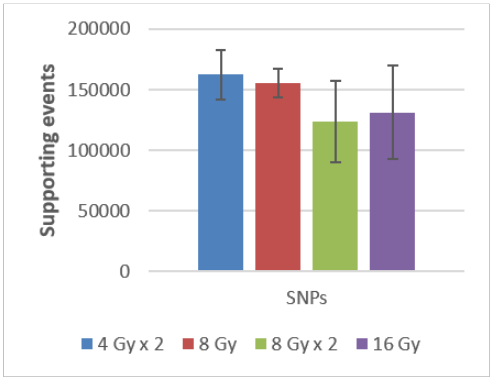

B

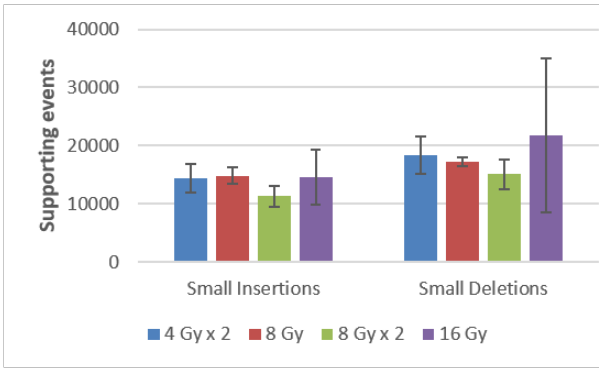

C

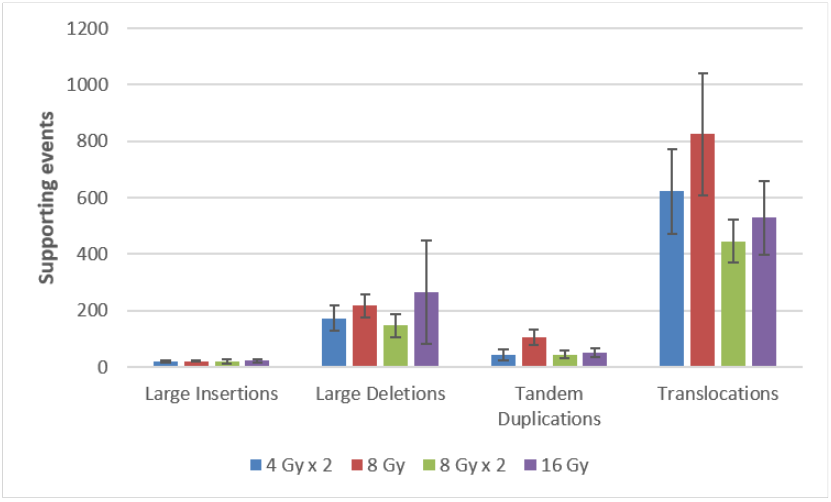

D

Sample ID	SNPs	Small Insertions	Small deletions	Large Insertions	Large Deletions	Tandem Duplications	Translocations
4 Gy x2-1	178033	16648	21106	25	234	73	781
4 Gy x2-2	175558	15587	20025	21	164	30	662
4 Gy x2-3	133781	10849	13777	17	123	27	424
8 Gy-1	142106	15729	16374	26	268	145	1107
8 Gy-2	170351	15887	18186	21	212	93	790
8 Gy-3	153350	12826	17127	18	172	81	577
8 Gy x2-1	104264	9607	13811	12	95	25	347
8 Gy x2-2	95687	10487	12722	24	154	57	465
8 Gy x2-3	170925	13841	18694	25	195	54	527
16 Gy-1	105117	11132	12048	17	127	42	447
16 Gy-2	185519	21223	40412	29	525	73	714
16 Gy-3	103440	11214	12843	23	149	36	428

Figure 6.2 Single cell amplified whole genome sequencing analysis of mutations following single and fractionated doses of IR.

Asynchronous 1BR3 hTERT human fibroblasts were given single and fractionated dose courses (second dose after 8 hours) with a 24 hours period for repair from the first dose, prior to single cell sorting and genome amplification. ***A & B)*** *Small scale mutations (<100bp) called by Isaac variant caller following removal of shared mutations found in the 0 Gy control cells. Error bars represent the standard deviation between 3 single cell genomes.* ***C)*** *Large scale mutations (>50bp) called by Manta following removal of shared mutations found in the 0 Gy control cells. Error bars represent the standard deviation between 3 single cell genomes.* ***D)*** *All mutation calls for each single cell genome.*

performed to the human reference genome as part of the HiSeq Analysis Software by Genewiz. We performed variant filtering to remove all calls from the 0 Gy samples that were in any of the IR samples. We then additionally filtered to remove any shared variant calls between the IR samples.

We found that there was no substantial change in the number of identified single-nucleotide polymorphisms (SNP) across the samples (Figure 6.2 A), suggesting that these are not spared by fractionation. Next, we found that there was an increase of small deletions with dose. Moreover, there was a clear decrease in the number of small insertions and deletions between the 16 Gy samples and the 8 Gy x2 samples (Figure 6.2 B). This result suggests that irradiation-induced indels could be spared by fractionation.

For large scale genome rearrangements, the variants were called using Manta (Illumina) by Alice Gao. Post variant call filtering was performed to remove calls found in the 0 Gy samples from the IR-treated samples. Notably, a decrease in the number of both large (>50bp) deletions and translocations

was seen when the irradiation was delivered in split doses. While there was not a decrease in the number of tandem duplications between 16 Gy and 8 Gy x2, the 8 Gy compared with 4 Gy x2 did show a difference, suggesting these events might also be spared by fractionation. However, the average is disproportionately affected by one sample (8 Gy-1), which might be an outlier. Large insertions were not spared by splitting the irradiation dose.

6.2 Discussion

6.2.1 A broad range of misrepair damage occurs following IR induced damage

Our data from both the population and single cell approaches, suggests that single nucleotide changes, small insertions and deletions along with large scale insertions, deletions and translocations occur following damage repair following irradiation in 1BR3 hTERT cells. The small indels complement the analysis by Kucab et al. (2019) and are likely to represent microhomology-mediated end-joining misrepair (Löbrich and Jeggo 2017). The greater level of SNPs we see in the single cell analysis is likely to be due to the approach used to call small indels. An updated approach was used to call the large-scale mutations; this is further discussed in the methodology. We would expect that when this updated methodology is applied, the pattern of small-scale SNPs and indels differences or lack thereof will remain similar, but the overall supporting events will decrease in an equal manner for each condition.

Large scale translocations denote interchromosomal translocations and have been demonstrated using classical cytogenetic approaches, but our data

suggest that the extent of this damage is more substantial than can be seen at the resolution of existing cytogenetic analyses. G-banding reaches a maximum resolution of 5Mb and mBAND technology reaches slightly lower at 6Mb but allows for a greater understanding of locational changes. However, mBAND technology is prohibitively expensive and technically difficult and most studies rarely target its use past one chromosome, with whole chromosome level resolution mFISH preferred to examine the whole genome at a lower resolution (Chudoba et al. 1999, Hu et al. 2006). The two single cell WGS analysis approaches we use together in theory give single bp resolution to insertions and deletions. Whilst detectable deletion sizes are only limited by chromosome size, the power of Manta to identify large insertions is limited to around double the read length (~600bp in our analysis).

We note that the 16 Gy samples do not have an increased number of mutations compared to cells irradiated with 8 Gy. One potential explanation for this result is the repair time given: a 24-hour period for 8 Gy is sufficient for almost complete repair, whilst a proportion of repair would be yet to complete with 16 Gy. If this is the case, then it would suggest that the rate of misrepair is constant despite the size of dose received. It would be beneficial to perform analysis on a range of doses at the time-point whereby damage (potentially measured by γ-H2AX foci clearance) was complete as well as at multiple time-points across repair for the same dose.

6.2.2 Large Scale deletions and translocations are spared by dose fractionation.

Our analysis suggests that deletions and translocations are spared with fractionation. This finding is complementary to the sparing of exchange aberrations seen by cytogenetic analysis for interchromosmal translocations, but additionally supports a sparing of intrachromosomal translocations (Bedford and Cornforth 1987). Contrastingly, large insertions are not spared with fractionation; this distinction is limited by the inability to resolve insertions of over 600bp in size. We are yet to examine the size distribution of the structural misrepair seen. If we see deletions between 50bp and 600bp the lack of insertions would suggest that these lengths of DNA are lost from one region but do not translocate and become inserted elsewhere during repair. There could therefore be a size dependent bias within repair where small fragments are lost. There is the suggestion that small indels could also be spared with fractionation. Until we complete the further analysis described, we must be cautious to interpret this, but if they are spared, determining the location of the damage spared to examine effects on viability will be vital as we discuss below.

6.2.3 Population distribution of irradiation-induced damage

We would expect that within a population of cells, there would be a close to a normal distribution of the amount of misrepair damage. Whist sequencing with sufficient depth in populations of cells has the potential to capture the full spectrum of misrepair, it is impossible to relate these mutations to individual cells and therefore only create averages through simulation. In contrast, single cell sequencing in our senescent model has a greater potential to examine the distribution of misrepair events. By definition, it only picks up one cell from

anywhere in the distribution, allowing us to directly relate the damage seen. However, this comes with the downside that we do not know where in the distribution the cells selected are and therefore calculating average mutational damage robustly is likely to require more than three cells per a condition. We were therefore encouraged to observe a lower level of standard deviation than we expected between three cells per condition, with only a few substantially different numbers of the same mutation type identified for the same treatment. These outliers are likely to represent closer to either end of the distribution for the misrepair they represent.

6.2.4 Considering mutation location

Whilst a sparing in the number of misrepair aberrations types is the most likely cause for improved survival, whether the locality of the damage changes with fractionation is an important consideration we are yet to probe in the data. For example, it is possible to hypothesise that translocations between actively transcribed genes might be disproportionately spared by fractionation due to damage induced transcriptional repression between fractions. This could lessen the impact on survival further than purely a decrease in translocation number suggests with fractionation of the dose. This may also be the case for misrepair aberrations where we do not see consistent differences in the number of aberrations between single and fractionated dose courses, such as SNPs, but locational pattern changes could have significant effects on viability. In order to perform this analysis, we will have to take the location of the misrepair seen with and without fractionation and compare it to genome-wide chromatin accessibility profiles that have been drawn from integrating

sequencing data from chromatin immunoprecipitation, RNA expression, epigenetic modifications and chromosome interaction experiments.

This research presents a stepping stone to applying single cell genome sequencing to the conundrum of fraction size sensitivity. Whilst the best practice data analysis methodology is still evolving, the early indications suggest that the approach will be a valuable tool. Final results and raw data will be accessible via publication to follow.

7 Final Discussion

7.1 Aims Revisited

"1. Elucidate the contribution of the cell cycle stage that repair occurs within to fractionation sensitivity."

In our repair-competent fraction size sensitive model cell line, we demonstrate by cell cycle phase-specific FACS clonogenic survival analysis that fraction size sensitivity does not change significantly in G_1, S and G_2 phases despite the availability of HR repair in S and G_2. These assays were performed in the absence of cell cycle progression. We replicate previously reported associations between cell viability and chromosome exchange aberrations during G_1 phase repair, and we demonstrate chromatid exchange type aberrations in G_2. Both are spared by split dose fractionation. We have not tested usage of HR in normal cell lines with low sensitivity to fraction size, but our results suggest that progression with an unrejoined DSB and/or misrepair past G_1 or G_2 cell cycle checkpoints is more likely to explain the lack of correlation between cell cycle phase and fraction size sensitivity in our research. It is difficult to apply the same assays to cells deficient in either HR or NHEJ to further assess a repair pathway specific affect due to low survival. It would however be beneficial to perform them in an HR positive cancer cell line with higher HR usage.

"2. Determine whether the kinetics of repair remain constant with dose fractionation."

Using γ-H2AX foci as a proxy for DSBs, we do not see a change in the induction of damage between fractions both when a second fraction is given in the presence or absence of ongoing repair. Furthermore, the kinetics of foci clearance do not alter significantly between split fractions. However, the number of unresolved persistent foci increases with dose and is spared with fractionation. If persistent foci correspond to un-repaired DSBs it suggests that unrepaired DSBs influence fraction size sensitivity. It is possible that the complexity of DNA damage and the location within higher order chromatin structure may determine this. Other explanations include that the persistent foci may stem from a continuation or alternate signalling after repair associated with the senescent fibroblast phenotype. If so, this could be modulated by the same suggestions and could be equally contributory to viability and fraction size sensitivity in our model system. Extending this analysis by capturing timepoints throughout repair would demonstrate when the un-repaired foci are formed; either directly following damage or as later derived breaks. Additionally, altering the time between fractions may provide further evidence of a correlation between unrepaired foci and the extent of fractionation. Finally, kinetic analysis within a fraction size insensitive cell line would provide a pertinent control.

"3. Investigate the contribution of the chromatin environment to fractionation sensitivity."

Using two different methodologies we targeted the global organisation of the chromatin architecture. Following HDAC inhibition, the increased acetylation and therefore a more open euchromatic chromatin structure did not

affect fraction size sensitivity. Neither did changes to the expression and likely function of BRG1, the catalytic ATPase of the PBAF and BAF SWI/SNF chromatin remodelling complexes, affect fraction size sensitivity.

The failure of detectable changes in chromatin organisation to affect fraction size sensitivity means that these changes are unlikely to play a major role in determining fraction size sensitivity in our model system. However, it remains possible that more specific changes, such as repression of transcription at sites of damage between fractions modulate sensitivity. In order to test this we could add transcriptional inhibition to the experiment.

"4. Define a mutational signature of irradiation, and determine whether this is altered by fractionation of the dose."

The assumed random distribution of radiation-induced DNA damage across the genome makes WGS analysis a technically challenging process. We demonstrate that it is possible to see radiation induced mutation patterns in a population of cells at a standard level of 30x depth. Additionally, upon moving to a single cell approach we are able to demonstrate individual cell mutational signatures following irradiation, which share the induction of small insertions, small and large deletions and translocations. Finally, whilst our analysis methodology is at an early stage, we see consistent decreases in these mutations with split dose fractionation, complementing the sparing of chromosome and chromatid exchange aberrations with dose seen using our cytogenetic approaches, and are now able to investigate for locational patterns for where mutational damage is spared.

“5. Investigate whether there are limiting factors to the fidelity of repair that modulate fractionation sensitivity.”

Whilst not yet presented, we have designed approaches to investigate potentially limiting factors of repair and research is ongoing. To give two examples, we are using cell lines with different levels of H1 expression to challenge whether the level of H1 can alter the recruitment of RNF168 and subsequently 53BP1-led pathway choice. The unexplained persistent γ-H2AX foci we see with increasing dose and their intriguing relationship with persistent 53BP1 foci, whereby 53BP1 almost always colocalise but γ-H2AX foci do not, along with a sparing of this unrelated γ-H2AX subset with split fractionation, suggests there could be more here to uncover. Finally, we consider the role of proteomic analysis following chromatin fractionation to uncover whether there are repair associated proteins whose recruitment to chromatin with dose plateaus at a threshold level, suggesting a limitation to its abundance.

7.2 Closing Thoughts

On balance, the research presented here supports exchange misrepair as the preeminent source of cell lethality that is spared with fractionation. We demonstrate for the first time, that regardless of the cell cycle phase in which repair occurs, exchange type aberration formation and survival are spared with split dose fractionation. Additionally, the large mutations that we see spared with split dose fractionation from single cell sequencing suggest both interchromosomal and intrachromosomal exchanges are spared with fractionation. Despite this, however, there are clear indications that other

mechanisms may contribute to the sparing effect of fractionation. In particular, the novel suggestions that small insertions and deletions (indels) and the number of unrepaired breaks at late timepoints can be spared with fractionation. Determining the locality of mutational damage spared with fractionation will be instrumental to viability if they interfere with transcription and replication and could therefore inhibit gene expression and cell division. At a cellular level, sparing could be a consequence of unrepaired or misrepaired DSBs, but these are not mutually exclusive. Both or either may be the culprit.

The chromatin environment, transcriptional activity, genetic background and cell cycle are all factors that could individually impact each of these potential sources. Our cellular and chromosomal experiments do not support the hypothesis that utilisation of high fidelity homologous recombination repair in the G_2 and S phases of immortalised human fibroblasts is associated with lower sensitivity to fraction size than in G_1 phase cells. There must be an alternative explanation for the tight inverse association between fraction size sensitivity and proliferation rates of human normal tissues during fractionated radiotherapy. Single cell WGS has allowed patterns of mutational damage to be uncovered for the first time. The level of mutational damage seen in our cell line is surprising. The fact that we see clonogenic survival of clones at the doses used for sequencing studies, despite the senescent fibroblast response to damage, suggests that survivors have the ability to deal with a considerable level of misrepair in the genome. Combining these findings, a next focus for us would be on the transition between cell cycle phases, or more precisely; the

pressure to proceed past cell cycle checkpoints with damage in highly proliferative cells. Fraction size sensitivity could be determined by different genetic pressures to progress past cell cycle checkpoints with a greater amount of misrepair, or indeed unrepaired DSBs.

Finally, the findings presented here in a single repair-proficient fraction size sensitive cell line might not reflect what happens in other fraction size sensitive cells including sensitive cancer cell lines. Further, whilst we demonstrate that cell cycle stage during repair and substantial chromatin state alterations do not alter fractionation sensitivity in our model, they may be vital contributors within a cancer genetic background. To move forward we must begin to examine the response at a cellular level of a greater range of models, especially those of fraction-size insensitive healthy cell lines and cancers. This work results in considerable issues to overcome to be able to compare results between cell lines, not least differences in radiosensitivity affecting the ability to use the same dose courses. Novel methodologies may have to be developed to track extent of repair prior to cell death. Of course, beyond this at a whole organism level, other variables will contribute, for example hypoxia, bystander effects and immune responses. If so these areas also justify research to establish whether they can be leveraged to alter fraction size sensitivity to improve radiotherapy outcomes.

Appendix

A

PCR Product Identification		
Target	**Chromosome**	**Amplicon Length (bp)**
A	12p	91
B	5p	108-166
C	17p	299
D	6p	614

B

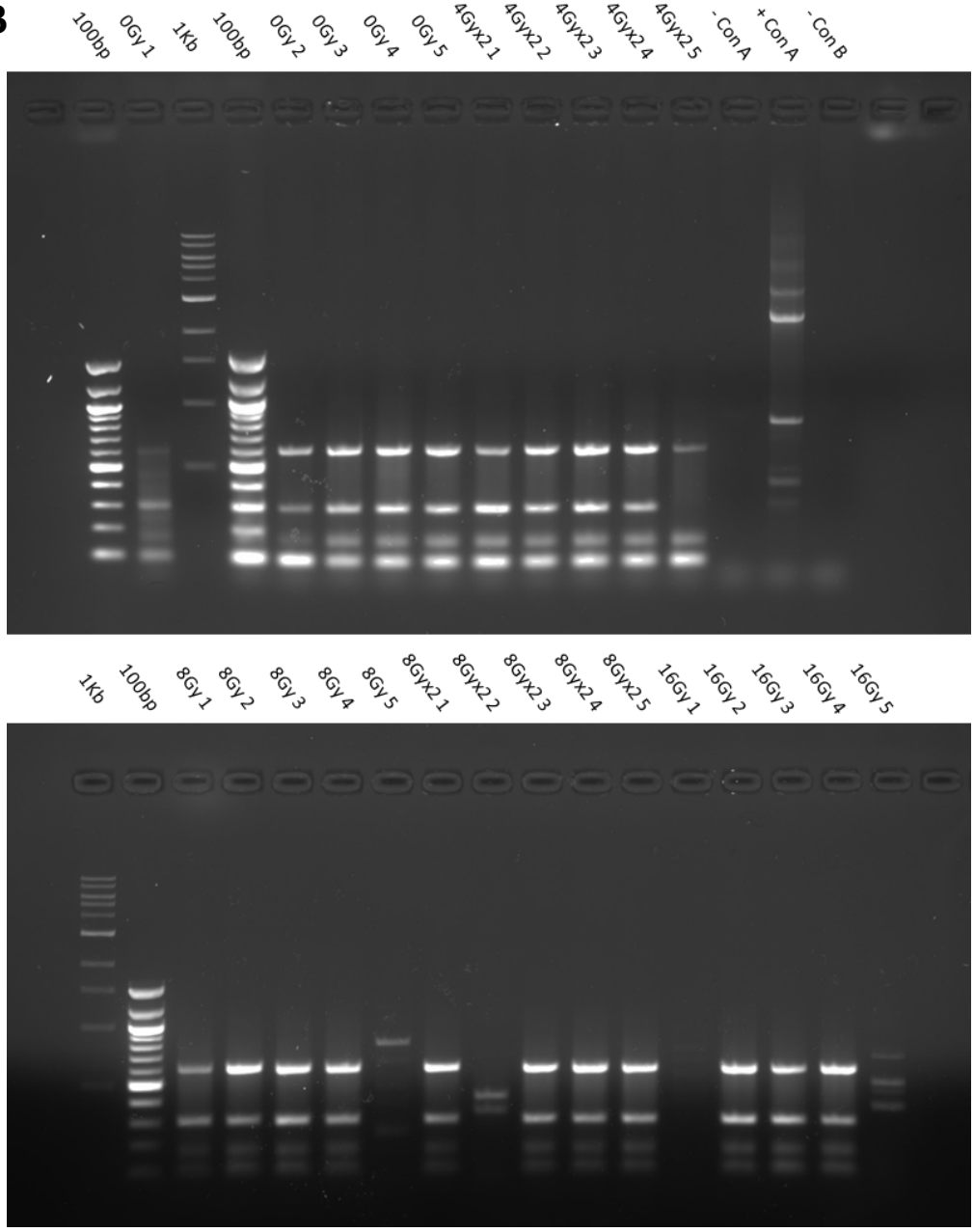

Appendix Figure 1: DNA Agarose gel of Ampli1 QC result.

A) *Location and lengths of test regions.* ***B)*** *15 single cell Ampli1 treated DNA samples tested with Ampli1 QC run on a 1% agarose gel. Two DNA free controls and a plasmid control (a standard GFP expression plasmid) were also loaded. The presence of 4 bands demonstrates a high quality of amplification for downstream assessment. 3 samples from each condition were chosen and renamed 1-3 for downstream sequencing assessment.*

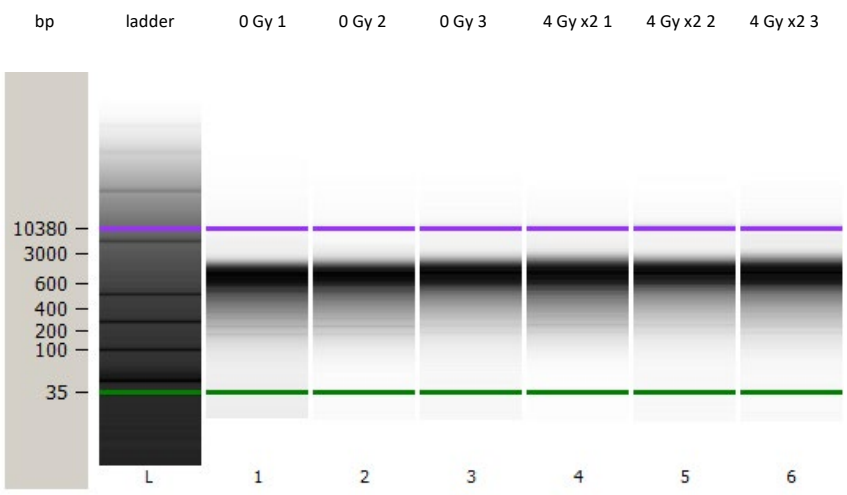

Appendix Figure 2: Bioanalyzer High Sensitivity DNA chip result visualised with the gel-like output for 6 representative Ampli1 samples.

Sample ID	Number of Mapped Reads	% Mapped Whole Genome	% Duplicate Mapped Reads	Mean Coverage (Depth)
0 Gy	1.21E+09	99.81	1.92	40.16
8 Gy	1.26E+09	99.76	1.98	41.15

Appendix Figure 3: Selected statistics from post alignment QC analysis of whole population WGS data.

Sample ID	Number of Mapped Reads	% Mapped Whole Genome	% Duplicate Mapped Reads	Mean Coverage (Depth)	% Variant Allele Frequency =1
0 Gy-1	6.19E+08	93.38	42.22	15.48	43.67
0 Gy-2	6.43E+08	95.77	40.49	16.21	43.24
0 Gy-3	7.22E+08	92.97	38.10	18.95	45.35
4 Gyx2-1	6.22E+08	95.51	38.01	16.25	40.57
4 Gyx2-2	5.67E+08	95.53	38.62	14.89	40.58
4 Gyx2-3	6.40E+08	95.69	35.98	17.17	43.08
8 Gy-1	6.63E+08	95.63	37.97	17.57	41.05
8 Gy-2	7.11E+08	95.56	43.70	17.11	42.36
8 Gy-3	6.11E+08	95.51	37.24	16.09	43.40
8 Gyx2-1	6.30E+08	95.75	39.44	16.23	43.24
8 Gyx2-2	6.44E+08	95.27	37.74	17.03	43.63
8 Gyx2-3	6.42E+08	95.85	36.98	16.73	43.90
16 Gy-1	6.61E+08	95.98	37.78	17.23	43.63
16 Gy-2	5.84E+08	92.95	37.82	15.10	48.20
16 Gy-3	6.54E+08	95.43	34.76	17.76	41.75
Average	6.41E+08	95.12	38.46	16.65	43.18

Appendix Figure 4: Selected statistics from post alignment QC analysis of single cell amplified WGS data.

		Biological Replicate				Average
Cell Cycle Stage	Course	1	2	3	4	
Asynchronous	0 Gy	1.0000	1.0000	1.0000	1.0000	1.0000
	2 Gy	0.3480	0.2963	0.3981	0.2765	0.3297
	4 Gy	0.0841	0.0664	0.0967	0.0501	0.0743
	8 Gy	0.0033	0.0042	0.0067	0.0037	0.0044
	4 Gy x2	0.0063	0.0078	0.0091	0.0084	0.0079
	2 Gy x4	0.0057	0.0116	0.0097	0.0084	0.0088
G_1	0 Gy	1.0000	1.0000	1.0000	1.0000	1.0000
	2 Gy	0.3625	0.2909	0.2576	0.2826	0.2984
	4 Gy	0.0694	0.0266	0.0461	0.0463	0.0471
	8 Gy	0.0032	0.0015	0.0021	0.0011	0.0020
	4 Gy x2	0.0044	0.0067	0.0033	0.0047	0.0048
	2 Gy x4	0.0039	0.0033	0.0043	0.0048	0.0041
S	0 Gy	1.0000	1.0000	1.0000	1.0000	1.0000
	2 Gy	0.3566	0.1407	0.3158	0.3135	0.2817
	4 Gy	0.0557	0.0786	0.0853	0.0732	0.0732
	8 Gy	0.0038	0.0043	0.0070	0.0049	0.0050
	4 Gy x2	0.0074	0.0109	0.0149	0.0090	0.0106
	2 Gy x4	0.0090	0.0153	0.0188	0.0152	0.0146
G_2	0 Gy	1.0000	1.0000	1.0000	1.0000	1.0000
	2 Gy	0.5086	0.2222	0.2222	0.2373	0.2976
	4 Gy	0.1102	0.0593	0.0531	0.0825	0.0763
	8 Gy	0.0050	0.0033	0.0038	0.0055	0.0044
	4 Gy x2	0.0082	0.0054	0.0062	0.0058	0.0064
	2 Gy x4	0.0086	0.0063	0.0100	0.0103	0.0088

Appendix Figure 5: Table of individual biological replicate survival for cell cycle stage sorted clonogenic survival analysis *(Figure 3.2)*

References

Alagoz, M., Y. Katsuki, H. Ogiwara, T. Ogi, A. Shibata, A. Kakarougkas, and P. Jeggo. 2015. "SETDB1, HP1 and SUV39 promote repositioning of 53BP1 to extend resection during homologous recombination in G2 cells." *Nucleic Acids Research* 43 (16):7931-7944. doi: 10.1093/nar/gkv722.

Alsbeih, M. G., B. Fertil, C. F. Arlett, and E. P. Malaise. 1996. "High split-dose recovery in hypersensitive human fibroblasts: a case of induced radioresistance?" *International Journal of Radiation Biology* 69 (2):225-39. doi: 10.1080/095530096146075.

Arlett, C. F., M. H. L. Green, A. Priestley, S. A. Harcourt, and L. V. Mayne. 1988. "Comparative Human Cellular Radiosensitivity: I. The Effect of SV40 Transformation and Immortalisation on the Gamma-irradiation Survival of Skin Derived Fibroblasts from Normal Individuals and from Ataxia-telangiectasia Patients and Heterozygotes." *International Journal of Radiation Biology* 54 (6):911-928. doi: 10.1080/09553008814552321.

Aymard, F., B. Bugler, C. K. Schmidt, E. Guillou, P. Caron, S. Briois, J. S. Iacovoni, V. Daburon, K. M. Miller, S. P. Jackson, and G. Legube. 2014. "Transcriptionally active chromatin recruits homologous recombination at DNA double-strand breaks." *Nature Structural & Molecular Biology* 21:366. doi: 10.1038/nsmb.2796.

Bakr, A., S. Köcher, J. Volquardsen, C. Petersen, K. Borgmann, E. Dikomey, K. Rothkamm, and W. Y. Mansour. 2016. "Impaired 53BP1/RIF1 DSB mediated end-protection stimulates CtIP-dependent end resection and switches the repair to PARP1-dependent end joining in G1." *Oncotarget* 7 (36):57679-57693. doi: 10.18632/oncotarget.11023.

Bartek, J., and J. Lukas. 2003. "Chk1 and Chk2 kinases in checkpoint control

and cancer." *Cancer Cell* 3 (5):421-429. doi: 10.1016/S1535-6108(03)00110-7.

Barton, O., S. C. Naumann, R. Diemer-Biehs, J. Kunzel, M. Steinlage, S. Conrad, N. Makharashvili, J. Wang, L. Feng, B. S. Lopez, T. T. Paull, J. Chen, P. A. Jeggo, and M. Lobrich. 2014. "Polo-like kinase 3 regulates CtIP during DNA double-strand break repair in G1." *Journal of Cell Biology* 206 (7):877-94. doi: 10.1083/jcb.201401146.

Baujat, B., J. Bourhis, P. Blanchard, J. Overgaard, K. K. Ang, M. Saunders, A. Le Maitre, J. Bernier, J. C. Horiot, E. Maillard, T. F. Pajak, M. G. Poulsen, A. Bourredjem, B. O'Sullivan, W. Dobrowsky, H. Andrzej, K. Skladowski, J. H. Hay, L. H. Pinto, K. K. Fu, C. Fallai, R. Sylvester, and J. P. Pignon. 2010. "Hyperfractionated or accelerated radiotherapy for head and neck cancer." *Cochrane Database Syst Rev* (12):Cd002026. doi: 10.1002/14651858.Cd002026.

Bedford, J. S., and M. N. Cornforth. 1987. "Relationship between the recovery from sublethal X-ray damage and the rejoining of chromosome breaks in normal human fibroblasts." *Radiation Research* 111 (3):406-23. doi: 10.2307/3576927.

Bentzen, S. M., R. K. Agrawal, E. G. Aird, J. M. Barrett, P. J. Barrett-Lee, J. M. Bliss, J. Brown, J. A. Dewar, H. J. Dobbs, J. S. Haviland, P. J. Hoskin, P. Hopwood, P. A. Lawton, B. J. Magee, J. Mills, D. A. Morgan, J. R. Owen, S. Simmons, G. Sumo, M. A. Sydenham, K. Venables, and J. R. Yarnold. 2008. "The UK Standardisation of Breast Radiotherapy (START) Trial A of radiotherapy hypofractionation for treatment of early breast cancer: a randomised trial." *Lancet Oncology* 9 (4):331-41. doi: 10.1016/s1470-2045(08)70077-9.

Bernier, J., E. J. Hall, and A. Giaccia. 2004. "Radiation oncology: a century of achievements." *Nature Reviews Cancer* 4 (9):737-747. doi: 10.1038/nrc1451.

Bétermier, M., P. Bertrand, and B. S. Lopez. 2014. "Is Non-Homologous End-Joining Really an Inherently Error-Prone Process?" *PLOS Genetics* 10 (1):e1004086. doi: 10.1371/journal.pgen.1004086.

Beucher, A., J. Birraux, L. Tchouandong, O. Barton, A. Shibata, S. Conrad, A. A. Goodarzi, A. Krempler, P. A. Jeggo, and M. Löbrich. 2009. "ATM and Artemis promote homologous recombination of radiation-induced DNA double-strand breaks in G2." *The EMBO journal* 28 (21):3413-3427. doi: 10.1038/emboj.2009.276.

Biechonski, S., L. Olender, A. Zipin-Roitman, M. Yassin, N. Aqaqe, V. Marcu-Malina, M. Rall-Scharpf, M. Trottier, M. S. Meyn, L. Wiesmüller, K. Beider, Y. Raz, D. Grisaru, A. Nagler, and M. Milyavsky. 2018. "Attenuated DNA damage responses and increased apoptosis characterize human hematopoietic stem cells exposed to irradiation." *Scientific Reports* 8 (1):6071. doi: 10.1038/s41598-018-24440-w.

Boesch, M., D. Wolf, and S. Sopper. 2016. "Optimized Stem Cell Detection Using the DyeCycle-Triggered Side Population Phenotype." *Stem cells international* 2016:1652389-1652389. doi: 10.1155/2016/1652389.

Bolzer, A., G. Kreth, I. Solovei, D. Koehler, K. Saracoglu, C. Fauth, S. Müller, R. Eils, C. Cremer, M. R. Speicher, and T. Cremer. 2005. "Three-Dimensional Maps of All Chromosomes in Human Male Fibroblast Nuclei and Prometaphase Rosettes." *PLOS Biology* 3 (5):e157. doi: 10.1371/journal.pbio.0030157.

Bonner, W. 2003. "Low-dose radiation: Thresholds, bystander effects, and adaptive responses." *Proceedings of the National Academy of Sciences* 100 (9):4973. doi: 10.1073/pnas.1031538100.

Borgmann, K., M. Dede, A. Wrona, I. Brammer, J. Overgaard, and E. Dikomey. 2004. "For X-irradiated normal human fibroblasts, only half of cell inactivation results from chromosomal damage." *International Journal of Radiation Oncology • Biology • Physics* 58 (2):445-52. doi:

10.1016/j.ijrobp.2003.09.036.

Brouwer, I., G. Sitters, A. Candelli, S. J. Heerema, I. Heller, A. J. Melo de, H. Zhang, D. Normanno, M. Modesti, E. J. G. Peterman, and G. J. L. Wuite. 2016. "Sliding sleeves of XRCC4–XLF bridge DNA and connect fragments of broken DNA." *Nature* 535:566. doi: 10.1038/nature18643.

Brownlee, P. M., A. L. Chambers, R. Cloney, A. Bianchi, and J. A. Downs. 2014. "BAF180 promotes cohesion and prevents genome instability and aneuploidy." *Cell Reports* 6 (6):973-981. doi: 10.1016/j.celrep.2014.02.012.

Buerstedde, Jean-Marie, and Shunichi Takeda. 2006. *Reviews and Protocols in DT40 Research : Subcellular Biochemistry*, *Subcellular Biochemistry 40*. Dordrecht: Springer Netherlands : Imprint: Springer.

Buisson, R., and J-Y. Masson. 2012. "PALB2 self-interaction controls homologous recombination." *Nucleic Acids Research* 40 (20):10312-10323. doi: 10.1093/nar/gks807.

Burma, S., B. P. Chen, and D. J. Chen. 2006. "Role of non-homologous end joining (NHEJ) in maintaining genomic integrity." *DNA Repair (Amst)* 5 (9-10):1042-8. doi: 10.1016/j.dnarep.2006.05.026.

Butler, L. M., D. B. Agus, H. I. Scher, B. Higgins, A. Rose, C. Cordon-Cardo, H. T. Thaler, R. A. Rifkind, P. A. Marks, and V. M. Richon. 2000. "Suberoylanilide hydroxamic acid, an inhibitor of histone deacetylase, suppresses the growth of prostate cancer cells in vitro and in vivo." *Cancer Research* 60 (18):5165-70.

Catton, C. N., H. Lukka, C-S. Gu, J. M. Martin, S. Supiot, P. W. M. Chung, G. S. Bauman, J-P. Bahary, S. Ahmed, P. Cheung, K. H. Tai, J. S. Wu, M. B. Parliament, T. Tsakiridis, T. B. Corbett, C. Tang, I. S. Dayes, P. Warde, T. K. Craig, J. A. Julian, and M. N. Levine. 2017. "Randomized Trial of a Hypofractionated Radiation Regimen for the Treatment of

Localized Prostate Cancer." *Journal of Clinical Oncology* 35 (17):1884-1890. doi: 10.1200/JCO.2016.71.7397.

Chadwick, K. H., and H. P. Leenhouts. 1973. "A molecular theory of cell survival." *Physics in Medicine and Biology* 18 (1):78-87. doi: 10.1088/0031-9155/18/1/007.

Chakraborty, A., N. Tapryal, T. Venkova, N. Horikoshi, R. K. Pandita, A. H. Sarker, P. S. Sarkar, T. K. Pandita, and T. K. Hazra. 2016. "Classical non-homologous end-joining pathway utilizes nascent RNA for error-free double-strand break repair of transcribed genes." *Nature Communications* 7:13049. doi: 10.1038/ncomms13049.

Chapman, J. R., M. R. Taylor, and S. J. Boulton. 2012. "Playing the end game: DNA double-strand break repair pathway choice." *Molecular Cell* 47 (4):497-510. doi: 10.1016/j.molcel.2012.07.029.

Chiolo, I., J. Tang, W. Georgescu, and S. V. Costes. 2013. "Nuclear dynamics of radiation-induced foci in euchromatin and heterochromatin." *Mutation Research* 750 (1-2):56-66. doi: 10.1016/j.mrfmmm.2013.08.001.

Chudoba, I., A. Plesch, T. Lörch, J. Lemke, U. Claussen, and G. Senger. 1999. "High resolution multicolor-banding: a new technique for refined FISH analysis of human chromosomes." *Cytogenetic and Genome Research* 84 (3-4):156-160. doi: 10.1159/000015245.

Cornforth, M. N., and J. S. Bedford. 1987. "A Quantitative Comparison of Potentially Lethal Damage Repair and the Rejoining of Interphase Chromosome Breaks in Low Passage Normal Human Fibroblasts." *Radiation Research* 111 (3):385-405. doi: 10.2307/3576926.

Craxton, A., J. Somers, D. Munnur, R. Jukes-Jones, K. Cain, and M. Malewicz. 2015. "XLS (c9orf142) is a new component of mammalian DNA double-stranded break repair." *Cell Death & Differentiation* 22 (6):890-7. doi:

10.1038/cdd.2015.22.

Curtis, S. B. 1986. "Lethal and potentially lethal lesions induced by radiation--a unified repair model." *Radiation Research* 106 (2):252-70. doi: 10.2307/3576798.

Dasu, A., and I. Toma-Dasu. 2012. "Prostate alpha/beta revisited – an analysis of clinical results from 14 168 patients." *Acta Oncologica* 51 (8):963-974. doi: 10.3109/0284186X.2012.719635.

Davis, A. J., and D. J. Chen. 2013. "DNA double strand break repair via non-homologous end-joining." *Translational Cancer Research* 2 (3):130-143. doi: 10.3978/j.issn.2218-676X.2013.04.02.

Delaney, G., S. Jacob, C. Featherstone, and M. Barton. 2005. "The role of radiotherapy in cancer treatment: estimating optimal utilization from a review of evidence-based clinical guidelines." *Cancer* 104 (6):1129-37. doi: 10.1002/cncr.21324.

Desouky, Omar, Nan Ding, and Guangming Zhou. 2015. "Targeted and non-targeted effects of ionizing radiation." *Journal of Radiation Research and Applied Sciences* 8 (2):247-254. doi: 10.1016/j.jrras.2015.03.003.

Djordjevic, B., and L. J. Tolmach. 1967. "X-ray sensitivity of HeLa S3 cells in the G2 phase comparison of two methods of synchronization." *Biophysical Journal* 7 (1):77-94. doi: 10.1016/s0006-3495(67)86576-7.

Falk, M., E. Lukasova, and S. Kozubek. 2008. "Chromatin structure influences the sensitivity of DNA to gamma-radiation." *Biochimica et Biophysica Acta* 1783 (12):2398-414. doi: 10.1016/j.bbamcr.2008.07.010.

Falk, M., E. Lukasova, and S. Kozubek. 2010. "Higher-order chromatin structure in DSB induction, repair and misrepair." *Mutation Research* 704 (1-3):88-100. doi: 10.1016/j.mrrev.2010.01.013.

Fernandez-Capetillo, O., A. Celeste, and A. Nussenzweig. 2003. "Focusing on

Foci: H2AX and the Recruitment of DNA-Damage Response Factors." *Cell Cycle* 2 (5):425-426. doi: 10.4161/cc.2.5.509.

Flinterman, M., J. Gaken, F. Farzaneh, and M. Tavassoli. 2003. "E1A-mediated suppression of EGFR expression and induction of apoptosis in head and neck squamous carcinoma cell lines." *Oncogene* 22 (13):1965-77. doi: 10.1038/sj.onc.1206190.

Fowler, J. F. 2005. "The radiobiology of prostate cancer including new aspects of fractionated radiotherapy." *Acta Oncologica* 44 (3):265-76. doi: 10.1080/02841860410002824.

Fradet-Turcotte, A., M. D. Canny, C. Escribano-Diaz, A. Orthwein, C. C. Leung, H. Huang, M. C. Landry, J. Kitevski-LeBlanc, S. M. Noordermeer, F. Sicheri, and D. Durocher. 2013. "53BP1 is a reader of the DNA-damage-induced H2A Lys 15 ubiquitin mark." *Nature* 499 (7456):50-4. doi: 10.1038/nature12318.

Frame, F. M., D. Pellacani, A. T. Collins, M. S. Simms, V. M. Mann, G. D. Jones, M. Meuth, R. G. Bristow, and N. J. Maitland. 2013. "HDAC inhibitor confers radiosensitivity to prostate stem-like cells." *British Journal of Cancer* 109 (12):3023-33. doi: 10.1038/bjc.2013.691.

Frank, K. M., N. E. Sharpless, Y. Gao, J. M. Sekiguchi, D. O. Ferguson, C. Zhu, J. P. Manis, J. Horner, R. A. DePinho, and F. W. Alt. 2000. "DNA ligase IV deficiency in mice leads to defective neurogenesis and embryonic lethality via the p53 pathway." *Molecular Cell* 5 (6):993-1002. doi: 10.1016/S1097-2765(00)80264-6.

Garcia, L. M., D. E. Wilkins, and G. P. Raaphorst. 2007. "α/β ratio: A dose range dependence study." *International Journal of Radiation Oncology • Biology • Physics* 67 (2):587-593. doi: 10.1016/j.ijrobp.2006.10.017.

Geuting, V., C. Reul, and M. Lobrich. 2013. "ATM release at resected double-strand breaks provides heterochromatin reconstitution to facilitate

homologous recombination." *PLOS Genetics* 9 (8):e1003667. doi: 10.1371/journal.pgen.1003667.

Ghezraoui, H., M. Piganeau, B. Renouf, J. B. Renaud, A. Sallmyr, B. Ruis, S. Oh, A. E. Tomkinson, E. A. Hendrickson, C. Giovannangeli, M. Jasin, and E. Brunet. 2014. "Chromosomal translocations in human cells are generated by canonical nonhomologous end-joining." *Molecular Cell* 55 (6):829-842. doi: 10.1016/j.molcel.2014.08.002.

Goodarzi, A. A., and P. A. Jeggo. 2012. "Irradiation induced foci (IRIF) as a biomarker for radiosensitivity." *Mutation Research* 736 (1-2):39-47. doi: 10.1016/j.mrfmmm.2011.05.017.

Goodarzi, A. A., and P. A. Jeggo. 2013. "The repair and signaling responses to DNA double-strand breaks." *Advances in Genetics* 82:1-45. doi: 10.1016/b978-0-12-407676-1.00001-9.

Goodarzi, A. A., P. Jeggo, and M. Lobrich. 2010. "The influence of heterochromatin on DNA double strand break repair: Getting the strong, silent type to relax." *DNA Repair* 9 (12):1273-1282. doi: 10.1016/j.dnarep.2010.09.013.

Gotoh, E., Y. Asakawa, and H. Kosaka. 1995. "Inhibition of protein serine/threonine phosphatases directly induces premature chromosome condensation in mammalian somatic cells." *Biomedical Research* 16 (1):63-68. doi: 10.2220/biomedres.16.63.

Gotoh, E., and M. Durante. 2006. "Chromosome condensation outside of mitosis: mechanisms and new tools." *Journal of Cellular Physiology* 209 (2):297-304. doi: 10.1002/jcp.20720.

Green, C. M., and G. Almouzni. 2003. "Local action of the chromatin assembly factor CAF-1 at sites of nucleotide excision repair in vivo." *The EMBO Journal* 22 (19):5163-5174. doi: 10.1093/emboj/cdg478.

Gudjonsson, T., M. Altmeyer, V. Savic, L. Toledo, C. Dinant, M. Grofte, J. Bartkova, M. Poulsen, Y. Oka, S. Bekker-Jensen, N. Mailand, B. Neumann, J. K. Heriche, R. Shearer, D. Saunders, J. Bartek, J. Lukas, and C. Lukas. 2012. "TRIP12 and UBR5 suppress spreading of chromatin ubiquitylation at damaged chromosomes." *Cell* 150 (4):697-709. doi: 10.1016/j.cell.2012.06.039.

Hall, E. J., and A. J. Giaccia. 2012. *Radiobiology for the radiologist*. 7th ed. Philadelphia: Wolters Kluwer Health/Lippincott Williams & Wilkins.

Hanahan, D., and R. A. Weinberg. 2011. "Hallmarks of cancer: the next generation." *Cell* 144 (5):646-74. doi: 10.1016/j.cell.2011.02.013.

Her, J., N. Soo Lee, Y. Kim, and H. Kim. 2016. "Factors forming the BRCA1-A complex orchestrate BRCA1 recruitment to the sites of DNA damage." *Acta Biochimica et Biophysica Sinica* 48 (7):658-664. doi: 10.1093/abbs/gmw047.

Hill, M. A. 2004. "The variation in biological effectiveness of X-rays and gamma rays with energy." *Radiation Protection Dosimetry* 112 (4):471-81. doi: 10.1093/rpd/nch091.

Horsman, M. R., and J. Overgaard. 2016. "The impact of hypoxia and its modification of the outcome of radiotherapy." *Journal of Radiation Research* 57 Suppl 1 (Suppl 1):i90-i98. doi: 10.1093/jrr/rrw007.

Hoskin, P. et al. 2019. Radiology dose fractionation, third edition. In *Royal College of Radiologists*.

Hrzenjak, A., F. Moinfar, M-L. Kremser, B. Strohmeier, E. Petru, K. Zatloukal, and H. Denk. 2010. "Histone deacetylase inhibitor vorinostat suppresses the growth of uterine sarcomas in vitro and in vivo." *Molecular Cancer* 9:49-49. doi: 10.1186/1476-4598-9-49.

Hu, Jie, Malini Sathanoori, Sally J. Kochmar, and Urvashi Surti. 2006.

"Application of multicolor banding for identification of complex chromosome 18 rearrangements." *Journal of Molecular Diagnostics : JMD* 8 (4):521-528. doi: 10.2353/jmoldx.2006.060001.

Huang, J., X. Liang, Y. Xuan, C. Geng, Y. Li, H. Lu, S. Qu, X. Mei, H. Chen, T. Yu, N. Sun, J. Rao, J. Wang, W. Zhang, Y. Chen, S. Liao, H. Jiang, X. Liu, Z. Yang, F. Mu, and S. Gao. 2017. "A reference human genome dataset of the BGISEQ-500 sequencer." *Gigascience* 6 (5):1-9. doi: 10.1093/gigascience/gix024.

Huang, L., and A. B. Pardee. 2000. "Suberoylanilide hydroxamic acid as a potential therapeutic agent for human breast cancer treatment." *Molecular Medicine* 6 (10):849-66. doi: 10.1007/BF03401823.

Iliakis, G. 1991. "The role of DNA double strand breaks in ionizing radiation-induced killing of eukaryotic cells." *BioEssays* 13 (12):641-8. doi: 10.1002/bies.950131204.

Iliakis, G., T. Murmann, and A. Soni. 2015. "Alternative end-joining repair pathways are the ultimate backup for abrogated classical non-homologous end-joining and homologous recombination repair: Implications for the formation of chromosome translocations." *Mutation Research/Genetic Toxicology and Environmental Mutagenesis* 793:166-175. doi: 10.1016/j.mrgentox.2015.07.001.

Isono, M., A. Niimi, T. Oike, Y. Hagiwara, H. Sato, R. Sekine, Y. Yoshida, S. Y. Isobe, C. Obuse, R. Nishi, E. Petricci, S. Nakada, T. Nakano, and A. Shibata. 2017. "BRCA1 Directs the Repair Pathway to Homologous Recombination by Promoting 53BP1 Dephosphorylation." *Cell Reports* 18 (2):520-532. doi: 10.1016/j.celrep.2016.12.042.

Jackson, S. P. 2002. "Sensing and repairing DNA double-strand breaks." *Carcinogenesis* 23 (5):687-696. doi: 10.1093/carcin/23.5.687.

Jackson, S. P., and J. Bartek. 2009. "The DNA-damage response in human

biology and disease." *Nature* 461:1071. doi: 10.1038/nature08467

Jain, S., N. Sugawara, and J. E. Haber. 2016. "Role of Double-Strand Break End-Tethering during Gene Conversion in Saccharomyces cerevisiae." *PLOS Genetics* 12 (4):e1005976. doi: 10.1371/journal.pgen.1005976.

Janssen, A., G. A. Breuer, E. K. Brinkman, A. I. van der Meulen, S. V. Borden, B. van Steensel, R. S. Bindra, J. R. LaRocque, and G. H. Karpen. 2016. "A single double-strand break system reveals repair dynamics and mechanisms in heterochromatin and euchromatin." *Genes & Development* 30 (14):1645-57. doi: 10.1101/gad.283028.116.

Jasin, M., and R. Rothstein. 2013. "Repair of strand breaks by homologous recombination." *Cold Spring Harbor Perspectives in Biology* 5 (11):a012740-a012740. doi: 10.1101/cshperspect.a012740.

Joiner, M., and A. van der Kogel. 2019. *Basic Clinical Radiobiology*. Boca Raton ; London ; New York: CRC Press, Taylor & Francis Group.

Kakarougkas, A., A. Ismail, A. L. Chambers, E. Riballo, A. D. Herbert, J. Kunzel, M. Lobrich, P. A. Jeggo, and J. A. Downs. 2014. "Requirement for PBAF in transcriptional repression and repair at DNA breaks in actively transcribed regions of chromatin." *Molecular Cell* 55 (5):723-32. doi: 10.1016/j.molcel.2014.06.028.

Kakarougkas, A., A. Ismail, K. Klement, A. A. Goodarzi, S. Conrad, R. Freire, A. Shibata, M. Lobrich, and P. A. Jeggo. 2013. "Opposing roles for 53BP1 during homologous recombination." *Nucleic Acids Research* 41 (21):9719-31. doi: 10.1093/nar/gkt729.

Karanam, K., R. Kafri, A. Loewer, and G. Lahav. 2012. "Quantitative live cell imaging reveals a gradual shift between DNA repair mechanisms and a maximal use of HR in mid S phase." *Molecular Cell* 47 (2):320-9. doi:

10.1016/j.molcel.2012.05.052.

Kent, W. J., C. W. Sugnet, T. S. Furey, K. M. Roskin, T. H. Pringle, A. M. Zahler, and D. Haussler. 2002. "The human genome browser at UCSC." *Genome Research* 12 (6):996-1006. doi: 10.1101/gr.229102.

Kim, H-J., and S-C. Bae. 2011. "Histone deacetylase inhibitors: molecular mechanisms of action and clinical trials as anti-cancer drugs." *American Journal of Translational Research* 3 (2):166-179. doi: 10.1007/s12094-008-0221-x.

Krejci, L., V. Altmannova, M. Spirek, and X. Zhao. 2012. "Homologous recombination and its regulation." *Nucleic Acids Research* 40 (13):5795-5818. doi: 10.1093/nar/gks270.

Kucab, J. E., X. Zou, S. Morganella, M. Joel, A. S. Nanda, E. Nagy, C. Gomez, A. Degasperi, R. Harris, S. P. Jackson, V. M. Arlt, D. H. Phillips, and S. Nik-Zainal. 2019. "A Compendium of Mutational Signatures of Environmental Agents." *Cell* 177 (4):821-836.e16. doi: 10.1016/j.cell.2019.03.001.

Kumagai, T., N. Wakimoto, D. Yin, S. Gery, N. Kawamata, N. Takai, N. Komatsu, A. Chumakov, Y. Imai, and H. P. Koeffler. 2007. "Histone deacetylase inhibitor, suberoylanilide hydroxamic acid (Vorinostat, SAHA) profoundly inhibits the growth of human pancreatic cancer cells." *International Journal of Cancer* 121 (3):656-65. doi: 10.1002/ijc.22558.

Kuo, L. J., and L. X. Yang. 2008. "Gamma-H2AX - a novel biomarker for DNA double-strand breaks." *In Vivo* 22 (3):305-9.

Lagendijk, J. J., B. W. Raaymakers, A. J. Raaijmakers, J. Overweg, K. J. Brown, E. M. Kerkhof, R. W. van der Put, B. Hardemark, M. van Vulpen, and U. A. van der Heide. 2008. "MRI/linac integration." *Radiotherapy and Oncology* 86 (1):25-9. doi: 10.1016/j.radonc.2007.10.034.

Li, H., and R. Durbin. 2010. "Fast and accurate long-read alignment with Burrows-Wheeler transform." *Bioinformatics* 26 (5):589-95. doi: 10.1093/bioinformatics/btp698.

Li, X., and W-D. Heyer. 2008. "Homologous recombination in DNA repair and DNA damage tolerance." *Cell Research* 18 (1):99-113. doi: 10.1038/cr.2008.1.

Litwin, I., E. Pilarczyk, and R. Wysocki. 2018. "The Emerging Role of Cohesin in the DNA Damage Response." *Genes* 9 (12):581. doi: 10.3390/genes9120581.

Llorente, B., C. E. Smith, and L. S. Symington. 2008. "Break-induced replication: what is it and what is it for?" *Cell Cycle* 7 (7):859-64. doi: 10.4161/cc.7.7.5613.

Lobachev, K., E. Vitriol, J. Stemple, M. A. Resnick, and K. Bloom. 2004. "Chromosome Fragmentation after Induction of a Double-Strand Break Is an Active Process Prevented by the RMX Repair Complex." *Current Biology* 14 (23):2107-2112. doi: 10.1016/j.cub.2004.11.051.

Löbrich, M., and P. Jeggo. 2017. "A Process of Resection-Dependent Nonhomologous End Joining Involving the Goddess Artemis." *Trends in Biochemical Sciences* 42 (9):690-701. doi: 10.1016/j.tibs.2017.06.011.

Lobrich, M., M. Kuhne, J. Wetzel, and K. Rothkamm. 2000. "Joining of correct and incorrect DNA double-strand break ends in normal human and ataxia telangiectasia fibroblasts." *Genes Chromosomes Cancer* 27 (1):59-68.

Löbrich, M., M. Kühne, J. Wetzel, and K. Rothkamm. 2000. "Joining of correct and incorrect DNA double-strand break ends in normal human and ataxia telangiectasia fibroblasts." *Genes, Chromosomes and Cancer* 27 (1):59-68. doi: 10.1002/(sici)1098-2264(200001)27:1<59::Aid-

gcc8>3.0.Co;2-9.

Löbrich, M., B. Rydberg, and P. K. Cooper. 1995. "Repair of x-ray-induced DNA double-strand breaks in specific Not I restriction fragments in human fibroblasts: joining of correct and incorrect ends." *Proceedings of the National Academy of Sciences of the United States of America* 92 (26):12050-12054. doi: 10.1073/pnas.92.26.12050.

Löbrich, M., A. Shibata, A. Beucher, A. Fisher, M. Ensminger, A. A. Goodarzi, O. Barton, and P. A. Jeggo. 2010. "gammaH2AX foci analysis for monitoring DNA double-strand break repair: strengths, limitations and optimization." *Cell Cycle* 9 (4):662-9. doi: 10.4161/cc.9.4.10764.

Lorat, Y., S. Schanz, and C. E. Rübe. 2016. "Ultrastructural Insights into the Biological Significance of Persisting DNA Damage Foci after Low Doses of Ionizing Radiation." *Clinical Cancer Research* 22 (21):5300. doi: 10.1158/1078-0432.CCR-15-3081.

Lorat, Y., S. Schanz, N. Schuler, G. Wennemuth, C. Rübe, and Claudia E. Rübe. 2012. "Beyond Repair Foci: DNA Double-Strand Break Repair in Euchromatic and Heterochromatic Compartments Analyzed by Transmission Electron Microscopy." *PLOS One* 7 (5):e38165. doi: 10.1371/journal.pone.0038165.

Lorenzini, A., F. B. Johnson, A. Oliver, M. Tresini, J. S. Smith, M. Hdeib, C. Sell, V. J. Cristofalo, and T. D. Stamato. 2009. "Significant correlation of species longevity with DNA double strand break recognition but not with telomere length." *Mechanisms of Ageing and Development* 130 (11-12):784-792. doi: 10.1016/j.mad.2009.10.004.

Loucas, B. D., and M. N. Cornforth. 2013. "The LET Dependence of Unrepaired Chromosome Damage in Human Cells: A Break Too Far?" *Radiation Research*. doi: 10.1667/RR3159.1.

M'Kacher, R., E. E. L. Maalouf, M. Ricoul, L. Heidingsfelder, E. Laplagne, C.

Cuceu, W. M. Hempel, B. Colicchio, A. Dieterlen, and L. Sabatier. 2014. "New tool for biological dosimetry: reevaluation and automation of the gold standard method following telomere and centromere staining." *Mutation Research* 770:45-53. doi: 10.1016/j.mrfmmm.2014.09.007.

Mahaney, B. L., M. Hammel, K. Meek, J. A. Tainer, and S. P. Lees-Miller. 2013. "XRCC4 and XLF form long helical protein filaments suitable for DNA end protection and alignment to facilitate DNA double strand break repair." *Biochemistry and Cell Biology* 91 (1):31-41. doi: 10.1139/bcb-2012-0058.

Mansour, W. Y., T. Rhein, and J. Dahm-Daphi. 2010. "The alternative end-joining pathway for repair of DNA double-strand breaks requires PARP1 but is not dependent upon microhomologies." *Nucleic Acids Research* 38 (18):6065-77. doi: 10.1093/nar/gkq387.

Mao, Z., M. Bozzella, A. Seluanov, and V. Gorbunova. 2008. "Comparison of nonhomologous end joining and homologous recombination in human cells." *DNA Repair* 7 (10):1765-1771. doi: 10.1016/j.dnarep.2008.06.018.

Mao, Z., Y. Jiang, X. Liu, A. Seluanov, and V. Gorbunova. 2009. "DNA repair by homologous recombination, but not by nonhomologous end joining, is elevated in breast cancer cells." *Neoplasia* 11 (7):683-691. doi: 10.1593/neo.09312.

Marchese, M. J., M. Zaider, and E. J. Hall. 1987. "Potentially lethal damage repair in human cells." *Radiotherapy and Oncology* 9 (1):57-65. doi: 10.1016/S0167-8140(87)80219-0.

Marechal, A., and L. Zou. 2013. "DNA damage sensing by the ATM and ATR kinases." *Cold Spring Harbor Perspectives in Biology* 5 (9). doi: 10.1101/cshperspect.a012716.

Mariotti, L. G., G. Pirovano, K. I. Savage, M. Ghita, A. Ottolenghi, K. M. Prise,

and G. Schettino. 2013. "Use of the γ-H2AX Assay to Investigate DNA Repair Dynamics Following Multiple Radiation Exposures." *PLOS One* 8 (11):e79541. doi: 10.1371/journal.pone.0079541.

Martin, O. A., A. Ivashkevich, S. Choo, L. Woodbine, P. A. Jeggo, R. F. Martin, and P. Lobachevsky. 2013. "Statistical analysis of kinetics, distribution and co-localisation of DNA repair foci in irradiated cells: cell cycle effect and implications for prediction of radiosensitivity." *DNA Repair (Amst)* 12 (10):844-55. doi: 10.1016/j.dnarep.2013.07.002.

Matsumoto, H., A. Takahashi, and T. Ohnishi. 2004. "Radiation-Induced Adaptive Responses and Bystander Effects." *Biological Sciences in Space* 18 (4):247-254. doi: 10.2187/bss.18.247.

Mazin, A. V., O. M. Mazina, D. V. Bugreev, and M. J. Rossi. 2010. "Rad54, the motor of homologous recombination." *DNA Repair (Amst)* 9 (3):286-302. doi: 10.1016/j.dnarep.2009.12.006.

McKenna, A., M. Hanna, E. Banks, A. Sivachenko, K. Cibulskis, A. Kernytsky, K. Garimella, D. Altshuler, S. Gabriel, M. Daly, and M. A. DePristo. 2010. "The Genome Analysis Toolkit: a MapReduce framework for analyzing next-generation DNA sequencing data." *Genome Research* 20 (9):1297-303. doi: 10.1101/gr.107524.110.

McMillan, T. J., J. H. Peacock, and G. G. Steel. 1989. "The 5Rs of Radiobiology " *International Journal of Radiation Biology* 56 (6):1045-1048. doi: 10.1080/09553008914552491.

Meisenberg, C., S. I. Pinder, S. R. Hopkins, S. K. Wooller, G. Benstead-Hume, F. M. G. Pearl, P. A. Jeggo, and J. A. Downs. 2019. "Repression of Transcription at DNA Breaks Requires Cohesin throughout Interphase and Prevents Genome Instability." *Molecular Cell* 73 (2):212-223.e7. doi: 10.1016/j.molcel.2018.11.001.

Miller, K. M., J. V. Tjeertes, J. Coates, G. Legube, S. E. Polo, S. Britton, and

S. P. Jackson. 2010. "Human HDAC1 and HDAC2 function in the DNA-damage response to promote DNA nonhomologous end-joining." *Nature Structural & Molecular Biology* 17 (9):1144-1151. doi: 10.1038/nsmb.1899.

Morgan, W. F. 2003. "Is there a common mechanism underlying genomic instability, bystander effects and other nontargeted effects of exposure to ionizing radiation?" *Oncogene* 22 (45):7094-9. doi: 10.1038/sj.onc.1206992.

Najafi, M., R. Fardid, Gh Hadadi, and M. Fardid. 2014. "The mechanisms of radiation-induced bystander effect." *Journal of biomedical physics & engineering* 4 (4):163-172.

Neal, J. A., and K. Meek. 2011. "Choosing the right path: does DNA-PK help make the decision?" *Mutation Research* 711 (1-2):73-86. doi: 10.1016/j.mrfmmm.2011.02.010.

Nepomuceno, T. C., V. C. Fernandes, T. T. Gomes, R. S. Carvalho, G. Suarez-Kurtz, A. N. Monteiro, and M. A. Carvalho. 2017. "BRCA1 recruitment to damaged DNA sites is dependent on CDK9." *Cell Cycle* 16 (7):665-672. doi: 10.1080/15384101.2017.1295177.

Neumaier, T., J. Swenson, C. Pham, A. Polyzos, A. T. Lo, P. Yang, J. Dyball, A. Asaithamby, D. J. Chen, M. J. Bissell, S. Thalhammer, and S. V. Costes. 2012. "Evidence for formation of DNA repair centers and dose-response nonlinearity in human cells." *Proceedings of the National Academy of Sciences of the United States of America* 109 (2):443-8. doi: 10.1073/pnas.1117849108.

Noda, A., Y. Hirai, K. Hamasaki, H. Mitani, N. Nakamura, and Y. Kodama. 2012. "Unrepairable DNA double-strand breaks that are generated by ionising radiation determine the fate of normal human cells." *Journal of Cell Science* 125 (22):5280. doi: 10.1242/jcs.101006.

Ochs, F., K. Somyajit, M. Altmeyer, M. B. Rask, J. Lukas, and C. Lukas. 2016. "53BP1 fosters fidelity of homology-directed DNA repair." *Nature Structural & Molecular Biology* 23 (8):714-21. doi: 10.1038/nsmb.3251.

Osborne, C. S. 2014. "Molecular Pathways: Transcription Factories and Chromosomal Translocations." *Clinical Cancer Research* 20 (2):296. doi: 10.1158/1078-0432.CCR-12-3667.

Otani, K., Y. Naito, Y. Sakaguchi, Y. Seo, Y. Takahashi, J. Kikuta, K. Ogawa, and M. Ishii. 2016. "Cell-cycle-controlled radiation therapy was effective for treating a murine malignant melanoma cell line in vitro and in vivo." *Scientific Reports* 6:30689. doi: 10.1038/srep30689.

Panier, S., and S. J. Boulton. 2013. "Double-strand break repair: 53BP1 comes into focus." *Nature Reviews Molecular Cell Biology* 15:7. doi: 10.1038/nrm3719.

Pawelczak, K. S., S. M. Bennett, and J. J. Turchi. 2011. "Coordination of DNA-PK activation and nuclease processing of DNA termini in NHEJ." *Antioxidants & Redox Signaling* 14 (12):2531-2543. doi: 10.1089/ars.2010.3368.

Pawlik, T. M., and K. Keyomarsi. 2004. "Role of cell cycle in mediating sensitivity to radiotherapy." *International Journal of Radiation Oncology • Biology • Physics* 59 (4):928-42. doi: 10.1016/j.ijrobp.2004.03.005.

Pei, H., L. Zhang, K. Luo, Y. Qin, M. Chesi, F. Fei, P. L. Bergsagel, L. Wang, Z. You, and Z. Lou. 2011. "MMSET regulates histone H4K20 methylation and 53BP1 accumulation at DNA damage sites." *Nature* 470 (7332):124-8. doi: 10.1038/nature09658.

Polo, S. E., and S. P. Jackson. 2011. "Dynamics of DNA damage response proteins at DNA breaks: a focus on protein modifications." *Genes & Development* 25 (5):409-33. doi: 10.1101/gad.2021311.

Purrucker, J. C., A. Fricke, M. F. Ong, C. Rube, C. E. Rube, and U. Mahlknecht. 2010. "HDAC inhibition radiosensitizes human normal tissue cells and reduces DNA Double-Strand Break repair capacity." *Oncology Reports* 23 (1):263-9. doi: 10.3892/or_00000632.

Qi, X. S., J. White, and X. A. Li. 2011. "Is α/β for breast cancer really low?" *Radiotherapy and Oncology* 100 (2):282-288. doi: 10.1016/j.radonc.2011.01.010.

Raaphorst, G. P. 1992. "Recovery of sublethal radiation damage and its inhibition by hyperthermia in normal and transformed mouse cells." *International Journal of Radiation Oncology • Biology • Physics* 22 (5):1035-41. doi: 10.1016/0360-3016(92)90804-q.

Rausch, T., T. Zichner, A. Schlattl, A. M. Stütz, V. Benes, and J. O. Korbel. 2012. "DELLY: structural variant discovery by integrated paired-end and split-read analysis." *Bioinformatics* 28 (18):i333-i339. doi: 10.1093/bioinformatics/bts378.

Regaud, C. , and R. Ferroux. 1927. "Discordance des effets des rayons X, d'une part dans la peau, d'autre part dans le testicule, par le fractionnement de la dose: diminution de l'efficacité dans la peau, maintien de l'efficacité dans le testicule." *Comptes rendus hebdomadaires séances mémoires Soc biol* 97:431.

Revell, S. H. 1974. "The Breakage-and-Reunion Theory and the Exchange Theory for Chromosomal Aberrations Induced by Ionizing Radiations: A Short History." In *Advances in Radiation Biology*, edited by J. T. Lett, H. Adler and M. Zelle, 367-416. Elsevier.

Riballo, E., M. Kuhne, N. Rief, A. Doherty, G. C. Smith, M. J. Recio, C. Reis, K. Dahm, A. Fricke, A. Krempler, A. R. Parker, S. P. Jackson, A. Gennery, P. A. Jeggo, and M. Lobrich. 2004. "A pathway of double-strand break rejoining dependent upon ATM, Artemis, and proteins locating to gamma-H2AX foci." *Molecular Cell* 16 (5):715-24. doi:

10.1016/j.molcel.2004.10.029.

Rodgers, K., and M. McVey. 2016. "Error-Prone Repair of DNA Double-Strand Breaks." *Journal of Cellular Physiology* 231 (1):15-24. doi: 10.1002/jcp.25053.

Rodier, F., D. P. Muñoz, R. Teachenor, V. Chu, O. Le, D. Bhaumik, J-P. Coppé, E. Campeau, C. M. Beauséjour, S-H. Kim, A. R. Davalos, and J. Campisi. 2011. "DNA-SCARS: distinct nuclear structures that sustain damage-induced senescence growth arrest and inflammatory cytokine secretion." *Journal of Cell Science* 124 (1):68. doi: 10.1242/jcs.071340.

Rothkamm, K., I. Krüger, L. H. Thompson, and M. Löbrich. 2003. "Pathways of DNA Double-Strand Break Repair during the Mammalian Cell Cycle." *Molecular and Cellular Biology* 23 (16):5706-5715. doi: 10.1128/mcb.23.16.5706-5715.2003.

Roukos, V., T. C. Voss, C. K. Schmidt, S. Lee, D. Wangsa, and T. Misteli. 2013. "Spatial dynamics of chromosome translocations in living cells." *Science* 341 (6146):660-4. doi: 10.1126/science.1237150.

Roy, S., A. J. de Melo, Y. Xu, S. K. Tadi, A. Negrel, E. Hendrickson, M. Modesti, and K. Meek. 2015. "XRCC4/XLF Interaction Is Variably Required for DNA Repair and Is Not Required for Ligase IV Stimulation." *Molecular and Cellular Biology* 35 (17):3017-28. doi: 10.1128/mcb.01503-14.

Roy, Sunetra, Abinadabe J. de Melo, Yao Xu, Satish K. Tadi, Aurélie Négrel, Eric Hendrickson, Mauro Modesti, and Katheryn Meek. 2015. "XRCC4/XLF Interaction Is Variably Required for DNA Repair and Is Not Required for Ligase IV Stimulation." 35 (17):3017-3028. doi: 10.1128/MCB.01503-14 %J Molecular and Cellular Biology.

Ruprecht, N., M. N. Hungerbühler, I. B. Böhm, and J. T. Heverhagen. 2019. "Improved identification of DNA double strand breaks: γ-H2AX-epitope

visualization by confocal microscopy and 3D reconstructed images." *Radiation and Environmental Biophysics* 58 (2):295-302. doi: 10.1007/s00411-019-00778-1.

Ryan, L. A., C. B. Seymour, and C. E. Mothersill. 2009. "Investigation of non-linear adaptive responses and split dose recovery induced by ionizing radiation in three human epithelial derived cell lines." *Dose-response : a publication of International Hormesis Society* 7 (4):292-306. doi: 10.2203/dose-response.09-003.Mothersill.

Saini, N. 2015. "The journey of DNA repair." *Trends in Cancer* 1 (4):215-216. doi: 10.1016/j.trecan.2015.11.001.

Savage, J. R. K. 2004. "On the nature of visible chromosomal gaps and breaks." *Cytogenetic and Genome Research* 104 (1-4):46-55. doi: 10.1159/000077465.

Setiaputra, D., and D. Durocher. 2019. "Shieldin – the protector of DNA ends." *EMBO Reports* 20 (5):e47560. doi: 10.15252/embr.201847560.

Shain, A. H., and J. R. Pollack. 2013. "The spectrum of SWI/SNF mutations, ubiquitous in human cancers." *PLOS One* 8 (1):e55119. doi: 10.1371/journal.pone.0055119.

Shanbhag, N. M., I. U. Rafalska-Metcalf, C. Balane-Bolivar, S. M. Janicki, and R. A. Greenberg. 2010. "ATM-dependent chromatin changes silence transcription in cis to DNA double-strand breaks." *Cell* 141 (6):970-81. doi: 10.1016/j.cell.2010.04.038.

Shibata, A., S. Conrad, J. Birraux, V. Geuting, O. Barton, A. Ismail, A. Kakarougkas, K. Meek, G. Taucher-Scholz, M. Lobrich, and P. A. Jeggo. 2011. "Factors determining DNA double-strand break repair pathway choice in G2 phase." *The EMBO Journal* 30 (6):1079-92. doi: 10.1038/emboj.2011.27.

Shibata, A., and P. Jeggo. 2019. "A historical reflection on our understanding of radiation-induced DNA double strand break repair in somatic mammalian cells; interfacing the past with the present." *International Journal of Radiation Biology* 95 (7):945-956. doi: 10.1080/09553002.2018.1564083.

Shibata, A., D. Moiani, A. S. Arvai, J. Perry, S. M. Harding, M-M. Genois, R. Maity, S. van Rossum-Fikkert, A. Kertokalio, F. Romoli, A. Ismail, E. Ismalaj, E. Petricci, M. J. Neale, R. G. Bristow, J-Y. Masson, C. Wyman, P. A. Jeggo, and J. A. Tainer. 2014. "DNA double-strand break repair pathway choice is directed by distinct MRE11 nuclease activities." *Molecular Cell* 53 (1):7-18. doi: 10.1016/j.molcel.2013.11.003.

Sinclair, W. K. 1968. "Cyclic X-Ray Responses in Mammalian Cells in Vitro." *Radiation Research* 33 (3):620-643. doi: 10.2307/3572419.

Sinclair, W. K., and R. A. Morton. 1965. "X-Ray and Ultraviolet Sensitivity of Synchronized Chinese Hamster Cells at Various Stages of the Cell Cycle." *Biophysical Journal* 5 (1):1-25. doi: 10.1016/s0006-3495(65)86700-5.

Sinclair, W. K., and R. A. Morton. 1966. "X-Ray Sensitivity during the Cell Generation Cycle of Cultured Chinese Hamster Cells." *Radiation Research* 29 (3):450-474. doi: 10.2307/3572025.

Singh, S., H. Le, S-J. Shih, B. Ho, and A. T. Vaughan. 2010. "Suberoylanilide hydroxyamic acid modification of chromatin architecture affects DNA break formation and repair." *International Journal of Radiation Oncology • Biology • Physics* 76 (2):566-573. doi: 10.1016/j.ijrobp.2009.08.031.

Smith, J., L. Mun Tho, N. Xu, and D. A. Gillespie. 2010. "Chapter 3 - The ATM–Chk2 and ATR–Chk1 Pathways in DNA Damage Signaling and Cancer." In *Advances in Cancer Research*, edited by George F. Vande Woude and George Klein, 73-112. Academic Press.

Somaiah, N., K. Rothkamm, and J. Yarnold. 2015. "Where Do We Look for Markers of Radiotherapy Fraction Size Sensitivity?" *Clinical Oncology (Royal College Radiologists)* 27 (10):570-8. doi: 10.1016/j.clon.2015.06.006.

Somaiah, N., J. Yarnold, F. Daley, A. Pearson, L. Gothard, K. Rothkamm, and T. Helleday. 2012. "The relationship between homologous recombination repair and the sensitivity of human epidermis to the size of daily doses over a 5-week course of breast radiotherapy." *Clinical Cancer Research* 18 (19):5479-88. doi: 10.1158/1078-0432.Ccr-10-3297.

Somaiah, N., J. Yarnold, A. Lagerqvist, K. Rothkamm, and T. Helleday. 2013. "Homologous recombination mediates cellular resistance and fraction size sensitivity to radiation therapy." *Radiotherapy and Oncology* 108 (1):155-161. doi: 10.1016/j.radonc.2013.05.012.

Steel, G., J. M. Deacon, G. M. Duchesne, A. Horwich, L. R. Kelland, and J. H. Peacock. 1987. "The dose-rate effect in human tumour cells." *Radiotherapy and Oncology* 9 (4):299-310. doi: 10.1016/S0167-8140(87)80151-2.

Storch, K., I. Eke, K. Borgmann, M. Krause, C. Richter, K. Becker, E. Schrock, and N. Cordes. 2010. "Three-dimensional cell growth confers radioresistance by chromatin density modification." *Cancer Res* 70 (10):3925-34. doi: 10.1158/0008-5472.CAN-09-3848.

Suwaki, N., K. Klare, and M. Tarsounas. 2011. "RAD51 paralogs: Roles in DNA damage signalling, recombinational repair and tumorigenesis." *Seminars in Cell & Developmental Biology* 22 (8):898-905. doi: 10.1016/j.semcdb.2011.07.019.

Takata, H., T. Hanafusa, T. Mori, M. Shimura, Y. Iida, K. Ishikawa, K. Yoshikawa, Y. Yoshikawa, and K. Maeshima. 2013. "Chromatin Compaction Protects Genomic DNA from Radiation Damage." *PLOS*

One 8 (10):e75622. doi: 10.1371/journal.pone.0075622.

Takata, M., M. S. Sasaki, E. Sonoda, C. Morrison, M. Hashimoto, H. Utsumi, Y. Yamaguchi-Iwai, A. Shinohara, and S. Takeda. 1998. "Homologous recombination and non-homologous end-joining pathways of DNA double-strand break repair have overlapping roles in the maintenance of chromosomal integrity in vertebrate cells." *The EMBO Journal* 17 (18):5497-5508. doi: 10.1093/emboj/17.18.5497.

Terasima, T., and L. J. Tolmach. 1963. "Variations in several responses of HeLa cells to x-irradiation during the division cycle." *Biophysical Journal* 3:11-33. doi: 10.1016/s0006-3495(63)86801-0.

Thames, H D., Jr., H. Rodney Withers, L. J. Peters, and G. H. Fletcher. 1982. "Changes in early and late radiation responses with altered dose fractionation: Implications for dose-survival relationships." *International Journal of Radiation Oncology • Biology • Physics* 8 (2):219-226. doi: 10.1016/0360-3016(82)90517-X.

Thames, H. D., S. M. Bentzen, I. Turesson, M. Overgaard, and W. Van den Bogaert. 1990. "Time-dose factors in radiotherapy: a review of the human data." *Radiotherapy and Oncology* 19 (3):219-235. doi: 10.1016/0167-8140(90)90149-Q.

Thorslund, T., A. Ripplinger, S. Hoffmann, T. Wild, M. Uckelmann, B. Villumsen, T. Narita, T. K. Sixma, C. Choudhary, S. Bekker-Jensen, and N. Mailand. 2015. "Histone H1 couples initiation and amplification of ubiquitin signalling after DNA damage." *Nature* 527 (7578):389-93. doi: 10.1038/nature15401.

Tkach, J. M., A. Yimit, A. Y. Lee, M. Riffle, M. Costanzo, D. Jaschob, J. A. Hendry, J. Ou, J. Moffat, C. Boone, T. N. Davis, C. Nislow, and G. W. Brown. 2012. "Dissecting DNA damage response pathways by analysing protein localization and abundance changes during DNA replication stress." *Nature Cell Biology* 14 (9):966-976. doi:

10.1038/ncb2549.

Tobias, J. S. 1996. "The role of radiotherapy in the management of cancer--an overview." *Annals of the Academy of Medicine of Singapore* 25 (3):371-9.

Tomimatsu, N., B. Mukherjee, and S. Burma. 2009. "Distinct roles of ATR and DNA-PKcs in triggering DNA damage responses in ATM-deficient cells." *EMBO Reports* 10 (6):629-635. doi: 10.1038/embor.2009.60.

Truong, L. N., Y. Li, L. Z. Shi, P. Y. Hwang, J. He, H. Wang, N. Razavian, M. W. Berns, and X. Wu. 2013. "Microhomology-mediated End Joining and Homologous Recombination share the initial end resection step to repair DNA double-strand breaks in mammalian cells." *Proceedings of the National Academy of Sciences of the United States of America* 110 (19):7720-5. doi: 10.1073/pnas.1213431110.

Turesson, I., J. Nyman, F. Qvarnstrom, M. Simonsson, M. Book, I. Hermansson, S. Sigurdardottir, and K. A. Johansson. 2010. "A low-dose hypersensitive keratinocyte loss in response to fractionated radiotherapy is associated with growth arrest and apoptosis." *Radiotherapy & Oncology* 94 (1):90-101. doi: 10.1016/j.radonc.2009.10.007.

Venkata Narayanan, I., M. T. Paulsen, K. Bedi, N. Berg, E. A. Ljungman, S. Francia, A. Veloso, B. Magnuson, F. di Fagagna, T. E. Wilson, and M. Ljungman. 2017. "Transcriptional and post-transcriptional regulation of the ionizing radiation response by ATM and p53." *Scientific Reports* 7:43598-43598. doi: 10.1038/srep43598.

Wang, H., Z-C. Zeng, T-A. Bui, E. Sonoda, M. Takata, S. Takeda, and G. Iliakis. 2001. "Efficient rejoining of radiation-induced DNA double-strand breaks in vertebrate cells deficient in genes of the RAD52 epistasis group." *Oncogene* 20 (18):2212-2224. doi: 10.1038/sj.onc.1204350.

Watts, F. Z. 2016. "Repair of DNA Double-Strand Breaks in Heterochromatin." *Biomolecules* 6 (4):47. doi: 10.3390/biom6040047.

Willis, N. A., G. Chandramouly, B. Huang, A. Kwok, C. Follonier, C. Deng, and R. Scully. 2014. "BRCA1 controls homologous recombination at Tus/Ter-stalled mammalian replication forks." *Nature* 510 (7506):556-9. doi: 10.1038/nature13295.

Wilson, G. D. 2007. "Cell Kinetics." *Clinical Oncology* 19 (6):370-384. doi: 10.1016/j.clon.2007.02.015.

Withers, H. R. 1985. "Biologic basis for altered fractionation schemes." *Cancer* 55 (S9):2086-2095. doi: 10.1002/1097-0142(19850501)55:9+<2086::AID-CNCR2820551409>3.0.CO;2-1.

Wolff, S. 1998. "The adaptive response in radiobiology: evolving insights and implications." *Environmental health perspectives* 106 Suppl 1 (Suppl 1):277-283. doi: 10.1289/ehp.98106s1277.

Zhou, H., M. Hong, Y. Chai, and T. K. Hei. 2009. "Consequences of cytoplasmic irradiation: studies from microbeam." *Journal of Radiation Research* 50 Suppl A (0 0):A59-A65. doi: 10.1269/jrr.08120S.

Zhu, J., M. Adli, J. Y. Zou, G. Verstappen, M. Coyne, X. Zhang, T. Durham, M. Miri, V. Deshpande, P. L. De Jager, D. A. Bennett, J. A. Houmard, D. M. Muoio, T. T. Onder, R. Camahort, C. A. Cowan, A. Meissner, C. B. Epstein, N. Shoresh, and B. E. Bernstein. 2013. "Genome-wide chromatin state transitions associated with developmental and environmental cues." *Cell* 152 (3):642-654. doi: 10.1016/j.cell.2012.12.033.